



**REPUBLIC OF IRAQ
MINISTRY OF HIGHER EDUCATION AND
SCIENTIFIC RESEARCH
AL-FURAT AL-AWSAT TECHNICAL UNIVERSITY
ENGINEERING TECHNICAL COLLEGE NAJAF**

**INVESTIGATION OF THE PERFORMANCE OF
DYE-SENSITIZED SOLAR CELLS BY COATING
WITH NATURAL DYES WITH NANOMATERIALS**

ZAINAB HAIDER ABD AL-REHMAN

**M.TECH.
IN MECHANICAL ENGINEERING TECHNIQUES
OF POWER**

2023



**INVESTIGATION OF THE PERFORMANCE OF DYE-SENSITIZED SOLAR
CELLS BY COATING WITH NATURAL DYES WITH NANOMATERIALS**

A THESIS

**SUBMITTED TO THE DEPARTMENT OF MECHANICAL
ENGINEERING TECHNIQUES OF POWER
IN PARTIAL FULFILLMENT OF THE REQUIREMENTS FOR
THE DEGREE OF MASTER OF THERMAL TECHNOLOGIES IN
MECHANICAL ENGINEERING TECHNIQUES OF POWER
(M. TECH)**

BY

ZAINAB HAIDER ABD AL-REHMAN

Supervised by:

Prof.

Dr. Dhafer Manea Hachim

Dr. Ahmed Salim Naser Al-murshedi

February/2023

بِسْمِ اللَّهِ الرَّحْمَنِ الرَّحِيمِ

وَمَنْ يَتَّقِ اللَّهَ يَجْعَلْ لَهُ مَخْرَجًا * وَيَرْزُقْهُ
مِنْ حَيْثُ لَا يَحْتَسِبُ وَمَنْ يَتَوَكَّلْ عَلَى اللَّهِ
فَهُوَ حَسْبُهُ إِنَّ اللَّهَ بَالِغُ أَمْرِهِ قَدْ جَعَلَ اللَّهُ
لِكُلِّ شَيْءٍ قَدْرًا

صدق الله العلي العظيم

الطلاق ﴿2-3﴾

DISCLAIMER

I confirm that the work submitted in this thesis is my own work and has not been submitted to any other organization or for any other degree.

Signature:

Name: Zainab Haider Abd AL-Rehman

Date: / / 2023

ACKNOWLEDGMENTS

First, I would like to thank the almighty ALLAH, all praise be to GOD for this. I wish to express my deep gratitude to my supervisor **Prof. Dr. Dhafer Manea Hachim** and **Dr. Ahmed Salim Naser Al Murshedi** for their valuable help, advice, and encouragement during the project.

Special thanks to the Dean of Engineering Technical College- Najaf **Asst.Prof. Dr. Hassanain Ghani Hameed** and Special thanks to the Head of the Department of Mechanical Engineering Techniques of Power **Dr. Ahmed Salim Naser Al Murshedi** in the Technical Engineering College /Al-Najaf, Al-Furat Al-Awsat Technical University, for their support and advice.

To the one who prayed for me, **my beloved father** ... with honor, love, and respect.

To my heaven in this world and the hereafter, **my beloved mother** ... in appreciation, love, and loyalty.

To the tender hearts that complete my happiness with **my brothers** and **my sisters** ... with love and pride.

To those with whom I shared the best times, **my friends** ... in appreciation and pride.

To everyone who has love and affection for me in his heart, to everyone who supported me and wished me well.

I dedicate the fruit of my humble effort.

Zainab Haider Abd AL-Rehman

2023

SUPERVISORS CERTIFICATION

We certify that the thesis entitled "**Investigation of the Performance of Dye-Sensitized Solar Cells by Coating with Natural Dyes with Nanomaterials**" submitted by **Zainab Haider Abd AL-Rehman** has been prepared under our supervision at the Department of Mechanical Engineering Techniques of Power, College of Technical Engineering-Najaf, AL-Furat Al-Awsat Technical University, as partial fulfillment of the requirements for the degree of Master of Techniques in Thermal Engineering.

Signature:

Name: Prof. Dr. Dhafer Manea Hachim
(Supervisor)

Date: / / 2023

Signature:

Name: Dr. Ahmed Salim Naser
Al Murshedi
(Co-Supervisor)

Date: / / 2023

In view of the available recommendation, we forward this thesis for debate by the examining committee.

Signature:

Name: Assis Prof. Dr Adel A.Eidan
Head mechanical Eng. Tech of power Dept.

Date: / / 2023

COMMITTEE CERTIFICATION

We certify that we have read the thesis entitled "**Investigation of The Performance of Dye-Sensitized Solar Cells by Coating with Natural Dyes with Nanomaterials**" submitted by **Zainab Haider Abd AL-Rehman** and, as the examining committee, examined the student's thesis in its contents. And that, in our opinion, it is adequate as a thesis for the degree of Master of Techniques in Thermal Engineering.

Signature:

Name: Prof. Dr. Dhafer Manea Hachim

(Supervisor)

Date: / / 2023

Signature:

Name: Dr. Ahmed Salim Naser Al
Murshedi

(Co-Supervisor)

Date: / / 2023

Signature:

Name: Prof. Dr. Qahtan A. Abed

(Member)

Date: / / 2023

Signature:

Name: Asst. Prof. Dr. Montadhar A.
M. AL-Moussawi

(Member)

Date: / / 2023

Signature:

Name: Asst. Prof. Dr. Amar Sadun Abdul-Zahra

(Chairman)

Date: / / 2023

Approval of the Engineering Technical College- Najaf

Signature:

Name: Asst. Prof. Dr. Hassanain Ghani

Dean of Engineering Technical College- Najaf

Date: / / 2023

LINGUISTIC CERTIFICATION

This is to certify that this thesis entitled “**Investigation of The Performance of Dye-Sensitized Solar Cells by Coating with Natural Dyes with Nanomaterials**” was reviewed linguistically. Its language was amended to meet the style of the English language.

Signature:

Name: Inst. Omar Ra'oof Marzah

Date: / / 2023

ABSTRACT

Solar cells (photovoltaic cells; PV) are considered the ideal solution to get rid of environmental pollution problems resulting from electrical energy production processes. PV converts solar energy directly into electrical energy by virtue of the Photovoltaic Effect without noise, environmental pollution, or moving parts, making solar cells the perfect choice for clean energy in the world. However, there are many environmental factors that limit the efficiency of solar cells and make them relatively low.

Dye-Sensitized solar cell (DSSC) is one of the third-generation photovoltaic cell types, which, like other solar cells, are defined as a device that converts solar photons (sunlight) into electrical energy. DSSC has attracted a lot of attention for its lower cost compared to other photovoltaics. In this work, DSSC cells were manufactured using natural dyes that are sensitive to light, as they are characterized by their ease of extraction and very low cost, as they are environmentally friendly. Titanium dioxide (TiO_2) layer which acts as an electron collector. It also consists of a liquid electrolyte solution to replace the lost electrons from the natural dye molecules.

In this study, DSSCs were synthesized using three different new natural dyes, which are dyes extracted from *Mentha* leaves (because they contain a high percentage of chlorophyll, which is the most important element in the absorption of solar energy) and *Helianthus Annus* leaves (because they contain the auxin hormone that causes this flower to rotate with the sun). And *Fragaria* fruit (because it contains anthocyanins). The best results obtained were for the DSSC based on the dye extracted from the sunflower flower, as it had the largest number of absorption peaks, as the cell results were $I_{sc} =$

1.19mA, $V_{oc} = 0.48V$, $FF = 50.77\%$ and $\eta = 0.29\%$, and to improve the performance efficiency. The cell three dyes were mixed to make a new cell based on the mixture of dyes in equal proportions as a dye, so the results for that cell were $I_{sc} = 1.59mA$, $V_{oc} = 0.59V$, $FF = 73.55$ and $\eta = 0.69\%$.

In other experiments, nanomaterials were mixed with dyes, but their results were negative, as the addition of nanomaterials caused the decomposition of the dye, and thus the light-sensitive part of the cell disappeared, and no results were shown for the cells.

Also in this study, the results were compared between a cell with one layer of TiO_2 and another with two layer; Both cells are based on a mixture of dyes as a photosensitizer, and after conducting a FESEM examination, the images showed that the single layer of TiO_2 shows more and larger cracks than it is for the two layers of TiO_2 . Thus, a basic defect of the DSSCs defects was addressed if there was a clear increase in the results of the cell consisting of two layers of TiO_2 . The efficiency of DSSCs increased from 0.69% to 1.13%.

The deterioration in the efficiency of DSSCs due to the increase in ambient temperature has been studied. Through the laboratory tests conducted using the (Keithlye 2400) device and shining a light with a radiation intensity of 1000 watts / m², the results noted that the efficiency of DSSCs decreases by a high percentage with the increase in temperature, as the efficiency decreased from 1.13% at the first temperature, which was equivalent to 23.8 °C, to 0.49%. at a temperature of 43.32 °C.

CONTENTS

DISCLAIMER	I
ACKNOWLEDGMENTS	II
SUPERVISORS CERTIFICATION	III
COMMITTEE CERTIFICATION	IV
LINGUISTIC CERTIFICATION	V
ABSTRACT	VI
LIST OF FIGURES	XII
LIST OF TABLES	XVII
CHAPTER ONE	1
INTRODUCTION	1
1.1 General Introduction	1
1.2 Photovoltaic Technology	1
1.3 Progress in PV technologies	2
1.4 Background of DSSCs	1
1.5 Principle and working of DSSCs	1
1.6 Development of constructional parameters of DSSC	2
1.6.1 substrate	3
1.6.2 Metal oxide semiconductor (MOS)	3
1.6.3 Dye photo-sensitizer	5
1.6.4 Electrolyte	7
1.6.5 Counter electrode (CE)	9
1.7 Aims of Present Work	10
CHAPTER TWO	11
LITERATURE REVIEW	11
2.1 INTRODUCTION	11
2.2 Substrates for DSSCs	11
2.2.1 type of substrates for DSSCs	11

2.2.2 Influence of substrate cleaning on DSSC performance _____	12
2.3 Semiconductors _____	13
2.4 Sensitizers (Dye) _____	14
2.4.1 Types of sensitizers (dye) _____	14
2.4.2 The condition of the plants before the extraction of the dye _____	17
2.4.3 The solvent used to extract the dye _____	18
2.5 Studies about electrolyte _____	20
2.6 Studies about counter electrode (CE) _____	21
2.7 Summary for Substrates _____	22
2.8 Summary For semiconductors (photoanodes) _____	22
2.9 Summary for Sensitizers (Dye) _____	24
2.10 Summary for Electrolyte _____	27
2.11 Scope of The Present Work _____	28
CHAPTER THREE _____	30
THEORETICAL CONCEPT _____	30
3.1 Introduction _____	30
3.2 Light Properties _____	30
3.3 Optical Properties _____	31
3.3.1 Electronic Transitions _____	31
3.3.2 Direct and indirect electronic transfers _____	32
3.3.3 The Optical Constants _____	35
3.4 Crystal Structure and Bragg's Law _____	38
3.5 The solar cells parameters _____	39
3.5.1 Short-circuit current density (I_{sc}) _____	40
3.5.2 Open circuit voltage (V_{oc}) _____	41
3.5.3 Fill factor (FF) _____	41
3.5.4 Power conversion efficiency (η) _____	41
CHAPTER FOUR _____	43
EXPERIMENTAL WORK _____	43
4.1 INTRODUCTION _____	43
4.2 Materials _____	43
4.2.1 Glass substrate _____	43

4.2.2 Titanium Dioxide (TiO ₂)	44
4.2.3 Other materials	45
4.3 Prepare each part for DSSC before assembly	45
4.3.1 Substrate cleaning	45
4.3.2 Preparation of TiO ₂ photoanode	46
4.3.3 Preparation of sensitizers (dyes)	48
4.3.4 Electrolyte preparation	50
4.3.5 Counter electrodes preparation	51
4.4 Fabrication of DSSCs	52
4.5 Steps of testing DSSC	56
4.6 Measurement Devices	57
4.6.1 Sensitive Electronic Scale	57
4.6.2 Magnetic Stirrer & Hot Plate	58
4.6.3 Ultrasonic Device	58
4.6.4 Ultraviolet-Visible Spectrometer (UV-Vis)	59
4.6.5 Field Emission Scanning electron microscopy (FESEM)	60
4.6.6 Furnace	61
4.6.7 X- Ray diffraction	62
4.6.8 Temperature Measurement	63
4.6.9 Keithley 2400 device	65
4.6.10 Coating Thickness Gauge	66
4.6.11 Solar Power Meter	67
CHAPTER FIVE	69
RESULTS AND DISCUSSION	69
5.1. Introduction	69
5.2. Experimental validation	69
5.3 Structural properties of TiO ₂	70
5.3.1 Characterization of TiO ₂ layer	70
5.3.2 X-Ray Measurement Results	72
5.3.3 Energy Dispersive Using X-Ray (EDX)	74
5.3.4 Field Emission Scanning Electron Microscopy (FESEM)	75
5.4. The results of optical measurements for TiO ₂	77
5.4.1 Absorption Coefficient	79

5.4.2 Reflectance	80
5.4.3 Refractive Index	80
5.4.4 Extinction Coefficient	81
5.4.5 Dielectric Constant	82
5.5. Optical characterization of dyes	84
5.6. Optical properties of electrolytes	88
5.7. Solar cell surface temperature with time	89
5.8. DSSCs measurement results	90
5.8.1. Study the effect of types of dyes on performance of DSSCs	90
5.8.2. Study the effect of types of counter electrodes	93
5.8.3. Study the effect of thickness of TiO ₂ Layers on Performances of DSSCs	95
5.8.4. Study the effect of temperature on performance of DSSCs	97
CHAPTER SIX	101
CONCLUSIONS AND RECOMMENDATIONS	101
6.1. Conclusion	101
6.2. Recommendations	102
References	103
Appendices:	118
Appendix -A: Titanium Dioxide certificate	118
Appendix –B: Water Bath Ultrasonic Device (Elmasonic P180H)	120
Appendix -C: Coating Thickness Gauge.	121
Appendix-D: Thermocouples calibration system.	122
Appendix-E. Solar Meter Calibration:	124
Appendix -F: List of publications	125
الخلاصة	128

LIST OF FIGURES

Chapter One

Figure 1.1: different generations of photovoltaic technology [8]. _____	1
Figure 1.2: (a) DSSC structure diagram; (b) Working principle of DSSC [10]. _____	2
Figure 1.3: Scheme of the modeled DSSCs [11]. _____	2
Figure 1.4: various band locations of semiconducting oxides for photo-anodes [15]. _____	4
Figure 1.5: Classification of dye sensitizer [15]. _____	5
Figure 1.6: various electrolytes utilized in DSSCs [1]. _____	8

Chapter Two

Figure 2.1: Absorption spectra of red, diluted, natural Malabar spinach extract and a mixture [32]. _____	15
Figure 2.2: In an ethanol solvent, the absorption spectra of dried and fresh lemon and parsley dye extracts in normalized form [38]. _____	18

Chapter Three

Figure 3.1: Spectrum wavelength [64]. _____	31
Figure 3.2: Electron transitions between ψ^* and ψ bands due to energy absorption [66]. _____	32
Figure 3.3: Electronic transmissions (a) permitted direct transmission; (b) prohibited direct transmission; (c) permitted indirect transmission; (d) prohibited indirect transmission [67]. _____	35
Figure 3.4: a) Crystal levels and Braque's law; b) X-ray diagnosis [76]. _	39
Figure 3.5: The standard current-voltage (I-V) and power-voltage (P-V) curves of a solar cell [77]. _____	40

Chapter Four

Figure 4.1: Glass substrates FTO type. _____	44
Figure 4.2: Crystalline Forms of Titanium Dioxide, Anatase, Rutile, and Brookite [81]. _____	44
Figure 4.3: Substrate cleaning steps. _____	46
Figure 4.4: Simple test steps to see if HNO ₃ is diluted or concentrated. ____	47
Figure 4.5: Nitric acid pH measurement device. _____	47
Figure 4.6: TiO ₂ paste and its texture. _____	48
Figure 4.7: Extraction steps for (a) Mentha leaves, (b) annual helianthus leaves. _____	49
Figure 4.8: Fragaria fruit tincture extraction steps. _____	50
Figure 4.9: nano silver. _____	50
Figure 4.10: stirring electrolytes in a dark container using a magnetic stirrer. _____	51
Figure 4.11: Counter electrodes preparation with pt. _____	52
Figure 4.12: Counter electrodes preparation with carbon soot. _____	52
Figure 4.13: Prepare FTO glass for casting TiO ₂ _____	53
Figure 4.14: TiO ₂ distribution using the doctor blade method. _____	54
Figure 4.15: Immersion of TiO ₂ -coated glass in dyes _____	54
Figure 4.16: Flowchart to facilitate DSSC fabrication preparation procedure. _____	55
Figure 4.17: The assembly procedure of FTO/TiO ₂ -dye/electrolyte/Pt DSSCs from several viewpoints: (a) side view, (b) front view (c) cross-section view. _____	56
Figure 4.18: solar cell measurement system. _____	57
Figure 4.19: Sensitive Electronic Scale. _____	57
Figure 4.20: Magnetic Stirrer Device. _____	58

Figure 4.21: Ultrasonic Device.	59
Figure 4.22: UV-V is spectrometer.	60
Figure 4.23: FESEM Electron Microscope.	61
Figure 4.24: Furnace device.	62
Figure 4.25: X-Ray device is used to diagnose the crystal structure of membranes.	63
Figure 4.26: Data logger.	64
Figure 4.27: Thermocouples K-types.	65
Figure 4.28: Keithley 2400 device.	66
Figure 4.29: Coating Thickness Gauge.	67
Figure 4. 30: Solar Power Meter.	68

Chapter Five

Figure 5.1: Verification results for I-V with Ref [31].	70
Figure 5.2 :Verification results for P-V with Ref [31].	70
Figure 5.3: X-ray diffraction of TiO ₂ before heat treatment.	73
Figure 5.4: X-ray diffraction of TiO ₂ after heat treatment.	73
Figure 5.5: XRD spectra of pure TiO ₂ and TiO ₂ -dye.	74
Figure 5.6: EDX spectra of TiO ₂ .	75
Figure 5.7: At 500 °C, FESEM pictures of a single TiO ₂ layer at 5µm and 10µm.	76
Figure 5. 8: At 500 °C, FESEM pictures of a two TiO ₂ layer at 5µm and 10µm.	76
Figure 5.9: FESEM image of TiO ₂	77
Figure 5.10: Absorption spectrum of TiO ₂ .	78
Figure 5.11: Transmitter spectra of FTO and TiO ₂ film cast on FTO.	78

Figure 5.12: Relationship of the absorption coefficient and wavelength of TiO ₂ .	79
Figure 5.13: The relationship between the reflection coefficient and the wavelength of the TiO ₂ film.	80
Figure 5.14: The relationship between the refractive index and the wavelength of the TiO ₂ film.	81
Figure 5.15: Relationship of the damping coefficient with the wavelength of the TiO ₂ film.	82
Figure 5.16: Relationship of the true dielectric constant with the wavelength of the TiO ₂ film.	83
Figure 5.17: Relationship of the imaginary dielectric constant with the wavelength of the TiO ₂ film.	83
Figure 5.18: UV-V is absorption spectra of Helianthus annuus in different solvents.	84
Figure 5.19: UV-V is absorption spectra of Mentha leaves in different solvents.	85
Figure 5.20: UV-V is absorption spectra of Fragaria in different solvents.	85
Figure 5.21: UV-V is absorption spectra of Mentha leaves, Helianthus annuus, Fragaria, and a mixture of the three with various peak locations.	88
Figure 5.22: Electrolyte absorption spectrum.	88
Figure 5.23: Electrolyte permeability spectrum.	89
Figure 5.24: DSSC surface temperature with time.	90
Figure 5. 25: I-V curve for DSSCs depends on dyes	92
Figure 5.26: P-V curve for DSSCs depends on dyes.	92
Figure 5.27: I-V of DSSCs with a) carbon soot b) pt.	94
Figure 5.28: P-V of DSSCs with a) carbon soot b) pt.	95
Figure 5.29: I-V diagram of DSSCs for TiO ₂ layers.	96

Figure 5.30: P-V diagram of DSSCs for TiO ₂ layers. _____	96
Figure 5.31: Current density-voltage curves of DSSC at 30 min of continuous light soaking. _____	97
Figure 5.32: Current density-voltage curves of DSSC at 30 min of continuous light soaking. _____	97
Figure 5.33: FF change with temperature. _____	98
Figure 5.34: voltage change with temperature. _____	99
Figure 5.35: current density changes with temperature. _____	99
Figure 5. 36: Efficiency change with temperature. _____	100

LIST OF TABLES

Chapter One

Table 1.1: List of solar cells based on their current efficiency[5]. _____	3
Table 1.2: Advantages and disadvantages of ZnO and TiO ₂ used as photoanodes. _____	4
Table 1.3: Advantages and disadvantages of different types of dye[1]._____	6
Table 1.4: Advantages and disadvantages of each type of electrolyte use in DSSCs [1]._____	9

Chapter Two

Table 2.1: Summary for Substrates._____	22
Table 2.2: Summary for Semiconductors (Photoanodes). _____	22
Table 2.3: Summary for Sensitizers (Dye)_____	24
Table 2.4: Summary for Electrolyte. _____	27

Chapter Four

Table 4.1: Glass substrates Properties._____	43
Table 4.2: General Properties of Titanium Dioxide. _____	45
Table 4.3: specification of Solar Power Meter. _____	68

Chapter Five

Table 5.1: TiO ₂ color at different temperatures and time. _____	71
Table 5.2: Absorption peaks and band gap energies of the isolated dyes. _	86
Table 5.3: Performance of DSSCs based on dyes. _____	93
Table 5.4: Comparison of experimental results of single-and two-layered DSSCs for TiO ₂ _____	96

NOMENCLATURE

Symbol	Definition	Unit
A	Absorbance	Absorbance unit (A.U)
d	Membrane thickness	m
E	Photon energy	Electron volt (eV)
E^{\wedge}	Amplitude of the electric field	V/m
E_g	Energy gap	eV
E_g^{\wedge}	Indirect energy gap	eV
E_i	Elementary electron energy	eV
FF	Fil factor	%
h	Planck's constant	6.63×10^{-34} J. s
I_{mp}	Maximum power current	mA
I_{ph}	Photocurrent	Ampere (A)
I_s	Diode saturation Current	Ampere (A)
I_{sc}	Short circuit current	mA
K	Wave vector	Nanometers (nm)
K^*	Represent the wave vector in space	-
K_f^{\wedge}	Final vector of the electron	-
K_i^{\wedge}	Primary vector of the electron	-
K_p	Wave vector of photon	Nanometers (nm)
N	Complex refractive index	-
n_B	Integer called the order of reflection	-
q^{\wedge}	Absorbed photon	Sievert (Sv)
V_{mp}	Maximum power voltage	Volt (V)
V_{oc}	Open circuit voltage	Volt (V)
W	Wave of frequency	rev/s
Subscripts		
ACN	Acetonitrile	-
AFM	Atomic force microscopy	-
CBD	Chemical bath deposition	-
CE	Counter electrode	-
DMII	Dimethyl 1-imidazoliumiodide	-
DSSCs	Dye-sensitized solar cells	-
FTO	Fluorine tin oxide	-
GuSCN	Guanidine thiocyanate	-
HUMO	Highest vacant moving orbital	-
ITO	Indium tin oxide	-
LUMO	Lowest vacant moving orbital	-

MOS	Metal oxide semiconductor	-
N-dc	Nitrogen-doped Carbon	-
PAN	Polyacrylonitrile	-
PEO	polyethylene oxide	-
PEs	Printable electrolytes	-
PIN	Polyindole	-
PV	Photovoltaic	-
TCO	Transparent conductive oxide	-
TiO ₂	Titanium Dioxide	-
UV-Vis	Ultraviolet-Visible Spectrometer	-
Chemical Symbols		
Ag	Silver	-
I ₂	Iodine	-
KI	Potassium Iodide	-
LiI	Lithium Iodide	-
MPN	3-Methoxy propionitrile	-
Nb ₂ O ₅	Niobium Oxide	-
OH	Hydroxide	-
PEO	Polyethylene Oxide	-
Pt	Platinum	-
PVDF	Polyvinylidene Fluoride	-
SnSe	Selenide Alqasdir	-
SrTiO ₃	Strontium Titanate Oxide	-
SnO ₂	Tin Oxide	-
TiO ₂	Titanium Dioxide	-
ZnO	Zinc Oxide	-
Zn ₂ SnO ₄	Zinc Stannate	-
Greek Symbols		
Ω	Ohm	-
r	Exponential coefficient	-
α	Absorption coefficient	cm ⁻¹
η	Efficiency	%
λ	Wavelength	Nanometers (nm)
ν	Frequency	Hertz (HZ)
ε	Molar absorptivity	L/(mol.cm)

CHAPTER ONE

INTRODUCTION

1.1 General Introduction

Electricity generation is one of the most amazing inventions that has changed human life. Electricity has many uses in our lives, such as domestic use, industrial and commercial sectors, transportation, communications, medical sectors, technology centers, etc. Therefore, it is not possible to imagine life without electricity. Electricity consumption varies from person to person and is increasing daily in all parts of the world, so more electricity must be produced to meet the requirements.

Coal is used to generate more than 80% of the electricity generated [1]. Coal mining has harmful effects on the environment and the atmosphere for several reasons, including the release of many gases such as sulfur dioxide, mercury, etc., which cause air pollution, and the excavation of the earth, which is the cause of population displacement [2]. Therefore, it is very important to promote the production of alternative energy resources such as solar energy, geothermal energy, wind energy, and tidal energy in order to preserve the environment and generate electricity.

1.2 Photovoltaic Technology

Photovoltaic (PV) technology is represented as one of the most promising developments because it can transform sunshine energy into electrical energy. Among the various PV technologies, the market is increasingly interested in dye-sensitized solar cells (DSSCs [1]. However, the following characteristics of DSSC make it particularly appealing:

- (i) Simple fabrication, low cost. Using existing materials in manufacturing without spending amount of money
- (ii) Creating a wide range of forms, sizes, colors, and transparencies.

These features make DSSCs attractive to technology in various areas of life, as they are widely used in architectural applications and systems[3][4].

1.3 Progress in PV technologies

PV cells evolved from the first crystalline silicon cell to today's solar cells in terms of cost and architecture. Cells of each generation show different efficiencies, as shown in Table (1-1), with three distinct generations depicted in Figure (1.1). [5].

- (i) First-generation solar cells are divided into two types: crystalline solar cells and silicon cells. Silicon cells are one of the most significant discoveries in the field of energy. Silicon cells dominate the PV energy market. However, the cells of this generation have a high manufacturing cost due to the high consumption of resources and the complexity of the manufacturing process[6].
- (ii) Second-generation solar cells have thin films, unlike the cells of the first generation, which have a lower manufacturing cost, fewer materials, and a larger deposit area. The materials used have a high energy gap and a high photovoltaic effect. The cells of the second generation have better absorption. Its optics are much better. Poor charge transfer is a major obstacle for the second-generation cells, which prevents the marketing of PV, and leads to the emergence of third-generation cells [7].

(iii) Third-generation solar cells: Researchers began to work on a new generation of solar cells known as the “third generation” or “emerging PV cells” to avoid the harm of the first and second-generation cells. The cells of this generation offer many advantages, such as their low-cost materials and the fact that their manufacturing processes are simple and abundant [7].

Table 1. 1: List of solar cells based on their current efficiency[5].

Type of Generation	Type of solar cell	η
1 st generation	Single Crystalline Solar cell	26.1%
	Multi crystalline Solar cell	23.3%
	Single Junction Gallium Arsenide Solar Cell	27.8%
2 nd generation	Amorphous Silicon Solar Cell	14%
	Cadmium Telluride	22.1%
	Copper Indium Gallium Diselenide	23.4%
3 rd generation	Quantum Dot Solar Cell	16.6%
	Perovskite Solar Cell	25.2%
	Organic Solar Cell	17.4%
	Dye Sensitized Solar Cell	14.3%

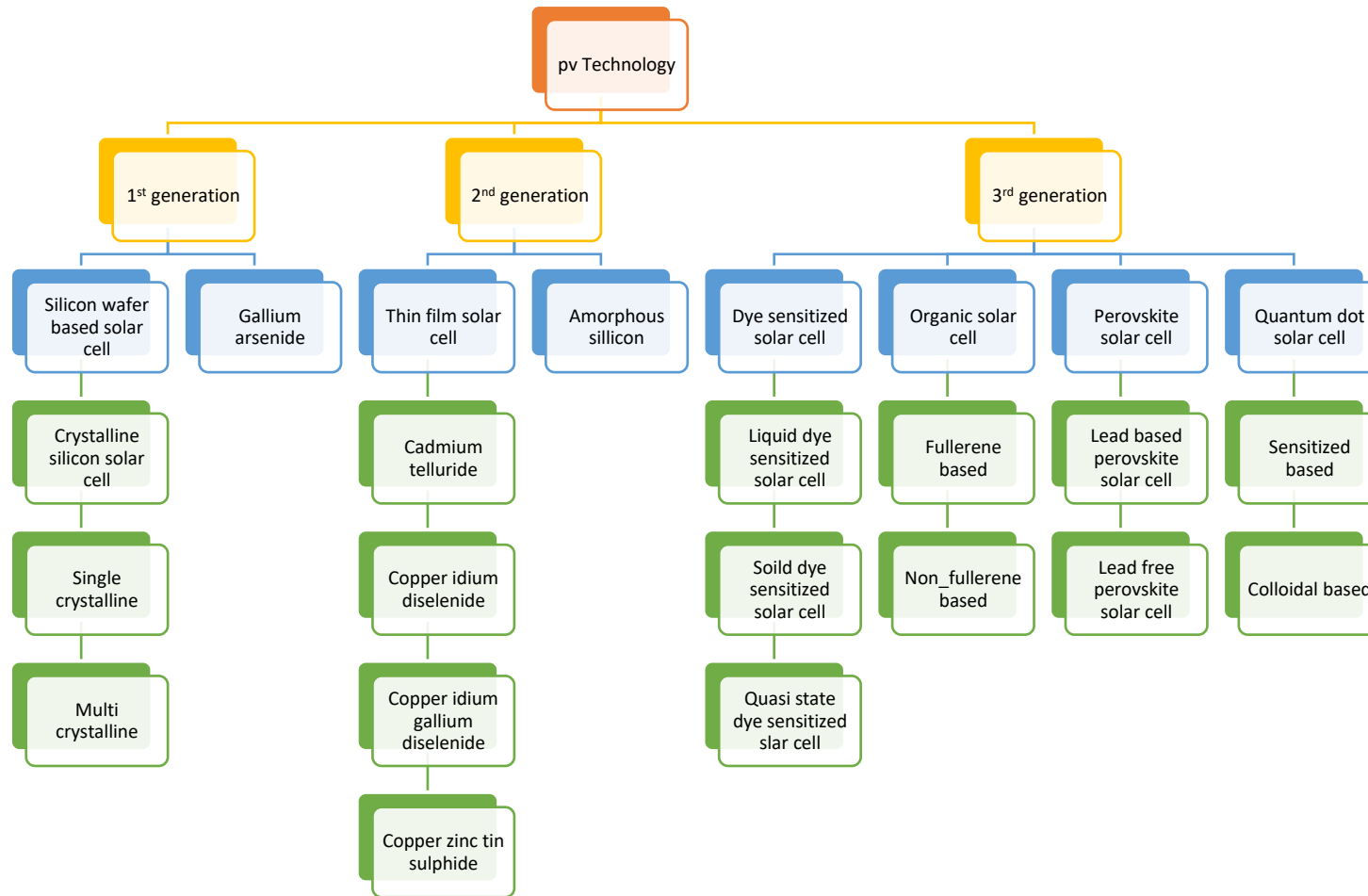


Figure 1. 1: different generations of photovoltaic technology [8]

1.4 Background of DSSCs

Dye sensitized solar cells are PVs that convert optical energy (artificial radiation or sunlight) into electrical energy by sensitizing wide bandgap semiconductors with a photosensitive dye. The first DSSCs were introduced by O'Regan and Gratzel in 1991[9]. They are a promising alternative to conventional solar cells. DSSCs are transparent, easy to manufacture, and cheaper, as the materials used to manufacture them are relatively cheap, and they are also environmentally friendly.

1.5 Principle and working of DSSCs

Basically, there are four basic steps that summarize the principle of work of DSSCs: Photon absorption, electron injection, electron transfer, and electric current generation. Figure (1.2) shows a schematic diagram of the structure and working principle of DSSCs.

Photons are defined as particles of light absorbed by transparent conductive oxide (TCO) from condensed dye molecules on the surface of the semiconductor. The electrons of the dye become excited, and then the electrons in the dye gain enough energy to break the atomic bonds and move from the valence band to the semiconductor layer, as the process of injecting the electron into the conduction band of the semiconductor occurs at a very high speed of picoseconds, a record time. Then the electrons will flow from the semiconductor films towards the negative electrode (the front photoelectrode), where they will travel through the external circuit until they reach the back electrode. Then, the electrolyte in contact with the semiconductor membranes, penetrating inside and in contact with the dye, gives it its electrons (oxidizes) and restores the dye, activating the oxidizing electrolyte by obtaining electrons from the counter electrode.

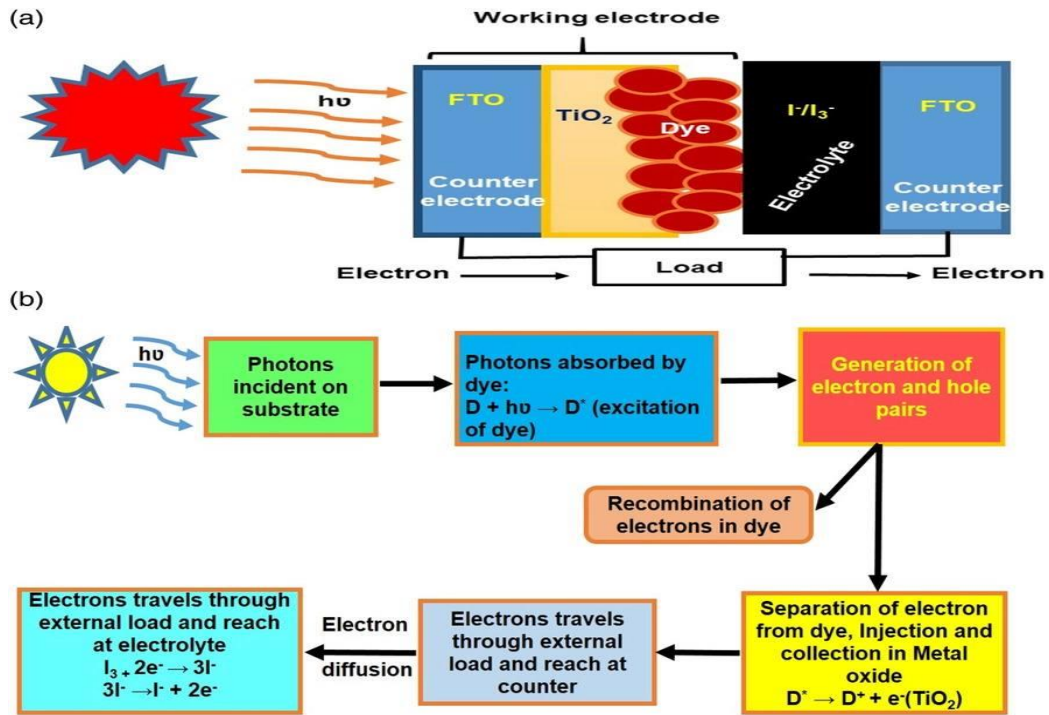


Figure 1. 2: (a) DSSC structure diagram; (b) Working principle of DSSC [10].

1.6 Development of constructional parameters of DSSC

The choice of parameters shown in Figure (1.3) is the most important aspect in building a DSSC in order to improve system performance [11].

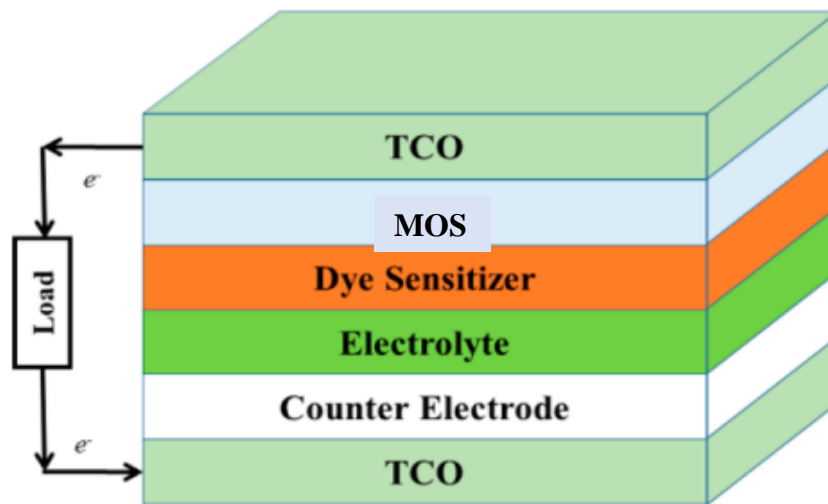


Figure 1. 3: Scheme of the modeled DSSCs [11].

1.6.1 substrate

DSSCs are typically made from two substrates with high transparency and conductivity. It was noted that the transparency should be greater than 80% to obtain the best light absorption and the best results [12]. The substrates must be highly conductive in order to minimize energy losses and obtain maximum charge transfer [12].

The substrates play an effective and essential role in achieving the overall efficiency of DSSCs. Substrates are defined as thin coating layers that act as collector currents and provide support for semiconductors in DSSCs. To reduce energy loss and facilitate electron transfer, the substrates must have low resistance [13].

According to the two most important properties (transparency and conductivity), there are different types of materials that are used as substrates in DSSCs. Glass is typically used as TCO substrate, i.e., indium tin oxide (ITO) and fluorine tin oxide (FTO).

1.6.2 Metal oxide semiconductor (MOS)

Semiconductors play a fundamental and important role in forming a strong bond with dye molecules and receiving photoelectrons from the sensitizers (dyes). The semiconductors used in DSSCs must have large surface area to improve dye absorption of light, high porosity and high bandgap for high electron mobility. It must match the properties of the sensitizer (dye) because the crystalline nanoparticles of the porous film must receive electrons from the sensitizer to generate electricity as their manufacture should be simple, stable, affordable and eco-friendly. There are various types of semiconductors, including titanium dioxide (TiO₂), zinc oxide (ZnO), tin

oxide (SnO_2), and Zinc stannate (Zn_2SnO_4), each of which has been extensively tested as a photoanode in DSSC applications. Yang et al. showed the different positions of the semiconductor oxide strands in the photoelectrode in Figure (1.4). Among these materials, TiO_2 and ZnO are the preferred materials in the application of DSSCs because of their properties [14][15]. However, there are advantages and disadvantages to each of them, which are shown in the table (1-2) [15].

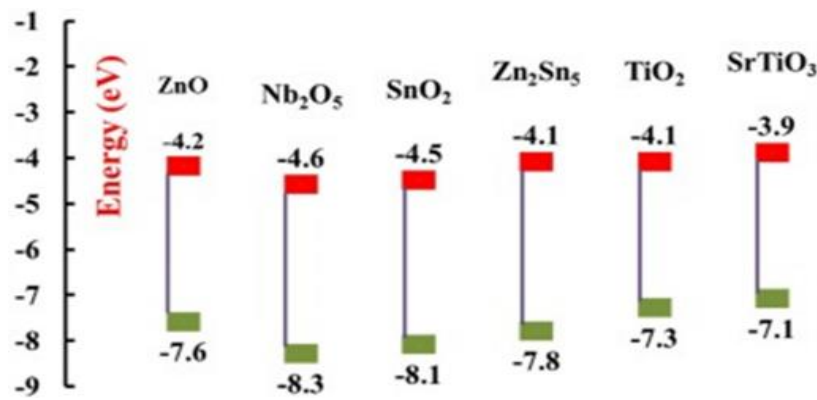


Figure 1. 4: various band locations of semiconducting oxides for photoanodes [15].

Table 1. 2: Advantages and disadvantages of ZnO and TiO_2 used as photoanodes.

Metal oxides	Advantages	Disadvantages	Ref.
ZnO	<ul style="list-style-type: none"> ZnO nanostructure heterogeneity Electron mobility is high. 	<ul style="list-style-type: none"> Dye-complexation of ZnO Performance depends on the dye. 	[16]
TiO_2	<ul style="list-style-type: none"> commercially available in large quantities, inexpensive, biocompatible, and non-toxic. Stable n-type semiconductor Fast electron injection rate Better photostability 	<ul style="list-style-type: none"> Electron mobility is restricted. High can recombine with others materials 	[17]

1.6.3 Dye photo-sensitizer

In general, dyes in DSSCs perform two basic functions: light absorption and electron transfer to semiconductors, so they have a fundamental and important role in the performance of DSSCs and the conversion of light energy into electrical energy. Pigments should have high absorption in the entire visible area and in the infrared region to get the most light [18][19]. Figure (1.5) shows the different forms of dye photo_sensitizer used in DSSCs [15]. The dye photo_sensitizer can be classified into metallic complexes. Photosensitizer, natural photosensitizer, organic photosensitizer. Each of these allergens has many advantages and disadvantages that are discussed in the Table (1-3) [15].

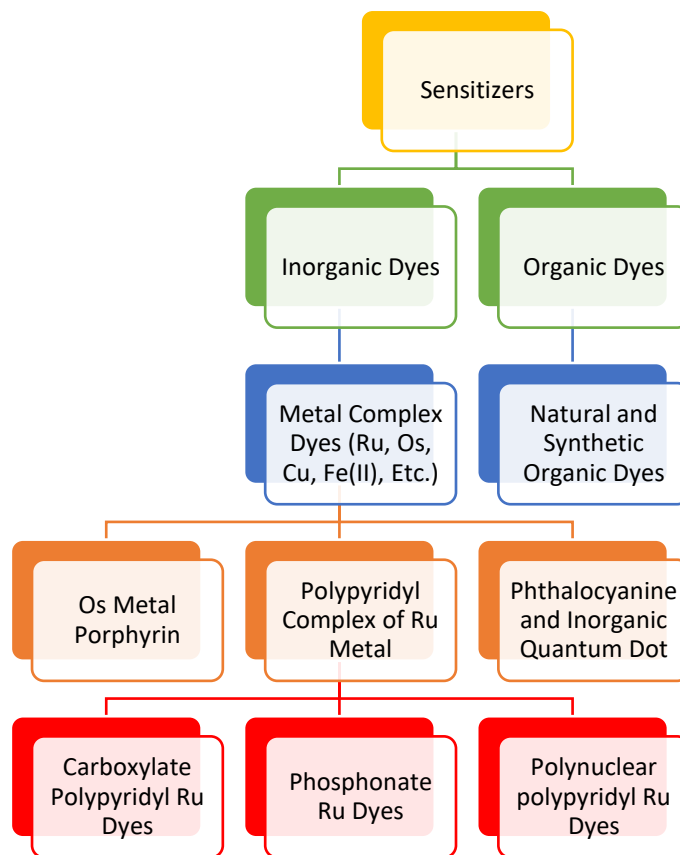


Figure 1. 5: Classification of dye sensitizer [15].

Table 1. 3: Advantages and disadvantages of different types of dye[1].

Types of Dye	Advantages	Disadvantages
Metal based	<ul style="list-style-type: none"> • Highly efficient DSSCs have been created with the use of noble metal-based sensitizers. • With MOS molecules, especially TiO₂, rapid electron injection and great anchoring capability are possible. • The photochemical, photophysical, and electrochemical characteristics of ruthenium dye are excellent. • it exhibits stable and useful oxidation states. • long excited lifetime. • Well soluble in all solvents. • high redox properties. • Absorption spectra ranging from visible to near-infrared. 	<ul style="list-style-type: none"> • harmful for nature. • Because of its scarcity, its prices are high. • Their use is limited due to their complex composition and purification. • The water molecules present in it trample the electrolyte allowing the dye to be absorbed by the MOS.
Metal Free	<ul style="list-style-type: none"> • Cost-effective DSSCs have been made with the use of metal-free organic sensitizers. • The organic dye is the preparation process is low-cost, simple, and non-toxic. because they do not contain noble metals like gold, Ru, Ir, etc. • high molar extinction coefficients. • stability when exposed to high temperatures and lengthy periods. • comparable η with metal complex dyes. • highly capable of harvesting a certain amount of light. 	<ul style="list-style-type: none"> • Due to the possibility for light absorption reductions, low absorption bands are seen in contrast to metal dye. • Because the qualities of the sensitizer degrade with time, there is a lack of stability. • It comprises substances that are both costly and difficult to get. • Purifying it is a lengthy process and needs to be repeated,

		causing a long preparation time.
		• poisonous in nature and have a negative impact on the environment.
		• Under high temperatures, the observed stability was not as robust as predicted.
		• η reported very poor results. Because the pigment deteriorates over time, it is unstable.
	• good photoreceptors.	
	• no use of noble metals.	
	• eco-friendly DSSCs can be fabricated.	
	• widely available and inexpensive.	
Natural	• completely biodegradable and easy to prepare.	
	• The quantity and wavelength of light absorbed may be changed using functional groups such as hydroxyl groups, carboxylic acid, and sulfonic acid.	

1.6.4 Electrolyte

Electrolytes are responsible for two main functions: (i) regeneration of the dye and (ii) transferring electrons from counter electrode (CE) to the dye through oxidation and reduction reactions. Electrolytes are classified according to their physical state into three main types: liquid, semi-solid, and solid. Figure (1.6) shows the many electrolytes that have been created for DSSCs, and their advantages and disadvantages are displayed in Table (1-4). In general, electrolytes should have excellent ionic conductivity, be non-corrosive and be transparent to visible light [20].

The lifespan of DSSCs depends on the nature of the electrolytes. In order for DSSCs to function well, the oxidation and reduction must have the following characteristics:

1. To keep dye absorption from deteriorating, there should be very little light absorption in the visible spectrum.
2. It must be chemically inert and will not react with the photoanode or dyes.
3. To ensure efficient transportation of electrons, the electrolyte solvent should have a high diffusion coefficient.
4. Non-toxic and readily available materials should be used.
5. To ensure that the electrolyte has a high concentration of charge carriers, it should be dissolvable to ensure that the redox pair essential for dye renewal is readily available[1].

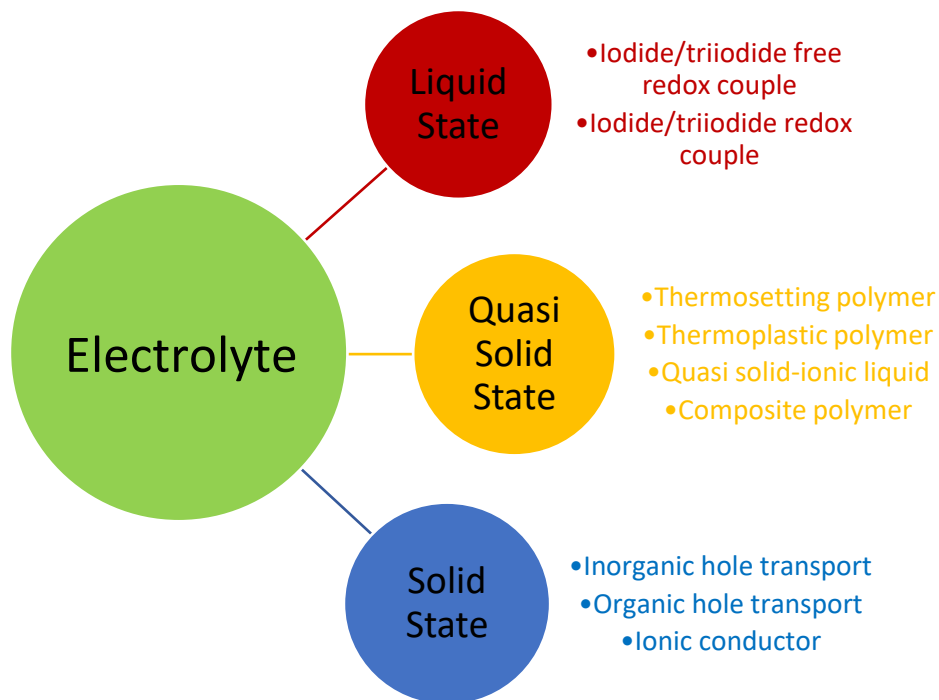


Figure 1. 6: various electrolytes utilized in DSSCs [1].

Table 1. 4: Advantages and disadvantages of each type of electrolyte use in DSSCs [1].

State	Advantages	Disadvantages
Liquid	<ul style="list-style-type: none"> • Easy of preparation • Low viscosity • High η • High conductivity 	<ul style="list-style-type: none"> • Because of the leakage from the cell, which reduces the performance. • Oxidation and reduction processes cause corrosion.
Quasi	<ul style="list-style-type: none"> • Excellent conductivity of ions • Good mechanical and chemical stability • Good bonding characteristics with MOS • High viscosity, compatible deposition methods • Low solvent volatility and low cost. 	<ul style="list-style-type: none"> • Leakage problem • Less stable • Low η as compared to liquid based DSSCs
Solid	<ul style="list-style-type: none"> • Not leak from the outer periphery of the cell 	<ul style="list-style-type: none"> • Low η as compared to liquid based DSSCs • cannot form proper bonds with MOS pores

1.6.5 Counter electrode (CE)

The counter electrode is the last part of the DSSC that aims to regenerate the dye by oxidation and reduction of electrolytes, which greatly and effectively affects the efficiency of the cell. The basic requirements for this CE are:

- High catalytic activity
- Low charge transfer resistance
- Chemically inert
- Reduce oxidized electrolyte by increasing exchange current density [21].

On top of the glass, the counter electrodes consist of TCO with platinum, silver, or carbon-coated materials to provide a reversible passage of electrons from an external circuit to the electrolyte through load [22].

1.7 Aims of Present Work

The purpose of this study is to manufacture DSSCs with the best possible efficiency. To achieve the specific objectives of the study, many of the following specific tasks must be performed:

- Fabrication of natural dye-sensitized solar cells and practical testing.
- Using cheap, not-toxic, natural dyes.
- Study the effect of temperature on performance of a dye-sensitized solar cell.
- Study the effects of different types of natural dyes on the performance of melanocytes.
- Studying the effect of the thickness of the main layer(bandgap) on dye-sensitized solar cell performance.

CHAPTER TWO

LITERATURE REVIEW

2.1 INTRODUCTION

Individual investigations into each component of the DSSCs play an important and instrumental role in its overall performance, so individual investigations into each component are critical. In this chapter, it will address several previous studies on DSSCs for all their parts, and recent developments in both substrates and their components, including the conductive transparent oxidation layer, sensitizer (dye), electrolyte, and counter electrode (CE), which are interested in improving the efficiency of solar cells.

2.2 Substrates for DSSCs

2.2.1 type of substrates for DSSCs

Cornelia Sima et al. (2010)[23] made a comparison of the two most common types of TCO (FTO and ITO) and obtained an efficiency of 9.6% for DSSCs manufactured using FTO substrates, while the efficiency they obtained using ITO substrates was only 2.24%. They mentioned that the reason for this is that the value of ITO substrates increases to 52 Ω /sq (after it was 18 Ω /sq) after exposure to 450 °C temperature for curing purposes, while the resistance of FTO substrates does not change (remaining at 8.5 Ω /sq), so the researchers recommended the use of FTO substrates to stabilize its resistance when exposed to heat and because it is less expensive.

Jasper Ejoywokoghene Ikpesu et al. (2020)[19] Reported that ITO and FTO are among the most transparent types of TCO, as their transparency is throughout the ultraviolet-visible spectrum, making them well suited for

DSSC fabrication. They also reported that ITO and FTO share a typical resistance of (10–20) Ω , but the resistance of ITO increases significantly with temperature, while this was not observed in FTO.

N. Ruba et al. (2021) [24] Mentioned that ITO is one of the unstable substrates of the resistance, as it increases during heat treatment, although it absorbs a good amount of visible light radiation. As for the FTO substrates, their stability resistance is better than that of ITO when treated with heat. Thus, FTO is one of the most promising substrates for the manufacture of DSSCs.

Mohamed Yahya et al. (2021) [25] Said that FTO substrates are more suitable to be used in the manufacture of DSSC due to their high stability (even at a temperature of 550 °C) and low cost, but ITO has higher optical transparency and conductivity compared to FTO.

2.2.2 Influence of substrate cleaning on DSSC performance

Katrin Gossen and Andrea Ehrmann (2019) [26] Through their study, they confirmed the effect of the solvent used to clean the substrates of DSSCs on their efficiency and lifespan. They cleaned the FTO with acetone once, water once, and isopropane (ethanol) again. They made DSSC based on anthocyanin dye with TiO_2 . Through the results they obtained, they concluded that the best efficiency was for DSSC in the case in which FTO was washed over ethanol because it caused a decrease in its resistance. While acetone caused an increase in the resistance of FTO, which caused the lowest efficiency.

2.3 Semiconductors

Aneel Pervez et al. (2018)[27] Compared the performance of DSSC in the presence of TiO₂ times and ZnO again, and made this comparison with five different dyes for each nanomaterial. The results they obtained confirmed that ZnO had lower photoelectric performance than TiO₂, as the best efficiency they obtained for DSSC was using Solanum Melongena dye (eggplant), as it was equalized using TiO₂ 1.10%, while it was with ZnO 0.67% better solidification of dye molecules with TiO₂.

D. Sinha et al. (2019)[28] Investigated the performance of TiO₂ and ZnO -based DSSCs utilizing a chlorophyll-based dye since it is stable on metal oxides (TiO₂ and ZnO). Under the same conditions, the two cells' performances were compared. The findings revealed that DSSCs based on TiO₂ had the best efficiency of 0.27%, while the efficiency of the other cell was 0.13%.

Mozhgan Hosseinnezhad et al. (2020)[29] Reported that the type of nanomaterial used in the manufacture of DSSCs has an effective and very significant effect on the photoconversion efficiency of the cell and its performance. For this reason, they made a comparison between the performance of the cell using TiO₂ and ZnO, and based on 6 different dyes, the best efficiency they obtained for the same dye was 12.5% for the cell based on TiO₂ while they obtained an efficiency of 7.5% for that based on ZnO, they also proved the preference of the cell based on TiO₂ over other dyes.

P. Dhamodharan et al. (2021)[30] Tested the ZnO-based DSSC, which was deposited on ITO substrates, and its performance was verified. By measuring it by atomic force microscopy (AFM), they noticed that its porous

nature has a small roughness, which is the main factor that made it achieve an efficiency of 1.09%.

Urenyang I. Ndeze et al. (2021) [31] prepared the photoanode by depositing a layer of TiO_2 on a FTO glass. They prepared a semiconductor paste by dissolving 3.5 g of nanoscale TiO_2 in 10 ml of ethanol. The best efficiency they obtained was 0.25% with a tincture extracted from shea leaves. They depicted the adsorption behavior of plasticized TiO_2 at 450°C , noting that the absorption peak was at 316 nm. They noticed that TiO_2 film absorbs ultraviolet rays in small amounts, while the transmission of visible light is 74.34%, and thus it can effectively transmit light to the dye and convert it into electrical energy in DSSC.

2.4 Sensitizers (Dye)

2.4.1 Types of sensitizers (dye)

F. Kabir et al. (2019) [32] Made DSSC based on natural red pigments extracted from anthocyanin-rich red spinach, and others based on green pigments extracted from chlorophyll-rich Malabar spinach. They also mixed 80% red spinach extract and 20% green spinach extract to form a third cell. Using a UV device, they observed that each dye had a different absorption atom than the other dye, as shown in Figure (2.1). The efficiency of DSSC based on spinach extract was red 0.531 and the efficiency of DSSC based on malabar spinach was 0.466, while the efficiency of DSSC based on the mixture of the two dyes was 0.847, which is the highest.

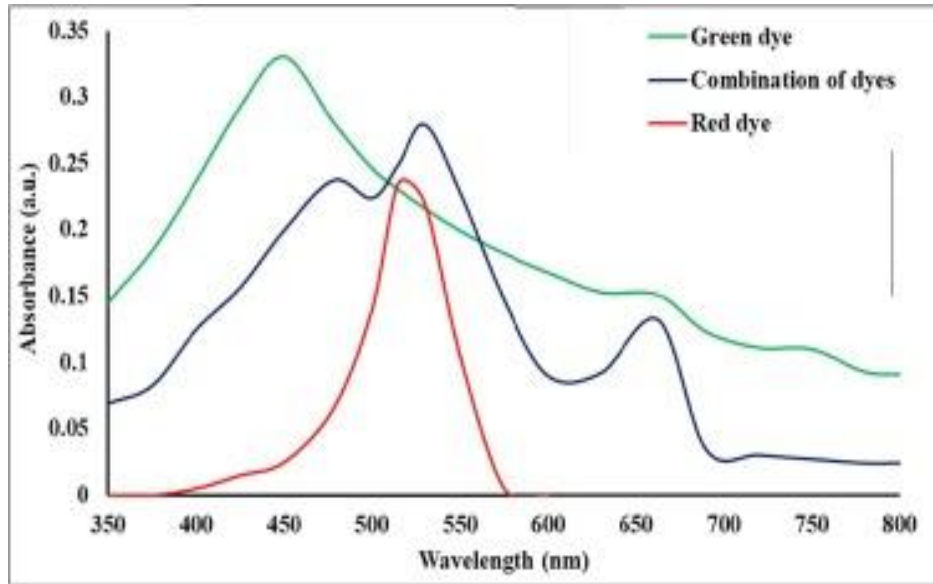


Figure 2. 1: Absorption spectra of red, diluted, natural Malabar spinach extract and a mixture [32].

F. Kabir et al. (2019) [33] Concentrated their efforts on extracting a red pigment from red spinach and a yellow pigment from turmeric, both of which have the potential to absorb and transform sunlight into electrical energy. They created three DSSCs using pigments taken from red spinach and turmeric, as well as one with a blend of the two pigments (60 percent turmeric extract and 40% extract), and found via Fourier transform infrared radiation (FTIR) that the natural pigments do not interact with one another, but rather coexist side by side. The greatest efficiency for DSSC based on a blend of the two colors was 1.079, whereas DSSC based on turmeric and red spinach yielded 0.378 and 0.134, respectively.

Tahmineh Jalali et al. (2020) [34] extracted four dyes from *Crocus sativus* (Saffron), *Malva sylvestris* (Mallow), *Oregano* (*Origanum vulgare*), and *Allium cepa* L (red onion) plants using a suitable solvent. The reason they use these dyes is that, they contain chlorophyll and anthocyanins, which are

excellent pigments for generating charge carriers in the process of collecting solar energy. They also contain hydroxyl and carbonyl groups (OH, C-H, N-H, and C = O) in their chemical structures, thus enabling them to bond with the ITO layer and thus enhance the efficiency of energy conversion because this causes an improvement in the transfer of electrons. The energy gap and energy level of LUMO enable them to be good and effective catalysts for use in DSSCs. Using a UV device, they discovered that the extracted dyes from Mallow had two distinct peaks, one at 470nm and the other at 665nm, due to the chlorophyll mixture in them. Peaks of oregano extract were observed at 420 nm and 320 nm due to the mixture of chlorophyll types A and B and their derivatives. While the red onion extract showed a broad peak from 310nm to 370nm, which is due to the anthocyanin mixture, the saffron extract showed two peaks consistent with the anthocyanins, which are about 325nm and 470nm. So, the best DSSC efficiency they got was 1.9% when they used the dye from oregano.

Malihe Golshan et al. (2021) [35] Made three cells based on three different dyes. The first cell was DSSC based on Malva verticillate dye, the second cell was based on Syzygium cumini dye, and the third cell was based on a dye represented by mixing the two previous dyes. By using a UV device, you can determine the spectral response of individual dyes and mixtures. The pigment extracted from Malva verticillate showed two absorption peaks, the first in the area of (400–450) nm and the other at 666 nm, which indicates the presence of chlorophyll pigment in this plant. As for the anthocyanins in the dye extracted from Syzygium cumini, the peak of its intense absorption was at 540nm. While the dye in the mixture showed the strongest absorption at a wavelength of 543nm, the highest result they found was 1.84% of the DSSC

dye-based mixture. They reported that the reasons for this were light-harvesting, good visual activities, and an appropriate energy level between LUMO and HOMO.

B. Arjun Kumar et al. (2021)[36] Extracted betalain and chlorophyll pigments from beet leaves and *Tridax procumbens* and used them as catalysts in the manufacture of two DSSC cells, one based on chlorophyll pigment extracted from beet leaves and the other based on a mixture of chlorophyll and Betalain in a 1:1 ratio. Compared with chlorophyll dye, they confirmed it using UV-vis. They also found that the efficiency of DSSC based on chlorophyll dye was 0.02%, while DSSC based on betalain dye showed 0.11%. They stated that the reason for this was the cross-sensitization to chlorophyll in betalain dye, which caused more electron transfer to TiO_2 .

2.4.2 The condition of the plants before the extraction of the dye

Sofyan A. Taya et al. (2013) [37] Made a comparison between the effects of dry and fresh natural dyes on the performance of DSSCs. They used five types of leaves from plants (parsley, spinach oleracea, green algae, watercress, and cemetery Anethum) and soaked them in ethanol before drying them once and again after drying. They observed that some dyes (parsley and green algae) caused better performance of DSSCs after drying, while others (spinach oleracea, watercress, and Anethum graveolens) performed better before drying. The best efficacy they obtained was 0.29% for antioxidants (DSSC) based on spinach extract after drying.

Sakshi et al. (2020) [38] They made a DSSC comparison based on natural dyes extracted from dried and fresh lemons. It showed maximum

absorption in dried lemon dye at 666nm, 542nm, and 607nm, while fresh absorption peaks were at 669nm, 505nm, and 602nm. Thus, dry lemon extract is better than fresh lemon extract because dry dye covers a wider wavelength. As illustrated in Figure (2.2). Likewise, parsley and spinach mentioned that their dry extracts were better than fresh.

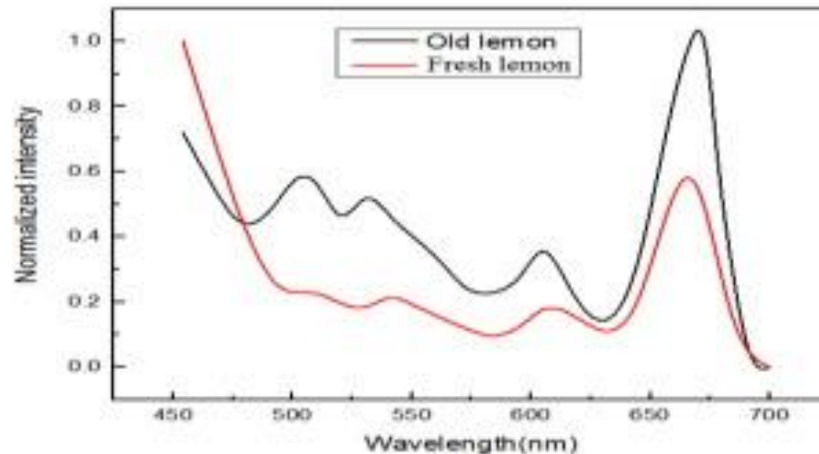


Figure 2. 2: In an ethanol solvent, the absorption spectra of dried and fresh lemon and parsley dye extracts in normalized form [38].

2.4.3 The solvent used to extract the dye

S. Sowmya et al. (2021) [39] Extracted the dyes using fresh and dried leaves of the henna plant. Using three different types of solvents (distilled water, acetone, and ethanol), these dyes were used as catalysts in the manufacture of DSSC, and from the results obtained using UV light, they observed that the dyes prepared using distilled water did not show an absorption peak in a visible area, making them insensitive for use in DSSC. While the other four dyes could be used as photosensitive materials because they showed clear peaks in the visible region. The results also showed that the efficiency of DSSC based on dyes extracted with acetone is the highest.

N. A. Norhisamudin et al. (2021) [40] Conducted a practical study to study the effects of the type of alcoholic solvent used to extract the natural dyes based on DSSCs, where they extracted dyes from green tea leaves and roselle by dissolving them with ethanol once, with methanol, and another time with a mixture of methanol and ethanol, where the efficiency result was equal to 0.00142% and 0.0000111% for Roselle and green tea, respectively. While they obtained an efficiency of 0.0000752% for DSSC based on green tea extracted using methanol and 0.00116% for Roselle extract, they were 0.0000959% and 0.0000257% for DSSC, based on Roselle extract and green tea using ethanol as a solvent.

M.Z. Najihah and Tan Winie (2021) [41] Confirmed that acetone is one of the best solvents used to extract natural dyes that are used as sensitizers in DSSC by extracting a dye from costus leaves, which they dissolved in three different solvents (acetone, ethanol, and methanol). The highest efficiency was obtained by using acetone extract 0.48%, while the efficiency of DSSC sensed with methanol and ethanol extracts was 0.23% and 0.37%, respectively.

S. Sowmya et al. (2021) [42] Manufactured a DSSC based on dyes extracted from the leaves of *Prosopis juliflora* (dry and fresh) and using different solvents (acetone once and ethanol again). The highest light conversion efficiency was obtained by using dried leaves that were dissolved in acetone, which equaled 0.322%, while DSSC based on fresh leaf extract and ethanol showed an efficiency of 0.017% and 0.225% with ethanol and acetone, respectively, while DSSC based on dry leaf extract and ethanol was 0.058%.

2.5 Studies about electrolyte

Shanmuganathan Venkatesan et al. (2019) [43] Used printable electrolytes (PEs) to get rid of the problem of precipitation of liquid electrolytes and evaporation of organic solvents. They prepared it by adding iodine (0.01 M), DMII (0.8 M), t-BP (0.5 M), and guanidine thio-cyanate (GuSCN (0.1 M)) in an MPN organic solvent. They prepared PEs by adding 9% (from the amount of liquid electrolyte) of a kind of polymer such as PEO/PVDF 9/1. With the prepared liquid, they added 4% of (TiO₂) NFs, then it was heated at 120°C to get rid of the additives in the liquid. They demonstrated by using this type of electrolyte in the fabrication of DSSC that the formation of the polymers has little effect on the efficiency of DSSC.

Rahul et al. (2020) [44] Used several different dyes, including spinach with quasi-solid electrolytes, where the electrolytes were prepared using polyethylene oxide (PEO) + KI + I₂. They obtained an efficiency of 0.002%. From the efficiency obtained, it can be concluded that the semi-solid electrolyte causes poor efficiency.

Phitchaphorn Khammee et al. (2021) [45] The electrolytes they injected into the DSSC consisted of 0.0075M of I₂, 0.6M of KI, 20 mL of acetonitrile, and 5 mL of ethylene glycone. The DSSC into which they injected this electrolyte was based on TiO₂ and Inthanin bok leaf extract. The best photoconversion efficiency they obtained was approximately 1.138%.

Soner Çakar et al. (2021) [46] Used a quasi-solid electrolyte as the first liquid electrolyte was prepared by adding 0.5 M 4-tert-butyl pyridine, 0.1 M Guanidine thiocyanate (GuSCN), 0.5 M 1-Methyl-3-propylimidazolium iodide (MPII), 0.1 M LiI, and 0.05 M I₂ in acetonitrile (ACN) Then 0.2 g of

synthesized polyacrylonitrile/polyindole (PAN/PIN) was added to the liquid electrolyte to convert it to a quasi-solid. They achieved an efficiency of 8.49 %. They concluded from their work that semi-solid electrolyte systems are a solution to evaporation and leakage problems, but their efficiency is lower compared to liquid electrolytes.

2.6 Studies about counter electrode (CE)

Mira Tol Zubaida Butt et al. (2018) [47] Reported through their study of DSSC that nitrogen-immersed biomass-derived carbonic aerogel (N_dC) is an effective alternative to conventional pt-based CE for DSSC because pt, due to its high cost, affects the cost of DSSC, unlike N_dC, which is characterized by low cost. They made CE cells based on Pt again and again on N_dC. They note that N_dC has good adhesion with FTO, and that DSSC based on it produced an efficiency of 4.68% after annealing at 450 °C, which is close to that of pt-based (which is equivalent to 0.85%), and the reason for this is that the high temperature annealing process leads to reducing the resistance by removing the buffer groups from N_dC.

D. Kishore Kumar et al. (2019) [48] Used selenide Alqasdir films (SnSe) as counter electrodes in DSSC to compare with others in which pt was used as a counter electrode. The actual cell area was 0.25%. By measuring the voltmeter, they revealed that the photoconversion performance of DSSC, in which SnSe was used as an antipolar electrode, is much lower than that based on pt if the efficiency of the first equals 5.76%, while the efficiency of the second equals 28.8%. They mentioned that the reason for this is the poor transfer of electrons between the CE and electrolytes.

Glennise Faye C. Mejica et al. (2021) [49] Performed a comparison of the performance of DSSC under different materials for CE. They used pt, which is expensive due to its scarcity of resources, and graphene, which is relatively inexpensive. With platinum, they achieved an efficiency of 0.0385%, but with graphene, they achieved an efficiency of 0.00067%. They came to the conclusion that graphene holds a lot of promise as an alternative to pt.

2.7 Summary for Substrates

Table 2. 1: Summary for Substrates.

Author	Type	Resistance	Cleaning method	Result
1- Cornelia Sima et al. (2010)[23]	FTO	8.5 Ω /sq	-----	η =9.6% Resistance constant
	ITO	18 Ω /sq		η =2.24% The resistivity rose to 52 Ω /sq.
2- Katrin Gossen, and Andrea Ehrmann (2019)[26]	FTO	76 Ω	used up water	The resistivity has dropped to 62 Ω .
		86 Ω	used up Ethanol	The resistivity has dropped to 61 Ω .
		76 Ω	used up Isopropanol	The resistivity rose to 102 Ω .
		71 Ω	used up Acetone	The resistivity rose to 177 Ω .
		80 Ω	Uncleaned	-----
3-Moustafa S. Abusaif et al. (2021) [50]	FTO	10 Ω	Acetone and distilled water	The resistivity rose to 35 Ω .

2.8 Summary For semiconductors (photoanodes)

Table 2. 2: Summary for Semiconductors (Photoanodes).

Author	type	Preparation of semiconductor dough	casting method	Result
1-Aneel Pervez et	ZnO	-Mix 30% distilled water with 70% ethanol. -Add 0.6g of ZnO.	Doctor blade	V_{oc} =0.28v I_{sc} =3.85mA/cm ²

al. (2018) [27]		-Mixed for 15 min. -Coated FTO was annealed at 400°C for 30 min.		$\eta = 0.67\%$ FF= 0.62
	TiO ₂	-Mixed 0.1ml triton, 0.8ml acetyl acetone and 4ml deionized water. -Add 2 g of TiO ₂ and mixed for 15 min. -Coated FTO was annealed at 400°C for 30 min.	Doctor blade	V _{oc} =0.33v I _{sc} =4.51mA/cm ² $\eta = 1.10\%$ FF= 0.74
2- D. Sinha et al. (2019) [28]	ZnO	-Mixing TiO ₂ or ZnO particles with drops of acetone -Coated FTO was annealed at 450°C for 30 min.	Chemical bath deposition (CBD)	V _{oc} =0.4v I _{sc} =0.66mA/cm ² $\eta = 0.13\%$ FF=0.5
	TiO ₂		rotating paint	V _{oc} =0.74v I _{sc} =1.02mA/cm ² $\eta = 0.27\%$ FF= 0.35
3- Mozghan Hosseinhezad et al. (2020) [29]	ZnO	-----	-----	$\eta = 0.13\%$
	TiO ₂	-----	-----	$\eta = 0.27\%$
4- P. Dhamodharan et al. (2021) [30]	ZnO	Coated ITO was annealed at 350°C for 30 min.	Spray pyrolysis	$\eta = 0.34\%$
5- Urenyang I. Ndeze et al. (2021) [31]	TiO ₂	-3.5 g of TiO ₂ dissolved in 10 ml of ethanol to form slurr. -Coated FTO was annealed at 450°C for 30 min.	Doctor's blade	V _{oc} =0.158 v I _{sc} =2.66mA/cm ² $\eta = 0.25\%$ FF= 0.596
6-Geetam Richhariya and Anil Kumar (2021) [51]	ZnO	-----	-----	V _{oc} =0.42 v I _{sc} =0.91mA/cm ² $\eta = 0.17\%$ FF= 0.46%
	TiO ₂	-The powder was milled of TiO ₂ -0.5 ml of nitric acid and 0.10 g of polyethylene glycol were added. -The mixture was stirred with the help of ultrasound for an hour.	-----	V _{oc} =0.51 V I _{sc} =1.39mA/cm ² $\eta = 0.33\%$ FF= 0.47%

		-It was annealed after casting on FTO by raising the temperature from 60 °C to 450 °C.		
7- Anupam Agrawal et al (2021) [52]	TiO ₂	-1 g of TiO ₂ was mixed and ground with 0.17 mL of acetic acid and 0.85 mL of DI water. -22 ml of ethanol was added and crushed for 25 minutes. -It was transferred to a beaker with magnetic stirring. -Ethyl cellulose and terpineol were added as binders. -After casting, it was annealed.	Doctor blade	V _{oc} =0.7276v I _{sc} =9.97mA/cm ² η= 4.86% FF= 0.6703
			Screen printing	V _{oc} =0.760 v I _{sc} =12.76mA/cm ² η= 6.72% FF= 0.6936
8- Ayesha Siddika et al. (2022) [53]	TiO ₂	-TiO ₂ was ground with mortar for an hour. -Drops of PEG (Sigma-Aldrich) were added, as well as Triton X-100.	Doctor's Blade	V _{oc} =0.6175 v I _{sc} =7.790mA/cm ² η= 1.24% FF= 0.279
			Screen Print	V _{oc} =0.6683 v I _{sc} =6.400mA/cm ² η= 1.47% FF= 0.344

2.9 Summary for Sensitizers (Dye)

Table 2. 3: Summary for Sensitizers (Dye)

Author	dye	Source	Preparation of the dye	Result
1- F. Kabir et al. (2019) [32]	Chlorophyll	Green spinach	-Spinach leaves washed. -dried for 2 hours at 50°C using an oven -It was cut into small pieces. - 0.363 g of it was dissolved in 5 ml of ethanol. -The mixture was kept out of the sun for 24 hours. -nominated.	V _{oc} =0.347 v I _{sc} =2.88mA/cm ² η= 0.466% FF= 0.486
	Anthocyanin	Red spinach		V _{oc} =0.383 v I _{sc} =2.81mA/cm ² η= 0.531% FF= 0.494
	Chlorophyll + Anthocyanin	Mixing (20% green + 80% red)		V _{oc} =0.385 v I _{sc} =4.27mA/cm ² η= 0.847% FF= 0.515
2- F. Kabir et al.	Betacyanin	Red spinach	-It has been carefully washed and chopped. -It was heated for 1 hour at 60 °C.	η=0.134%

(2019) [33]			- 1 g of it is dissolved in 10 ml of distilled water. -It was used.	
	Curcumin	Turmeric	-Washed, peeled and cut into thick pieces. -It was left for 12 hours to air dry. -It was crushed by a mortar pestle - 1 g of it was dissolved in 10 ml of ethanol. -The mixture was filtered and used.	$\eta=0.378\%$
	Betacyanin + Curcumin	Mixing (40% Red spinach +60% Turmeric)	-----	$V_{oc}=499.3 \text{ mV}$ $I_{sc}=4.26\text{mA}/\text{cm}^2$ $\eta= 1.078\%$
3- Ishwar Chandra Maurya et al. (2019) [54]	Anthocyanin	Cassia fistula	-Fresh flowers washed with water. -It was dried at room temperature. -It was crushed into a fine powder. - 2g of powder is dissolved in 50ml of ethanol. -It was stirred for 8 hours at room temperature. -It was in the dark for the whole day. -Filtered to get rid of solid residue.	$V_{oc} =0.549 \text{ V}$ $I_{sc}=0.5\text{mA}/\text{cm}^2$ $\eta= 0.21\%$
4-Ahmed M. Ammar et al. (2019) [55]	Anthocyanin	Onion peels	-Put 6 gm of onion peels and 147 gm of chopped red cabbage in 400ml of water. -The mixtures were heated for 24 hours at 90°C.	$V_{oc}=0.48 \text{ v}$ $I_{sc}=0.24\text{mA}/\text{cm}^2$ $\eta=0.064723\%$ FF= 46.63
	Anthocyanin	Red cabbage	-Cooled at room temperature. -filtered with filter paper to extract the pure dyes.	$V_{oc}=0.51 \text{ v}$ $I_{sc}=0.21\text{mA}/\text{cm}^2$ $\eta=0.060145\%$ FF= 46.61064

	Chlorophyll	Spinach leaves	-The spinach has been crushed into a fine powder. -11 gm of spinach was added to the acetone. -The solution has been filtered	$V_{oc}=0.59\text{ v}$ $I_{sc}=0.41\text{ mA/cm}^2$ $\eta=0.171253\%$ $FF= 58.75982$
5- K.B. Erande et al. (2020) [56]	Anthocyanin	Pomegranate	-The pomegranate has been washed -The pure juice was extracted by manual squeezing. -The dye was filtered using filter papers to obtain a pure dye.	$V_{oc}=304.07\text{ mv}$ $I_{sc}=1.62\text{ mA/cm}^2$ $\eta= 0.2\%$ $FF= 0.209\%$
6- Tahmineh Jalali et al. (2020) [34]	Anthocyanin	Saffron		$V_{oc}=0.43\text{ v}$ $I_{sc}=2.48\text{ mA/cm}^2$ $\eta= 0.51\%$ $FF= 48.04\%$
	Chlorophyll	Mallow		$V_{oc}=0.49\text{ v}$ $I_{sc}=2.16\text{ mA/cm}^2$ $\eta= 0.45\%$ $FF= 42.65\%$
	Anthocyanin	Red Onion		$V_{oc}=0.55\text{ v}$ $I_{sc}=2.12\text{ mA/cm}^2$ $\eta= 0.54\%$ $FF= 46.66\%$
	Chlorophyll	Oregano		$V_{oc}=0.43\text{ v}$ $I_{sc}=2.48\text{ mA/cm}^2$ $\eta= 0.51\%$ $FF= 47.82\%$
7- Kenneth Obi et al. (2020) [57]	Anthocyanin	Prickly pear	-Fresh fruits were ground using a pestle and mortar. -Different concentrations of water and ethanol (e.g., 90:10) were mixed and used as a solvent. -Three drops of dilute citric acid were added to adjust its pH.	$V_{oc}=0.589\text{ v}$ $I_{sc}=1.51\text{ mA/cm}^2$ $\eta= 0.57\%$ $FF= 57.6\%$
	Betalain	Mulberry		$V_{oc}=0.568\text{ v}$ $I_{sc}=1.39\text{ mA/cm}^2$ $\eta= 0.68\%$ $FF= 73.1\%$
8- Malihe Golshan et al.	Chlorophyll + Anthocyanin	Malva verticillate	The dye was extracted with the help of a microwave.	$V_{oc}=0.54\text{ v}$ $I_{sc}=1.42\text{ mA/cm}^2$ $\eta= 0.70\%$ $FF=55.4\%$

(2021) [35]	Chlorophyll + Anthocyanin	Syzygium cumini		$V_{oc}=0.20\text{ V}$ $I_{sc}=1.29\text{mA/cm}^2$ $\eta=0.27\%$ $FF=26.1\%$
9-Mona A. Almutair i et al. (2021) [58]	Chlorophyll	Beetroot	-The beetroot was washed with distilled water. -It was dried at room temperature. -It was crushed using a small home mill. -pressed with a piece of cloth to obtain a pure, concentrated mat. -stored in a dark place for use.	$V_{oc}=0.38\text{ V}$ $I_{sc}=1.29\text{mA/cm}^2$ $\eta=0.15\%$ $FF=0.32\%$
10- Amarach ukwu N. Ossai et al. (2021) [59]	Chlorophyll	Carica papaya leaf	-20 g of dried leaves and fruits are dissolved in 100 ml of ethanol	$V_{oc}=0.40\text{ V}$ $I_{sc}=1.77\text{mA/cm}^2$ $\eta=0.29\%$ $FF=0.42$
	Chlorophyll	Black cherry	-The dyes were filtered using filter paper.	$V_{oc}=0.38\text{ V}$ $I_{sc}=1.56\text{mA/cm}^2$ $\eta=0.25\%$ $FF=0.43$

2.10 Summary for Electrolyte

Table 2. 4: Summary for Electrolyte.

Author	Electrolyte status	type	Preparation of the electrolyte	Result
1- Rahul et al. (2020) [44]	quasi solid	KI/I_2	-KI, I_2 and polyethylene oxide are dissolved in acetonitrile. -The mixture was stirred for 3-4 hours at 500°C using a magnetic stirrer. -It was dried for a week at room temperature.	$V_{oc}=0.51\text{ v}$ $I_{sc}=0.006\text{mA/cm}^2$ $\eta=0.002\%$ $FF=0.55$
2- Phitchaphorn Khammee et al. (2021)[45]	Liquid	I^-/I_3	Prepared by mixing 0.6 mol/L of KI, 0.075 mol/l of I_2 , 20 ml of acetonitrile, and 5 mL of ethylene glycol.	$\eta=1.182\%$

3-Dong-Jin Yun et al. (2021) [60]	Liquid	I^-/I_3	It was prepared by mixing 0.03 M I_2 0.6 M 1-butyl-3-methyl imidazolium iodide, 0.1 M guanidinium thiocyanate, and 0.5 M 4-tert-butylpyridine in a solvent mixture of valeronitrile and acetonitrile (85:15 vol%).	$I_{sc}=3.1\text{mA}/\text{cm}^2$ $\eta=0.726\%$ FF=26.2%
4- Soner Çakar et al. (2021) [61]	quasi solid	I^-/I_3	-The liquid electrolyte was prepared by adding 0.5 M 4-tert-butyl pyridine, 0.1 M GuSCN, 0.5 M MPII, 0.1 M LiI and 0.05 M I_2 in CAN. -Added 0.2 g of synthesized PAN/PIN into liquid electrolyte	$V_{oc}=0.86\text{v}$ $I_{sc}=12.43\text{mA}/\text{cm}^2$ $\eta= 8.49\%$ FF=49%
5-Fadzai Lesley Chawaram bwa et al. (2021) [62]	Liquid	I^-/I_3	-0.1 M LiI, 1 M 1-butyl 3-methylimidazolium iodide, 0.1 M I_2 , 0.1 M guanidine thiocyanate, and 0.5 M 4-tert-butylpyridine were dissolved in MPN -2% of iso-octylphenoxy polyethoxyethanol was added to 1 ml of the above solution. -It was mixed using a magnetic stirrer for 24 hours.	$\eta= 5.02\%$
	quasi solid		-Added 10 wt% of TiO_2 and 9 wt% of poly ethylene with liquid electrolyte. -PEO has been added. -Mixed for 10 minutes.	$\eta= 4.59\%$

2.11 Scope of The Present Work

According to the previous literature, the following can be concluded:

- ❖ **Substrates:** According to previous studies, the best types of substrates are made of FTO glass, as their strength does not change with annealing, and the best way to wash and clean the substrates is by using ethanol.

- ❖ **Semiconductors film:** From the above, the best type of semiconductor used in the manufacture of DSSCs is TiO_2 .
- ❖ **Sensitizers (Dye):** According to previous studies, DSSCs based on natural dyes are a promising technology. However, more experiments are needed to obtain the best efficiencies.
- ❖ **Electrolyte:** From previous studies, it can be concluded that the most commonly used electrolyte is I^-/I_3 . It was also concluded that liquid electrolytes are the most efficient, but they are subject to evaporation and leakage, and vice versa in the case of quasi solid electrolytes.
- ❖ **Counter electrode:** Most of the previous research proves that Pt is the best so far, as many researchers have sought to obtain cells based on other elements that are incompatible with those based on Pt.

CHAPTER THREE**THEORETICAL CONCEPT****3.1 Introduction**

In this chapter, the main concept is the effect of important changes and reflection losses on the parameters of dyestuff solar cells. This is useful for estimating the performance of dye solar cells under various conditions and understanding the effects of reflectance loss and temperature differences. All equations that deal with solar cell parameters are here.

3.2 Light Properties

The light we see is only a small part of the total energy generated by the sun. Solar energy represents electromagnetic waves ranging from gamma rays to radio waves. Among these rays are X-rays, ultraviolet rays, infrared and visible rays, and microwave rays, as depicted in Figure (3.1).

Sunlight reaches the ground, where it contains about 6% ultraviolet radiation (400 nm), 45% visible radiation (400 nm-700 nm), and the remaining 49% infrared radiation (>700 nm). Photon energy(E), the wavelength (λ), and frequency (ν) are the most important characteristics of electromagnetic waves to distinguish between them. where the energy of photons and wavelength are inversely proportional to each other [63].

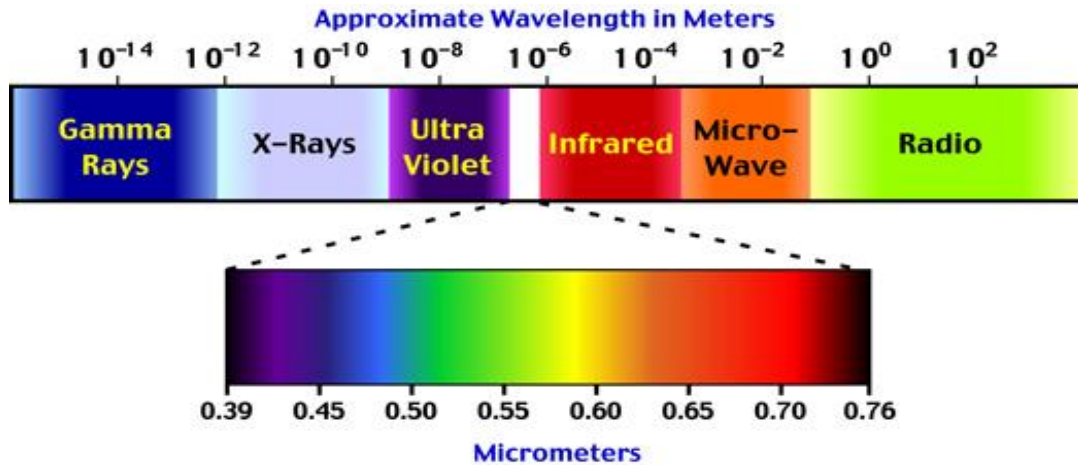


Figure 3.1: Spectrum wavelength [64].

3.3 Optical Properties

Knowing the absorbance, transmittance, and reflectivity spectra helps us determine many properties within different wavelengths. In the visible spectrum region, it gives enough information about how the material behaves for solar applications and how much it affects the light that gets through.

3.3.1 Electronic Transitions

When electromagnetic radiation falls on a semiconductor, a large and rapid increase in absorption will occur when the energy band of the absorbed radiation is equal to the frequency of the atoms and approximately equal to the energy gap between the conduction and valence bands, which is called the Fundamental Absorption Edge. The location and composition of this edge give us information about the value and type of the energy gap [65]. The interaction of the incident ray with the molecule works to irritate the atoms of the molecule and its energy is transferred. to the excited state as shown in Figure (3.2), where ψ and ψ^* represent the description of the molecular orbitals and the ground and excited states, respectively, which are separated by an energy of:[66]

$$\Delta E_e = h\nu = E_{\psi^*} - E_{\psi} \quad (3.1)$$

Where;

h: Planck's constant (6.63×10^{-34} J.S)

ν : frequency of the photon (HZ).

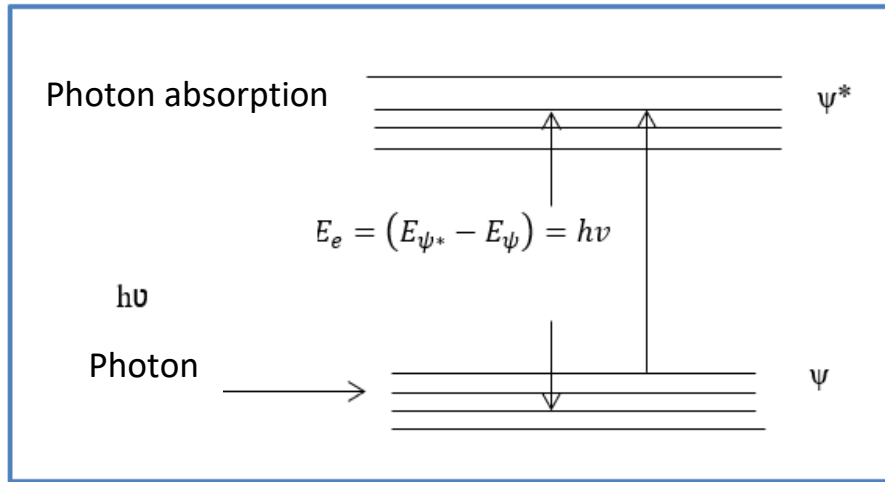


Figure 3. 2: Electron transitions between ψ^* and ψ bands due to energy absorption [66].

3.3.2 Direct and indirect electronic transfers

Direct transfer occurs when electrons move from the top of the valence band to the bottom of the conduction band directly as a result of energy absorption greater than or equal to the energy gap ($h\nu \geq E_g$). As shown in Figure (3.3). These transitions occur on the condition that the change in the value of the wave vector of the transferred electron is ($\Delta K = 0$) and that the direct transition occurs when ($K = 0$), and in this transition both the energy and momentum of the electron remain conserved, and they are described by the two relationships below:

$$E_f = E_i + h\nu \quad (3.2)$$

$$\mathbf{K}'_f = \mathbf{K}'_i + \mathbf{q}' \quad (3.3)$$

Where;

E_i : Elementary electron energy (eV).

E_f : The final electron energy (eV).

\mathbf{K}'_i : The primary vector of the electron.

\mathbf{K}'_f : The final vector of the electron.

The wave vector of the absorbed photon (\mathbf{q}') can be neglected because it is very small compared to (\mathbf{K}), meaning that ($\mathbf{K}'_f = \mathbf{K}'_i$) direct transitions are of two types (allowed transitions and forbidden transitions) that allowed direct transitions occur. When a transition occurs from the top of the valence band and of the atom to the bottom of the conduction band directly as a in Figure (3.3), the direct transmission is prohibited if the transition from the bottom of the valence band to the top of the conduction band is directly as b in Figure (3.3).

The absorption coefficient can be described as a function of the photon energy by the following relationship:

$$\alpha h\nu = B(h\nu - E_g)^r \quad (3.4)$$

where;

B: Constant quantity.

r: An exponential coefficient whose value is (1/2) for the permissible direct transmission and (3/2) for the direct transmission that is not allowed.

As for the indirect electronic transitions, they occur as a result of the electron moving indirectly from the valence band to the bottom of the conduction band. The permitted indirect transition occurs from the top of the valence band to the bottom of the conduction band, as c in Figure (3.3), while the forbidden indirect transition occurs from the bottom of the valence band to the top of the conduction band, as d in Figure (3.3). The valence and the bottom of the conduction band do not have the value of the wave vector ($\Delta K = 0$). These transitions are accompanied by the emission or absorption of a photon with a certain amount of energy, which conserves that makes both momentum and energy. The conservation law can be written in the following form:

$$E_f = E_i + h\nu \mp E_p \quad (3.5)$$

$$K_f = K_i \pm K \quad (3.6)$$

Where; K_p is the wave vector of the photon accompanying the indirect transition.

The energy required for the electron to move from the valence band to the conduction band when a photon is absorbed or emitted is by the following relationship:

$$h\nu = E'_g \pm E_p \quad (3.7)$$

Where;

E_p : the energy of the photon that goes along with the indirect transfer, the positive sign means the photon that was absorbed, and the negative sign means the photon that was sent out.

The absorption coefficient for indirect transmission is given by:

$$\alpha = \alpha_0 \frac{(hv - E'_g \pm E_p)^r}{hv} \quad (3.8)$$

Where;

E'_g : Indirect energy gap (eV)

r : exponential coefficient equal to (2) for the allowed indirect transitions and equal to (3) for the forbidden indirect transitions [67].

As for dyes as organic materials, the energy gap was calculated using the following equation:[68]

$$Eg = \frac{1.24}{\lambda (\mu m)} \quad (3.9)$$

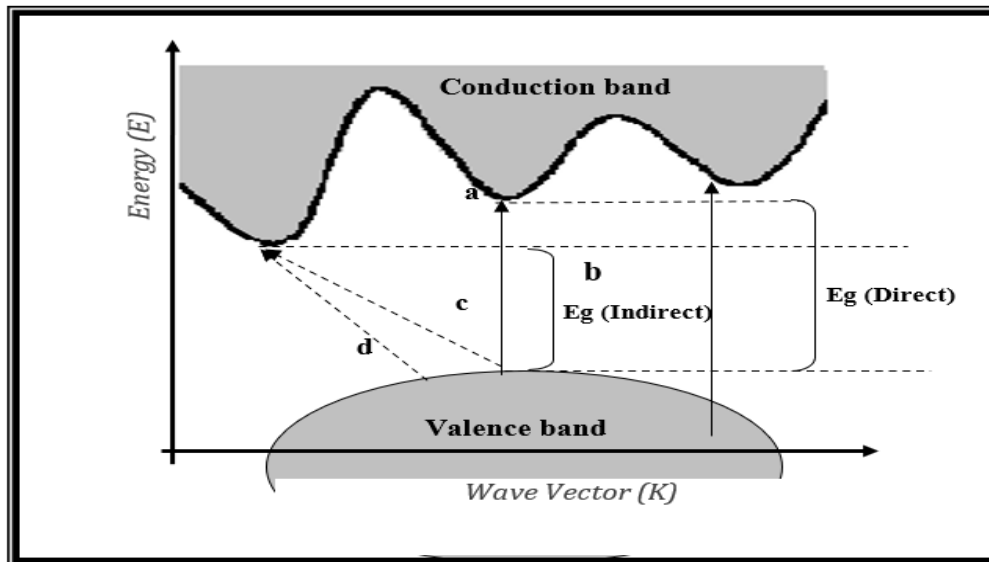


Figure 3.3: Electronic transmissions (a) permitted direct transmission; (b) prohibited direct transmission; (c) permitted indirect transmission; (d) prohibited indirect transmission [67].

3.3.3 The Optical Constants

Optical constants are one of the important factors that classify the optical behavior of materials. Each substance has its own characteristics when affected by light (or electromagnetic radiation) in terms of intensity of absorption, reflection and other characteristics. Therefore, the difference

between materials can be distinguished by optical constants such as the coefficient of refraction, as they are calculated. These are constants for a wave propagated in a medium using Maxwell's equations.

3.3.3.1 Refractive index

When a wave of frequency (ω) propagates through a given medium in a given direction (Z), the electric field strength (E) depends on time and location according to the equation: [69]

$$E = \hat{E} e^{-i(Nk^*z - \omega t)} \quad (3.10)$$

Where;

k^* : represents the wave vector in space ($2\pi/\lambda$).

\hat{E} : The amplitude of the electric field is at ($z=0$).

N : The complex refractive index is given by:

$$N = n + iK \quad (3.11)$$

The real part (n) of the relationship represents the normal refractive index, which is defined as the ratio between the speed of light in a vacuum to its average speed and is always greater than (1) [69]. From the value of the inertia coefficient (K) and the value of the reflectivity (R), the refractive index can be calculated from the following equation:[70][71]

$$n = \frac{1+R^{1/2}}{1-R^{1/2}} \quad (3.12)$$

3.3.3.2 Extinction Coefficient

The imaginary part (K) in equation (3.11) represents the attenuation coefficient (K), which is responsible for the decay of the wave exponentially within the material, for example, when a wave propagates within a solid

medium a distance equal to one wavelength of its wavelength in a vacuum, its amplitude will decrease by $(e^{-2\pi k})$ assuming that (k) is the damping coefficient for that substance. It is given by the following relationship:[72][73]

$$K = \frac{\lambda\alpha}{4\pi} \quad (3.13)$$

3.3.3.3 Absorption Coefficient

It is an amount that depends on the energy of the incident photon and represents the ratio between the number of photons actually absorbed per unit length of matter during one second and the number of photons incident per unit area per second [74]. The absorption coefficient is given by the following equation:[69]

$$\alpha = 2.303 \frac{A}{d} \quad (3.14)$$

Where;

A: Membrane absorbance (A.U).

d: membrane thickness (m).

3.3.3.4 Complex dielectric constant

The complex refractive index (N) is related to the nodal dielectric constant (ϵ) by the relationship :[75]

$$N = \sqrt{\epsilon} \quad (3.15)$$

The dielectric constant is a measurable quantity that describes the response of a material when it is affected by an electric field. It is caused by the propagation of an electromagnetic wave through it and can be represented

by two parts, the real part (ϵ_r) And the fictional part (ϵ_i) According to the relationship:

$$\epsilon = \epsilon_r + i \epsilon_i \quad (3.16)$$

And from the relations (3.14) (3.15) (3.10) it can be written:

$$(n + iK)^2 = (\epsilon_r + i \epsilon_i) \quad (3.17)$$

From equation 3.16, we get both the real dielectric constant and the imaginary dielectric constant in terms of the normal refractive index and the inertia coefficient.

$$\epsilon_r = n^2 - K^2 \quad (3.18)$$

$$\epsilon_i = 2nK \quad (3.19)$$

The real part of the dielectric constant controls how fast the wave moves through the medium, and the imaginary part controls how much energy is lost as heat or radiation [75].

3.4 Crystal Structure and Bragg's Law

Traditionally, X-rays have been used to identify the crystal structure of a substance, study the atomic arrangement, or even photograph it using rays with a wavelength that is within the space between atoms. The English scientist (W. L. Bragg) was able to deduce his law based on the fact that the difference in the paths of two rays is equal to multiples of wavelength, and Bragg's law is written follows: [76]

$$n_B \lambda = 2 d_{hkl} \sin (\theta) \quad (3.20)$$

Where;

n_B : An integer called the order of reflection ($n_B = 1, 2, 3, \dots$).

λ : X-ray wavelength (nm)

d_{hkl} : Interstitial distance of the set of levels (hkl)

θ : Bragg's angle

The basic inversion condition for Bragg's reflection to occur is the realization of the inequality ($\lambda < 2d_{hkl}$). As in Figure (3.4), the use of X-rays to study the crystal structure is one of the easiest ways. In order to obtain the X-ray diffraction pattern that occurs when Bragg's law is achieved, some experimental methods have been designed, such as the Laue method, the crystal rotation method, the crystal oscillation method, and the powder method, and all these methods are based on the principle of continuity (λ) continuously or changing (θ) continuously during experience.

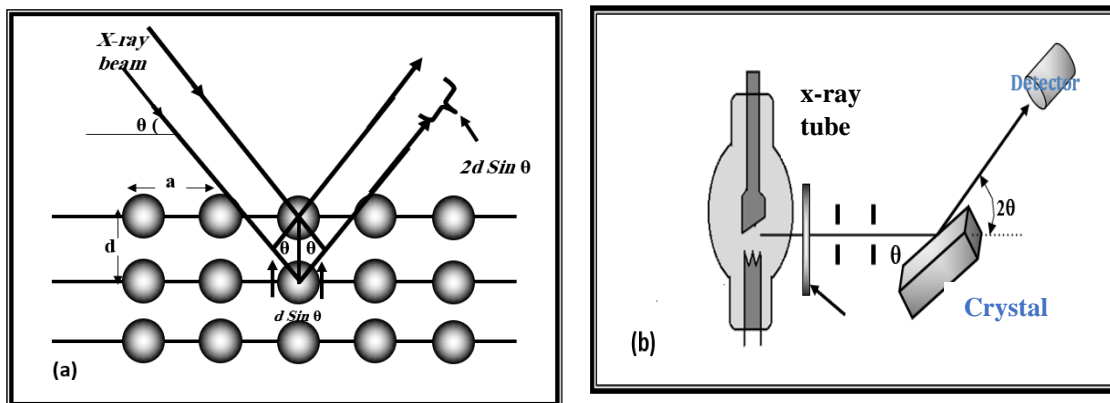


Figure 3.4: a) Crystal levels and Bragg's law; b) X-ray diagnosis [76].

3.5 The solar cells parameters

The most important PV parameters that determine the performance of DSSCs are open-circuit voltage (V_{oc}), short circuit current (I_{sc}), fill factor (FF), and photoelectric efficiency (η). All of which can be estimated from the I-V characteristics of the solar cell under illumination, as shown in

Figure(3.5)[77]. These parameters are optimized depending on the basic parts of the cell.

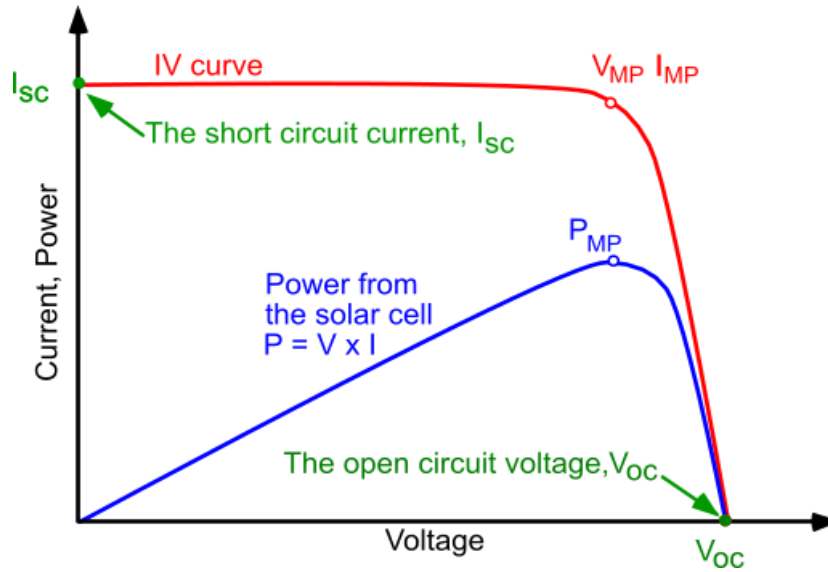


Figure 3.5: The standard current-voltage (I-V) and power-voltage (P-V) curves of a solar cell [77].

3.5.1 Short-circuit current density (I_{sc})

Short-circuit current density is the maximum current density generated when the voltage across the DSSC is zero. The interaction between the photoanode, the dye absorption coefficient, and the dye sensor affects the I_{sc} . The main factors affecting I_{sc} the photoelectric properties are the physical and molecular structures, which I_{sc} increase with the intensity of sunlight absorbed by the dye sensitizer (meaning it depends on the temperature). I_{sc} also equal to the absolute number of photons converted into electron-hole pairs. As in the following relationship [78].

$$I_{sc} = I_s \left[\exp \frac{q \cdot V_{oc}}{kT} - 1 \right] - I_{ph} \quad (3.21)$$

3.5.2 Open circuit voltage (V_{oc})

Open circuit voltage is the maximum voltage that can be obtained from DSSCs when the circuit is open, i.e., when ($I = 0$). It is also known as the "electrical difference" between the two ends of the cell. The open circuit voltage is strongly dependent on temperature as shown in the relationship below [78].

$$V_{oc} = \frac{kT}{q} I_n \left[\frac{I_{ph}}{I_s} \right] + 1 \quad (3.22)$$

Where:

K: Boltzmann constant,

T: Temperature,

q: electronic charge,

I_{ph} : photocurrent (A),

I_s : diode saturation current (A).

3.5.3 Fill factor (FF)

Fill factor is the ratio of the maximum output power (P_{max}) to the product of V_{oc} and I_{sc} . As shown in the Figure (3-5), where P_{max} is obtained by the multiplication of the voltage corresponding to the point P_{max} (V_m) by the photocurrent (I_m) [79].

$$FF = \frac{P_{max}}{I_{sc} \cdot V_{oc}} = \frac{I_{max} \cdot V_{max}}{I_{sc} \cdot V_{oc}} \quad (3.23)$$

3.5.4 Power conversion efficiency (η)

Power conversion efficiency is the ratio of P_{max} to the input power (P_{in}).

$$\eta = \frac{P_{max}}{P_{in}} = \frac{I_{max} \cdot V_{max}}{P_{in}} = \frac{I_{sc} \cdot V_{oc} \cdot FF}{P_{in}} \quad (3.24)$$

$$P_{in} = I \cdot A_{cell} \quad (3.25)$$

From the above equation, it is clear that the efficiency of DSSC is related to the greatest power density (I_{max} and V_{max}) and power density (I_{sc} and V_{oc}) [80].

CHAPTER FOUR

EXPERIMENTAL WORK

4.1 INTRODUCTION

This chapter focuses on the method of manufacturing dye-sensitized solar cells and the preparation of all layers that comprise the cell. DSSCs were tested in the laboratories of the Technical College of Engineering in Najaf. 1000W/m² fixed radiant flux with a light that is perpendicular to the surface of the solar cell. The optical properties of the natural dyes were first examined using (UV-vis) in addition to the curves of voltage, current and cell performance using (Keithulye2400) device, and finally the materials and techniques used in manufacturing DSSCs were explained.

4.2 Materials

4.2.1 Glass substrate

Table 4.1. & Figure (4.1) depict the dimensions, and specific properties of glass substrates which employed in this study.

Table 4. 1: Glass substrates Properties.

NO.	Item	Description
1	Type	FTO
2	Size (mm)	25 * 25 * 1.1
3	Resistance(Ω)	10–20
4	FTO Roughness	12.5 nm

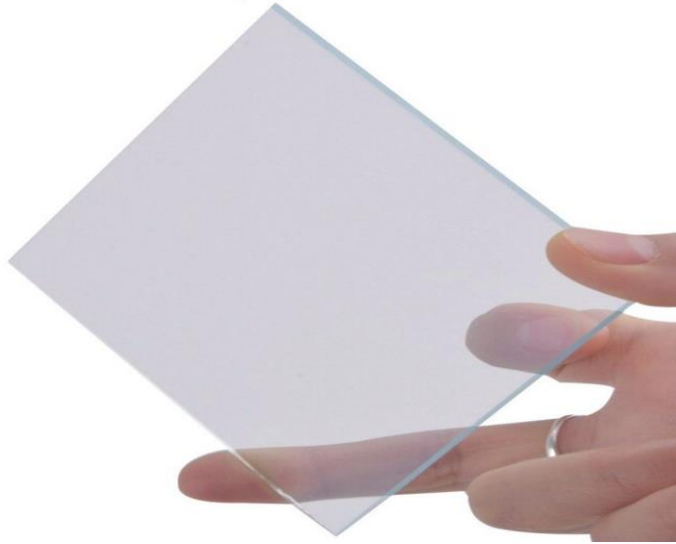


Figure 4. 1: Glass substrates FTO type.

4.2.2 Titanium Dioxide (TiO_2)

Titanium dioxide is a white, highly stable, and unreactive metal oxide found in three crystalline forms in nature: anatase, rutile, and brookite [81] as pictured in Figure (4.2).



Figure 4. 2: Crystalline Forms of Titanium Dioxide, Anatase, Rutile, and Brookite [81].

Unlike brookite and rutile, which are rarely used, anatase has been used in a variety of industrial fields since the 1920s. Titanium dioxide is naturally occurring, but the titanium is never found pure. Anatase-crystalline form titanium Dioxide (TiO_2) is semiconductor with an energy gap of about 3.2 eV and a refractive index of about ($n=2.52$) [81]. In the case of rutile and brookite, the energy gaps are 3.0 eV and 3.1 eV, respectively, and they have a refractive index ($n=2.76$) [82].

Table 4. 2: General Properties of Titanium Dioxide.

Properties	value
Chemical formula	TiO_2
Molar mass	79.86 g/mol
Density	3.78 g/cm ³
Appearance	White
Melting point	1843 °C
Refraction index (n)	2.52
Energy bandgap	3.2 e.v

4.2.3 Other materials

From local markets, acetone, ethanol, and methanol were purchased, which are used for cleaning and dissolving. and the natural plant (Mentha, Helianthus annuus, and Fragaria), which is used to extract pigments used as catalysts, was also purchased. Lithium iodide and iodine are used as oxidation-reduction pairs, among other substances to be taken up during preparation.

4.3 Prepare each part for DSSC before assembly

4.3.1 Substrate cleaning

In Figure (4.3), steps (a) Uncleaned FTO glass, as shown in (b) FTO was cleaned using deionized water, as in (c) and (d). Then the cleaning was carried out using the ultrasonic cleaning device and ethanol, where the ethanol

and FTO glass were placed in the ultrasonic device and it was turned on for cleaning for half hour, as in (e). The pedestals were carefully removed from the ultrasonic scrubber as they were grabbed by the tip with forceps, as in (f). Place them in Petri dishes to dry and maintain cleanliness.

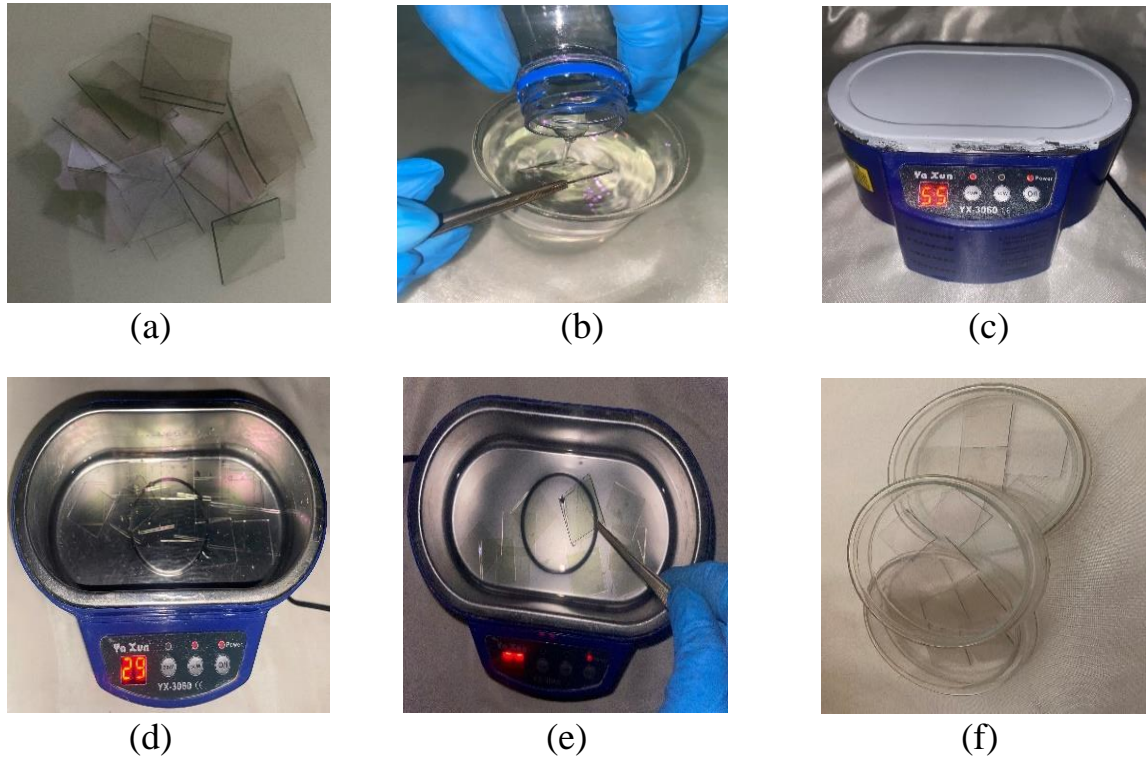


Figure 4. 3: Substrate cleaning steps.

4.3.2 Preparation of TiO_2 photoanode

First, the acidity of nitric acid (HNO_3) was confirmed if it was diluted by conducting a simple experiment shown in Figure (4.4), where an unspecified amount of HNO_3 was taken and a small amount of copper filings was added to it. It can be noticed that there is a change in the color of the mixture and a rise of vapors, which indicates that the acid is undiluted.

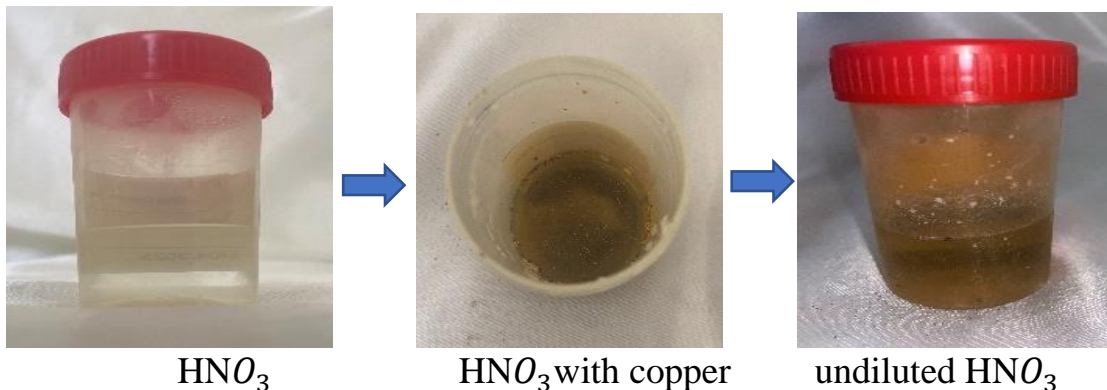


Figure 4.4: Simple test steps to see if HNO_3 is diluted or concentrated.

Concentrated nitric acid is diluted by dissolving 3 ml of it in 50 ml of water to make it diluted acidic (PH = 3). This was confirmed using a device (PH – Meter CG818). As shown in Figure (4.5).



Figure 4.5: Nitric acid pH measurement device.

After checking the acidity of HNO_3 , a TiO_2 paste was prepared by dissolving 2 g of TiO_2 powder of sizes (10 nm) separately with 6 ml of dilute HNO_3 . The mixture was mixed well using a pestle for half an hour, followed by magnetic stirring for another 30 min until it became homogeneous as shown in Figure (4.6), after that, one drop of ethylene glycone and two drops

of Triton X-100 were added to increase the adhesion of TiO_2 to the FTO glass, then it is magnetically stirred for an hour and a half.



Figure 4. 6: TiO_2 paste and its texture.

4.3.3 Preparation of sensitizers (dyes)

The dyes were prepared from *Mentha* leaves and annual *helianthus* leaves in the same way. After harvesting, the green leaves for *Mentha* and yellow leaves for annual *helianthus* were washed with distilled water first, and then the leaves were dried at room temperature in the dark. Then the leaves were dried and crushed separately using an electric grinder. Then 0.75 g of dried plant leaves were added to 60 ml of acetone (Also ethanol and methanol separately). It was placed in a sealed package in the dark and left for 24 hours, then filtered using filter papers to get rid of large pieces and obtain a clear extract without impurities. Then it was kept away from the light for use when needed. These steps are illustrated in Figure 4.7(a and b).



(a)



(b)

Figure 4. 7: Extraction steps for (a) *Mentha* leaves, (b) annual *helianthus* leaves.

While the anthocyanin dye was extracted by crushing *Fragaria* fruit after washing it with distilled water in a mortar and pestle, 2 g of it was placed in 5 ml of acetone (Also ethanol and methanol separately). It was left in the dark for 24 hours, after which it was filtered using filter papers to get rid of large pieces and obtain a pure extract, then it was kept in a tightly closed

package away from light for use when needed. These steps are illustrated in Figure (4.8).

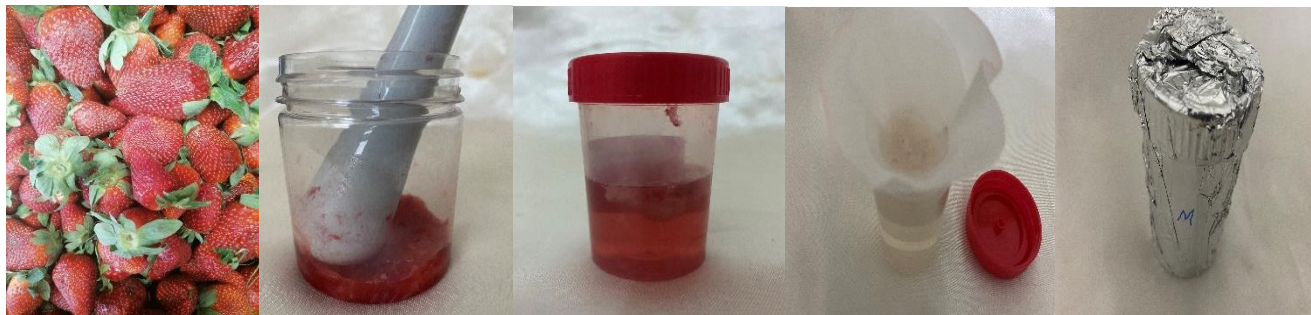


Figure 4. 8: Fragaria fruit tincture extraction steps.

The fourth dye was prepared by mixing equal amounts of all the aforementioned dyes, and the same method of preserving the other dyes was kept.

In other separate steps 0.08 g silver nanoparticles as shown in Figure 4.9 were added to the dye to see the effect of this on the performance of DSSCs.

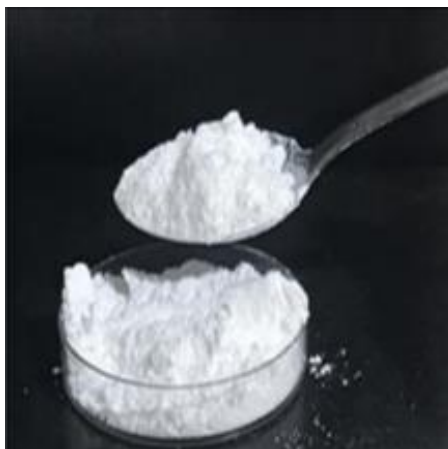


Figure 4. 9: nano silver.

4.3.4 Electrolyte preparation

The electrolyte was prepared by dissolving 3 g of I in 50 ml of ethylene glycone by stirring using a magnetic stirrer for 20 minutes, then 1.5 g of KI

was added to the solution and continued stirring for an hour and a half. Taking into account that the solution is in a dark container as shown in Figure (4.10).



Figure 4. 10: stirring electrolytes in a dark container using a magnetic stirrer.

4.3.5 Counter electrodes preparation

The platinum liquid is placed on a clean FTO glass and heated from 100°C to 450°C in 50°C increments over the course of five minutes in order to generate a cathode for the DSSC. For ten minutes, the temperature was raised to 450 degrees Celsius, after reaching 450 degrees. The glass was then removed from the furnace and allowed to cool to ambient temperature for an additional ten minutes. Because platinum oxidizes in the light, the heating was done in a dark environment.

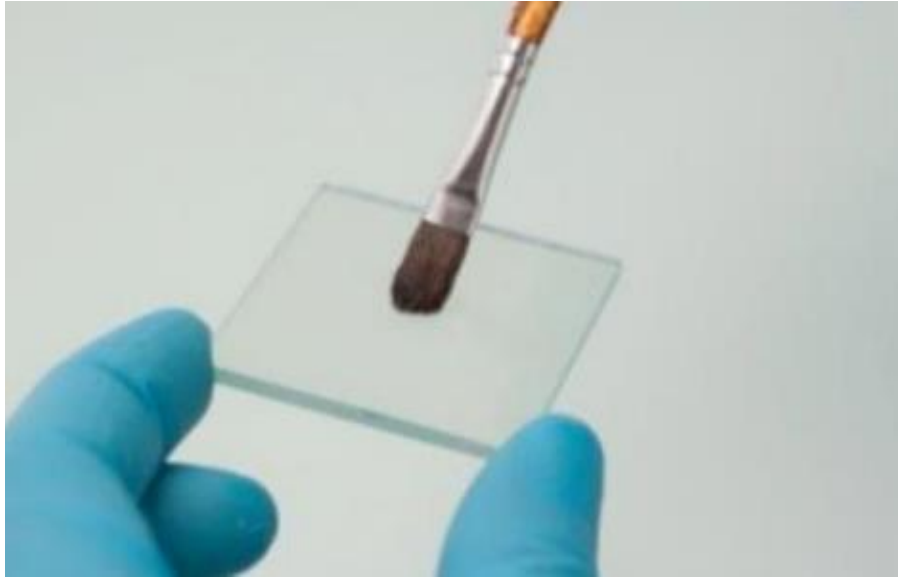


Figure 4.11: Counter electrodes preparation with Pt.

In other steps, carbon soot was relied upon instead of Pt as the counter electrode, as shown in Figure (4.12). as a cheap and easy component.

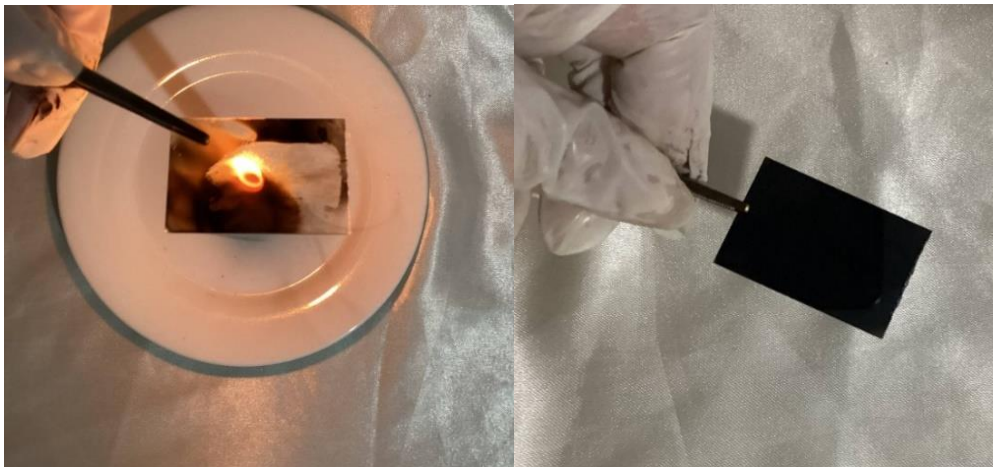


Figure 4.12: Counter electrodes preparation with carbon soot.

4.4 Fabrication of DSSCs

1. The working side of the FTO was determined with a voltmeter. For the purpose of defining the DSSC work area to the external circuit and to

control the thickness of the TiO_2 layer, adhesive tape was placed around three sides of the FTO glass. As shown in Figure (4.13).



Figure 4. 13: Prepare FTO glass for casting TiO_2

2. A TiO_2 paste was poured and distributed using a glass applicator. This method is called "blade doctor" and allowed to dry, then it is annealed for 100 minutes at 500°C gradually starting at 100°C .

As to the two-layer TiO_2 cell: The organic matter is then added to the TiO_2 paste, which is subsequently dried for 15 minutes at 100°C . TiO_2 paste is then poured over the first layer and annealed for a further 80 minutes at 500°C to form the second layer. In order to avoid the electrolyte coming into direct contact with the FTO glass, the second layer of TiO_2 is there to slow down the pace at which the TiO_2 film breaks down.

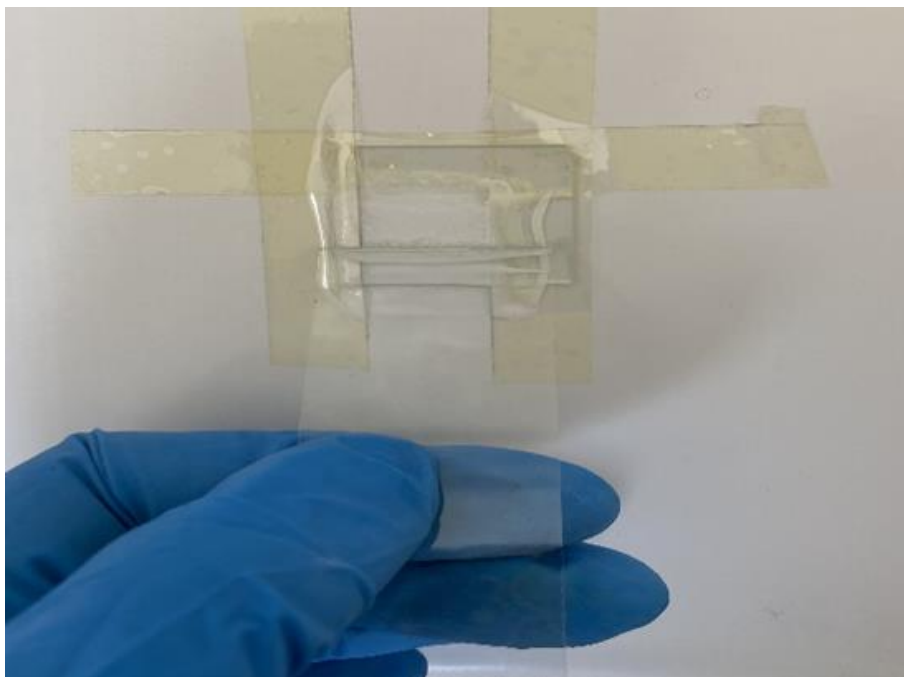


Figure 4.14: TiO₂ distribution using the doctor blade method.

3. The TiO₂-coated glass is placed in the dyes as shown in Figure (4.15) and left for 24 hours. Then lift it and leave it to dry at room temperature. This completes the anode electrode.

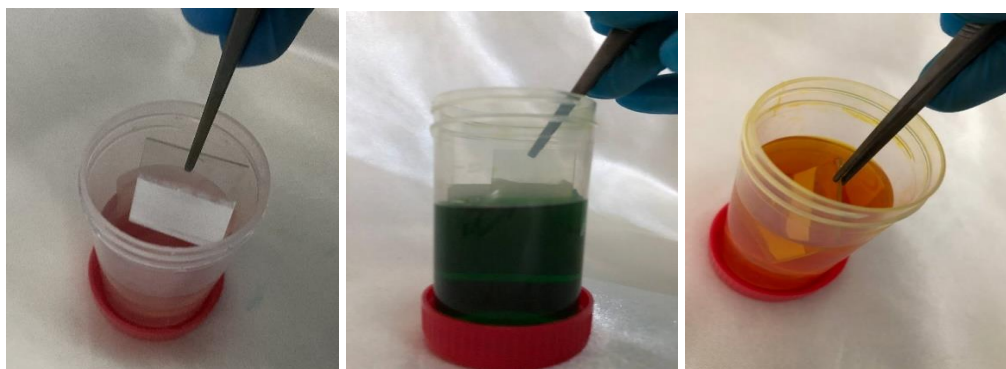


Figure 4.15: Immersion of TiO₂-coated glass in dyes

4. Electrolyte drops are placed.
5. Both electrodes (anode and counter electrodes) are placed opposite each other. The displacement of the poles from each other for a distance is

for the purpose of electrical connection of the solar cell to the external circuit. The resulting cell must be well sealed. In this study, paper clamp was used to keep the electrolyte from leaking out and to hold the electrodes together.

Figure 4.16 shows the detailed steps of the dye-based solar cell fabrication method.

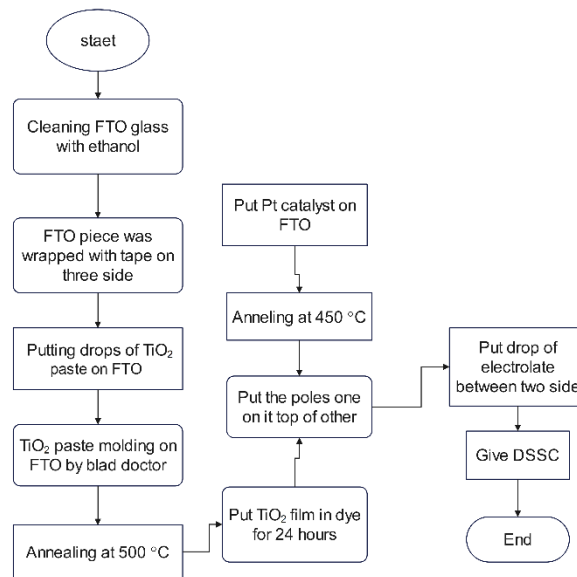


Figure 4. 16: Flowchart to facilitate DSSC fabrication preparation procedure.

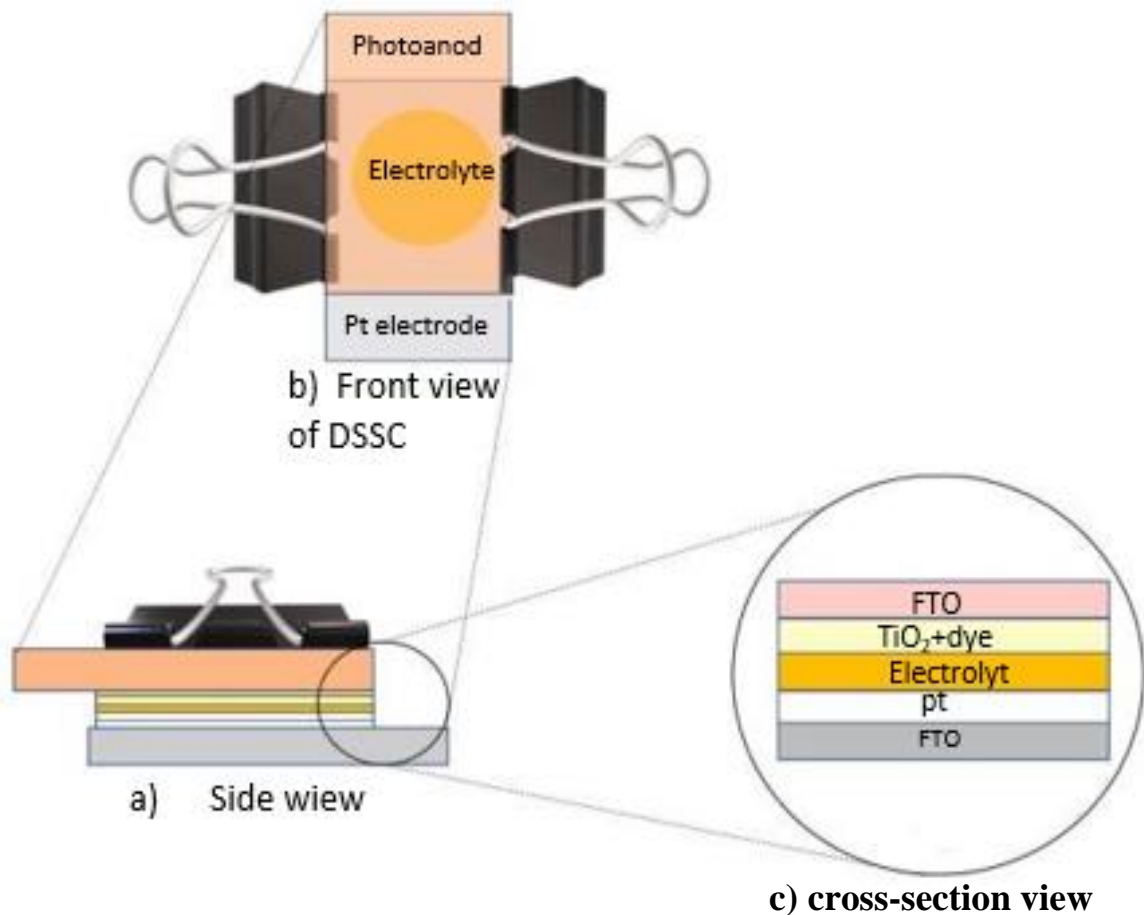


Figure 4. 17: The assembly procedure of FTO/TiO₂-dye/electrolyte/Pt DSSCs from several viewpoints: (a) side view, (b) front view (c) cross-section view.

4.5 Steps of testing DSSC

The photocell measurement circuit consists of a digital voltage and current meter (**Keithley 2400**) connected to both ends of the DSSC sample, as well as, a light source, which is a xenon lamp with an intensity of 1000 W/m², 11 cm away from the cell. The sample is connected by capillary wires using a wire clamp. Parts of an electrical circuit in a computer, as shown in the Figure (4.18).

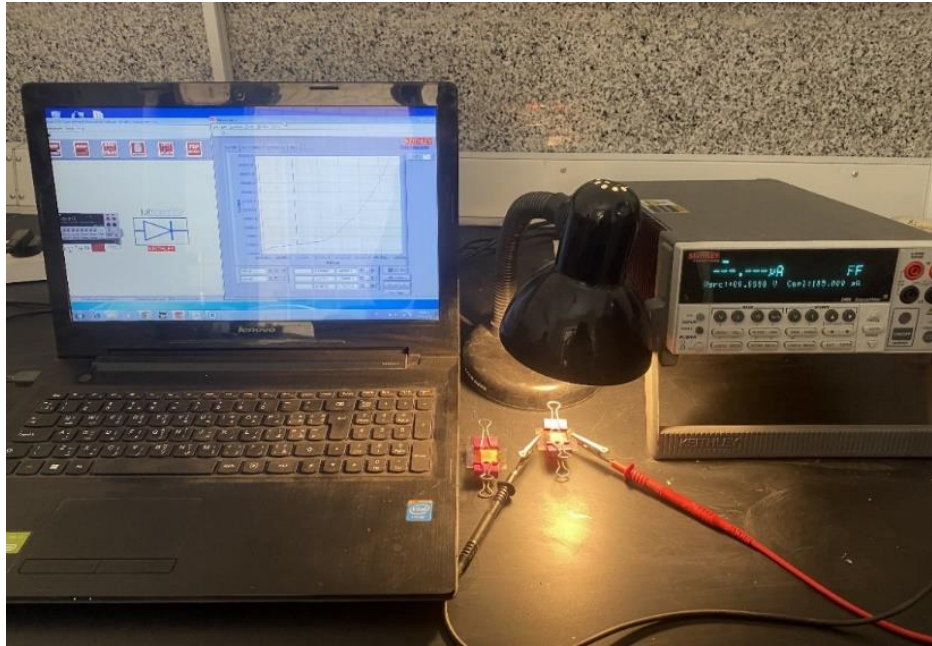


Figure 4. 18: solar cell measurement system.

4.6 Measurement Devices

4.6.1 Sensitive Electronic Scale

The high accuracy measurement of the genuine nanomaterial weight. KERN and Sohn GmbH's **ACS 200-4** four-digit sensitive electronic balance was employed as shown in Figure (4.19).



Figure 4. 19: Sensitive Electronic Scale.

4.6.2 Magnetic Stirrer & Hot Plate

Figure (4.20) shows the magnetic stirrer device, which contains hot plates and speed selectors. The magnetic field was the basis of its work, for which two magnetic poles were installed, one of which was installed in the bottom plate of the device and the second as a rod that was placed inside the beaker, and due to the magnetic repulsion, the strip rotates and agitates the solution. The purpose of this process in this paper is to mix the electrolyte and the semiconductor paste.

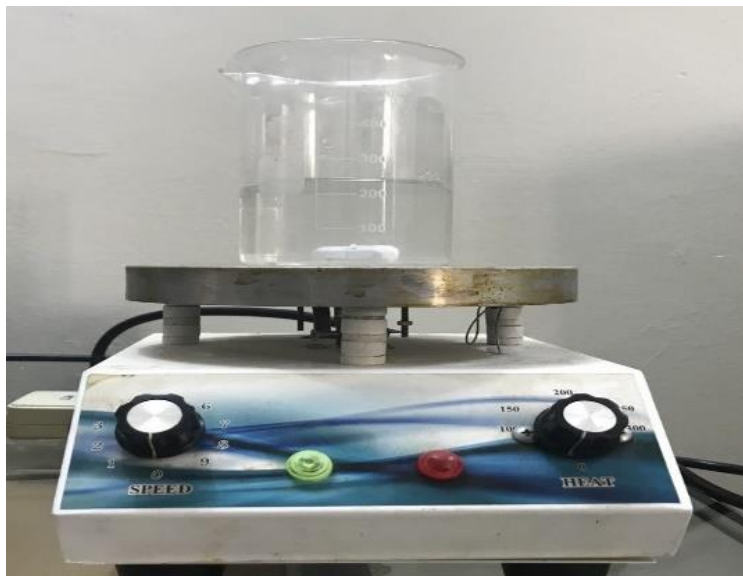


Figure 4. 20: Magnetic Stirrer Device.

4.6.3 Ultrasonic Device

This device as shown in Figure (4.21) was used to clean the FTO glass to get rid of dust and suspended impurities.

Principle work, the basis work of the device is an emission of Ultrasound waves at certain frequencies that hit the basic fluid to dispersion the Nanoparticles in it.



Figure 4. 21: Ultrasonic Device.

4.6.4 Ultraviolet-Visible Spectrometer (UV-Vis)

To study the absorption, transmittance, and reflection properties of the light falling on the solar cell. An Ultraviolet-Visible Spectrometer (**UV-Vis**) Type- Shimadzu 1800 was used. The principal work of the device is to emit light with wavelengths similar to that of incoming solar radiation, by measuring the intensity of the incident radiation and transmittance radiation, and by knowing the difference between them the absorbed radiation was measured. The same device is also used to measure the reflectivity of light, with the reflection measurement option. Where the emitted and received, light ratios are read using a lens, and by knowing the difference between them the transmitted and reflected light are measured. Figure (4.22) shows the **UV-Vis** spectrometer device. This device was used in this study to verify the wavelength and absorbance of dyes used as sensitizers in DSSCs. The test process took place at the University of Kufa - College of Science.

General specifications:

- Wavelength range: 190 – 1100 nm
- Wavelength accuracy: ± 0.3 nm (190 to 1100 nm)
- Wavelength repeatability: ± 0.1 nm
- Dimensions (W x H x D): 450 x 270 x 490 mm



Figure 4. 22: UV-V is spectrometer.

4.6.5 Field Emission Scanning electron microscopy (FESEM)

The FESEM apparatus was used to study the outer surface of the prepared TiO_2 and to show the micro-configurations of the membrane surface. Its working principle is to send a beam of electrons over the surface of the sample, which drives the coating. The metallic element causes a shower of electrons to shoot towards a fluorescent screen or photographic plate, which gives an image of the surface of the object. Scanning electron microscopes can magnify objects up to 100.000 times.



Figure 4. 23: FESEM Electron Microscope.

4.6.6 Furnace

Heat treatment means exposing the models to a certain temperature higher than room temperature for a specified period of time. Heat treatment helps to remove crystal defects, as it gives kinetic energy to the atoms of the material that works to rearrange them within the crystal structure, and thus works on the regularity of the grains and their merging with each other and then increasing their size; that is, it stimulates the crystals to grow.

The furnace device, shown in Figure (4.24), was used at Al-Qadisiya University-College of Engineering for the purpose of heat treatment of TiO_2 films. The temperature of this device ranges from (0–1,000 °C).



Figure 4. 24: Furnace device.

4.6.7 X- Ray diffraction

The crystal structure of TiO_2 has been studied, to reveal the effect of annealing at $500\text{ }^\circ\text{C}$ on the crystal structure of TiO_2 films. By studying the X-ray patterns, we can determine when a beam of X-rays is shed at a certain angle on the surface of the membrane as a result of Brack's reflections for parallel crystal surfaces, we get a diffraction pattern for these rays. When the film is of a random type, the reflected wave does not form any peaks; that is, the interference of the reflected beams is scoter. But when the membrane is arranged in a crystalline arrangement, the interference is constructive as a result of the fall of that beam and its reflection from the organized crystals, without any scattering of the beams reflected from those crystal surfaces as a result of their regularity. "**Bragg Law**".



Figure 4. 25: X-Ray device is used to diagnose the crystal structure of membranes.

4.6.8 Temperature Measurement

To study the effect of room temperature on the surface of a dye solar cell. An internal experiment was carried out in the engineering laboratories Najaf Technical College. Experiments were performed under Condition (1000 W/m², room temperature control 25 ° C, the total test time is half hour). K-type thermocouples are installed on the surface of the solar cell and connected to data logger type - **Anpat (AT4532)** for solar cell logging Temperature.

4.6.8.1 Data-Logger

A data logger is a temperature measuring device with multiple channels, as depicted in Figure (4.26). It was very important to study the effect of cell surface temperature on its efficiency. **Anpat (AT4532)** with (32) channels were chosen as the data logger in this thesis. Type K and Type T thermocouples can be used with this instrument, and the read accuracy is 0.2 percent $\pm 1^{\circ}\text{C}$.



Figure 4. 26: Data logger.

4.6.8.2 *Thermocouples*

Type K thermocouples, as shown in Figure (4.27), were used to check the surface temperature of the solar cell. Two K-type thermocouples were installed, one of which is on the back surface of the solar cells, and the second is fixed to record the room temperature. To obtain an actual reading, of the thermocouple, a calibration process was performed. Where the reading of the thermocouples was compared with the reading of the mercury thermometer at the freezing and boiling temperatures (0 °C and 100 °C) respectively, and different readings between (0 - 100 °C). More details on the calibration process are show in Appendix D.



Figure 4. 27: Thermocouples K-types.

4.6.9 Keithley 2400 device

Keithley's Source Measure Unit (SMU) Instruments in Series 2400 are specifically designed for test applications that require tightly coupled sourcing and measurement. All Source Meter models provide precision voltage and current sourcing, as well as, measurement capabilities. Each Source Meter SMU instrument is both a highly stable DC power source and a true instrument-grade 6.5-digit multimeter. The power source characteristics include low noise, precision, and readback. The multimeter capabilities include high repeatability and low noise. The result is a compact, single-channel, DC parametric tester. In operation, these instruments can act as a voltage source, a current source, a voltage meter, a current meter, and an ohmmeter.

Features:

- Five instruments in one (IV Source, IVR Measure)
- Five models: 20–100 W DC, 1000 W pulsed, 1100 V to 1 μ V
- Source and sink (4-quadrant) operation
- 0.012% basic measure accuracy with 6.5-digit resolution

- 1700 readings/second at 4.5 digits via GPIB
- Pass/Fail comparator for fast sorting/binning



Figure 4. 28: Keithley 2400 device.

4.6.10 Coating Thickness Gauge

To measure the thickness of the TiO_2 coating, the TT-260 was used as shown in Figure (4.29). According to the measuring principle, the probe and the magnetic metal substrate will form a closed magnetic circuit when the probe contacts the coating; the magnetic resistance of the closed magnetic circuit varies due to the existence of a non-magnetic coating. The thickness of the coating can be measured through the variation in magnetic resistance. The device is calibrated before initiation to measure the thickness of the layer. By knowing the difference between the two measurements before and after the coating process, the coating thickness was measured. To obtain a more accurate thickness, several readings at several positions are taken on the

surface of the solar cell and take the average readings are the average thin film thickness obtained (30 μm) and (12 μm)



Figure 4. 29: Coating Thickness Gauge.

4.6.11 Solar Power Meter

The device that measures the intensity of radiation reaching the solar cell it is called a solar power meter, or (Pyrometer). This device was used in this thesis to fit the height between the halogen light source and the solar cell, there by controlling the radiant flux at $1000\text{W}/\text{m}^2$. Indoor experimental work in the laboratories of the Engineering Technical College of Najaf was performed where the solar radiation intensity was constant as a function of time. The solar power meter (Pyrometer) is shown in Figure (4.30). Before using, the calibration process should be done, and it was performed by taken the reading of intensity light at dark, which record ($1000\text{ W}/\text{m}^2$). Several readings were taken to ensure the appropriate height between the halogen light source and the solar cell surface, which gave the light intensity $1000\text{W}/\text{m}^2$.

The device contains a sensing lens, control buttons, and an LCD monitor. Its specifications and calibration were listed in Table 4.3, and Appendix E.



Figure 4. 30: Solar Power Meter.

Table 4. 3: specification of Solar Power Meter.

Specifications	Details
Type	Tenmars TM-207
Reading range	0-2000 W /m ²
Accuracy	± 10 W/m ²
Reading time	0.25Second

CHAPTER FIVE

RESULTS AND DISCUSSION

5.1. Introduction

This chapter, present the experimental result obtained from testing the materials used in manufacturing of DSSCs, as well as, the performance of DSSCs such as efficiency, open circuit voltage, maximum power (η , FF , P_{max} , J_{sc} , V_{oc}). The results of the current study will be presented, which are represented by the optical properties such as the absorbance of the dyes used as sensitizers in this research, as well as, the structural properties of TiO_2 models (**FESEM, X-Ray**).

5.2. Experimental validation

Should be mentioned in the experimental section[31]. This was done to make sure that it would work and that the results would be reliable. DSSC is manufactured using dyes extracted from the leaves of the shea plant. The anode was also manufactured using FTO glass (with a resistance of 15Ω) with TiO_2 after the anneal it at a temperature of $450 \text{ }^\circ\text{C}$. Through the schemes shown in Figures 5.1 and 5.2, we note that the error rate is very low, which is equivalent to 1.3% for efficiency. The error rate was calculated based on the equation shown[83]:

$$\%Error = \frac{Exact\ value - Approx\ value}{Exact\ value} * 100 \quad 5.1$$

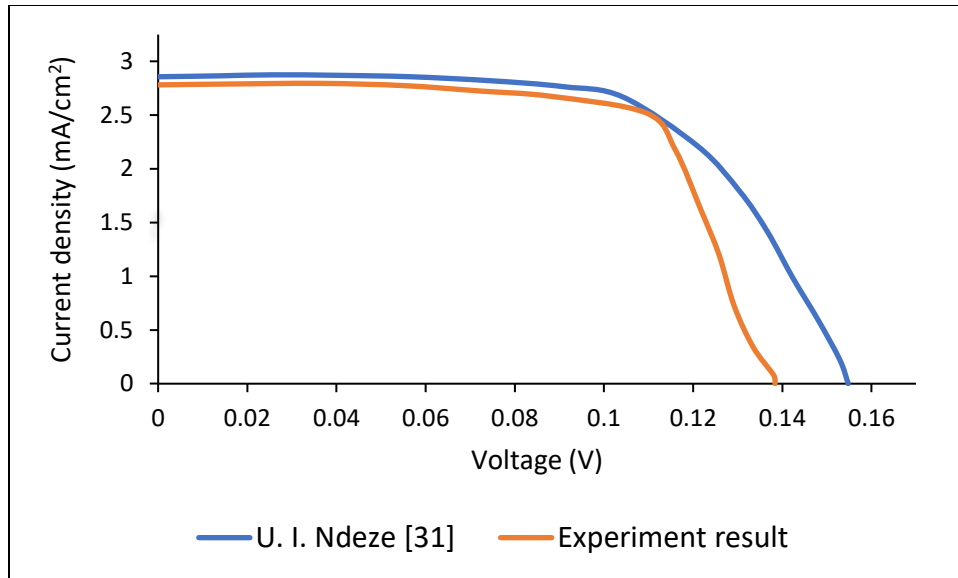


Figure 5. 1: Verification results for I-V with Ref [31].

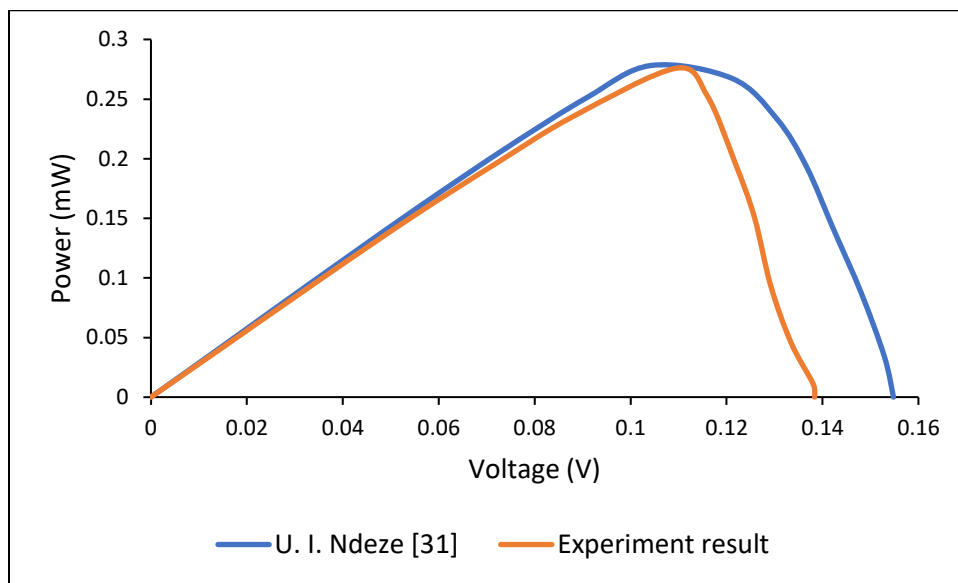


Figure 5. 2 : Verification results for P-V with Ref [31].



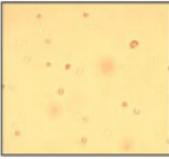
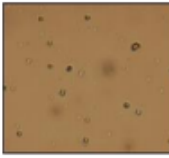
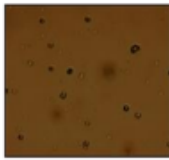

5.3 Structural properties of TiO_2


5.3.1 Characterization of TiO_2 layer

TiO_2 layer deposition on a conductive FTO glass substrate at $500\text{ }^\circ\text{C}$ was prepared by doctor blade technique. The experimental results showed that TiO_2 was transparent and porous.

The gradual increase in temperature upon annealing gave good results in preparing TiO₂ films. Taking into consideration that the models should not be raised immediately after heating to prevent their breakage, the models are left in the ovens until they cool down. The color difference of TiO₂ films at different temperatures is shown in Table 5.1.

Table 5. 1: TiO₂ color at different temperatures and time.

Temperature (°C)	Time (min)	Color	Figure
100	10	Milky	
150	10	Milky	
200	10	Light yellow	
250	10	Yellow-Brown	
300	10	Brown – Dark Brown	
350	10	Dark Brown	
400	10	Getting lighter color	
450	15	Color less	

500	15	Color less	
-----	----	------------	---

The TiO₂ film strengthens with the increase in temperature, as some of the materials that were placed during the preparation of the paste will volatilize with the increase in temperature.

5.3.2 X-Ray Measurement Results

X-ray test were carried out on the films prepared on FTO glass. The nature of TiO₂ plays a very important role in dye adsorption, as well as, controls of efficiency and photocatalytic processes due to the details of different binding patterns. These tests showed that all of these films are in the anatase phase through peaks (20.144, 25.005, 37.795, 47.776, 54.212, 62.370, and 75) with respect to TiO₂. The anatase phase is considered an active phase due to its surface chemistry and its high conduction band. This phase shows better performance for DSSCs than the rutile phase. This was extensively studied by Park et al. in 2000 [84]. Also, by examining the X-Rays, a noticeable increase in the height of the peaks was shown, as shown in Figures 5.3 and 5.4. These results are consistent with the tables of the American Society for Testing's Materials (**A.S.T.M.**). It is also observed from Figures 5.3 and 5.4 that there are no phases of impurities or other oxides in the crystal structure. We can determine the crystal size, which is the primary determinant in influencing the electron transport properties of materials, through the equation : [85]

$$d = \frac{0.9\lambda}{\beta \cos(\theta)} \quad 5.2$$

In this equation, θ is the diffraction angle, β is full width at half maximum for each peak, and λ is employed X-Ray wavelength.

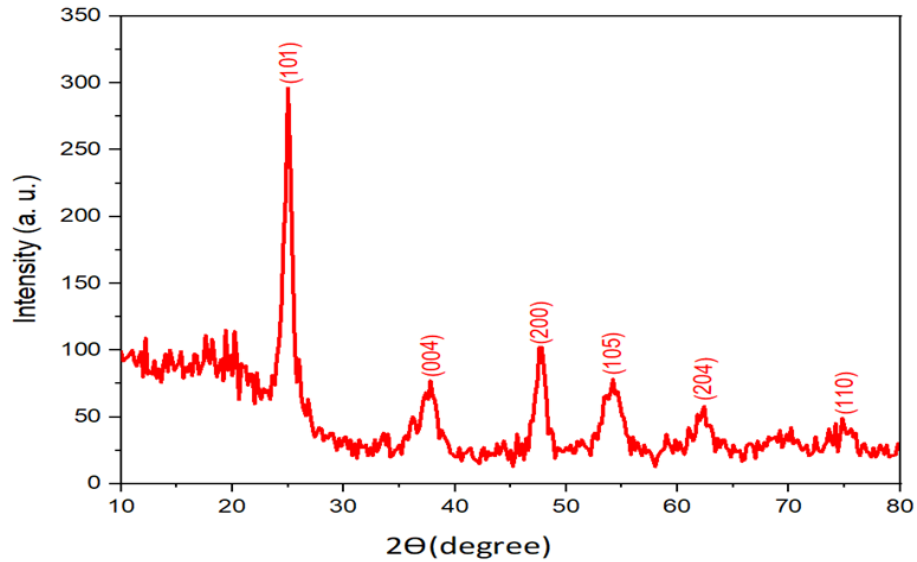


Figure 5. 3: X-ray diffraction of TiO₂ before heat treatment.

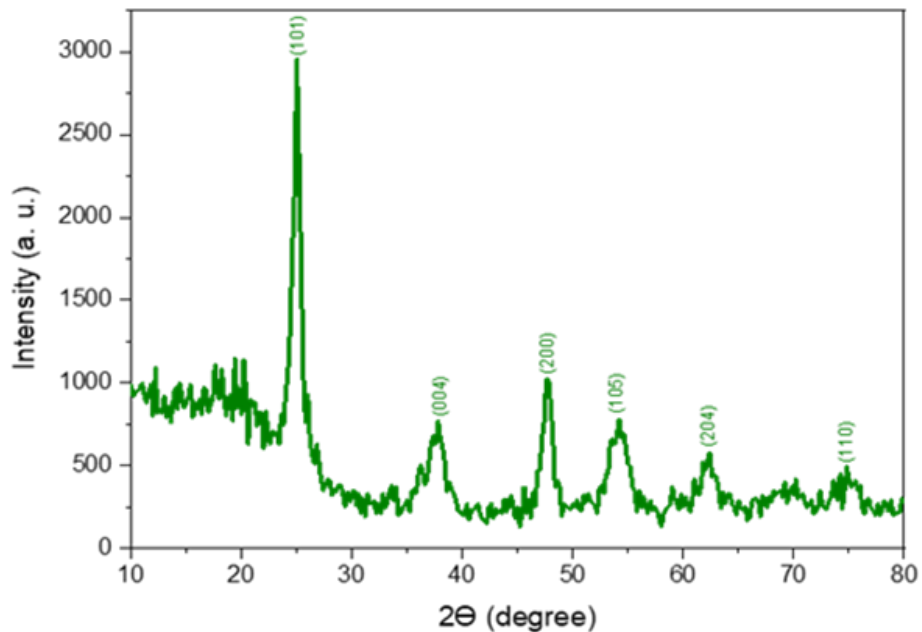


Figure 5. 4: X-ray diffraction of TiO₂ after heat treatment.

To ensure that the pigments extracted from the leaves were adsorbed on the surface of TiO₂, the inhibition of TiO₂ crystallization was verified by

XRD. The Figure (5.5) shows the TiO_2 spectra before and after dye adsorption. The main peak intensity at $2\theta = 25^\circ$ was high before dye adsorption and remained at its peak after dye adsorption.

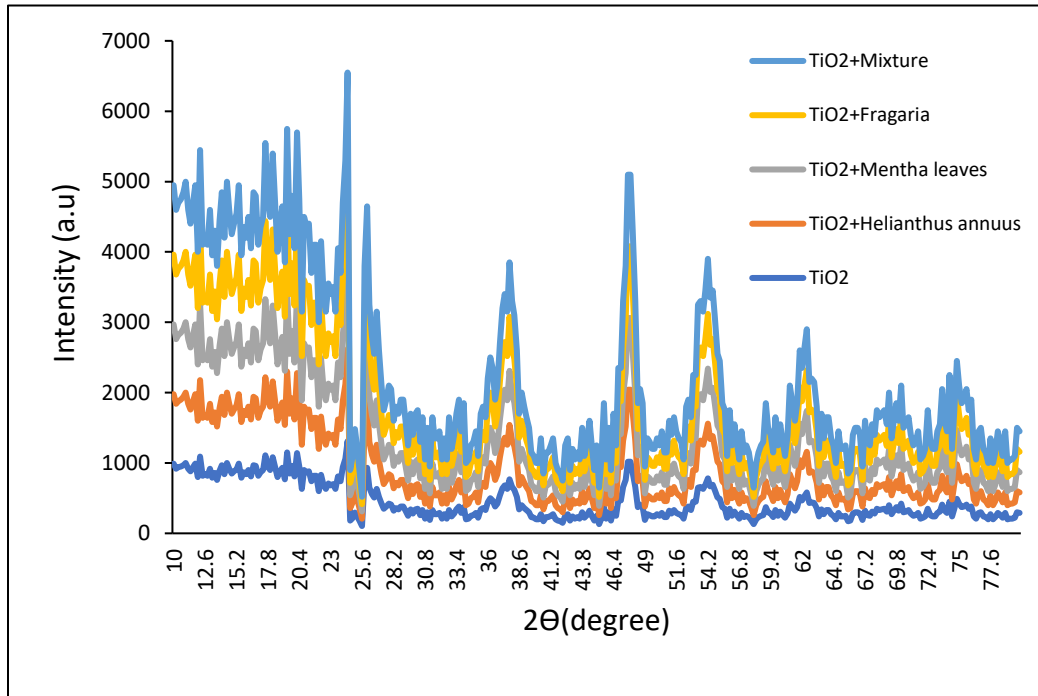


Figure 5. 5: XRD spectra of pure TiO_2 and TiO_2 -dye.

5.3.3 Energy Dispersive Using X-Ray (EDX)

Figure 5.6 shows the energy dispersive X-Ray spectroscopy. This was carried out to reveal the elements present in the deposited TiO_2 film. The analysis confirms the presence of titanium, oxygen, sodium, and calcium at 36.64 at.%, 55.64 at.%, 4.34 at.%, and 3.60 at.%, respectively. The presence of minor traces of other elements (calcium and sodium) could be attributed to interactions of secondary electrons from the FTO glass substrate. The higher percentage of atomic weight distribution of oxygen and titanium is confirmed by the EDX showing that TiO_2 film was deposited.

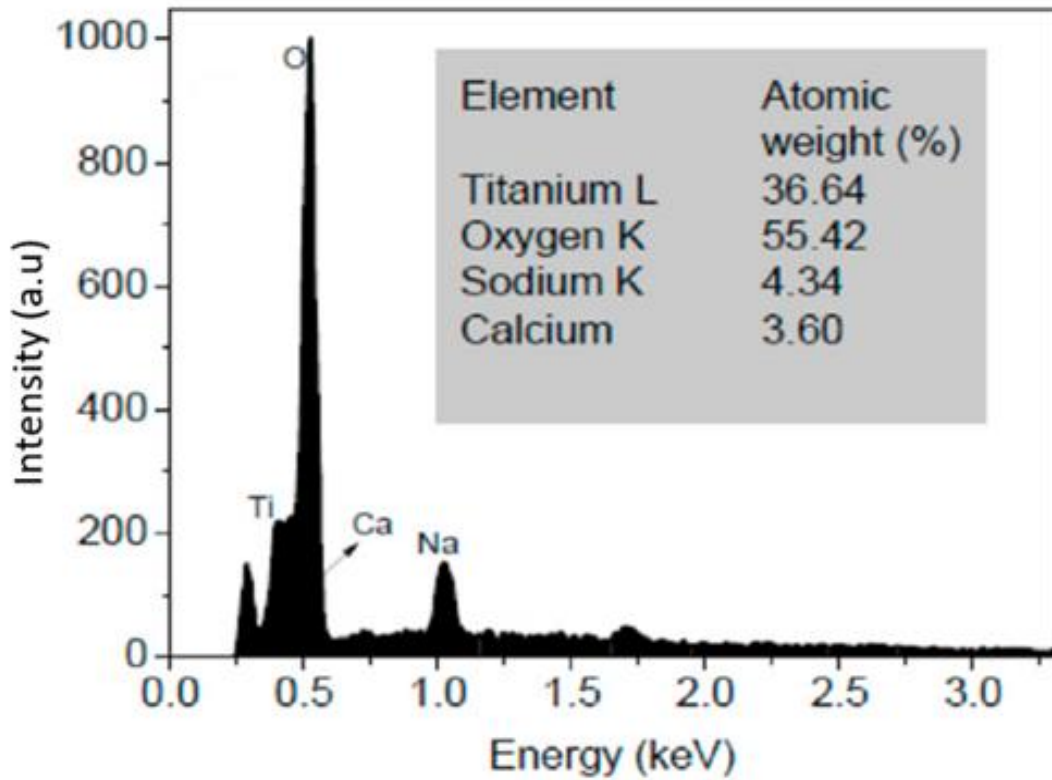


Figure 5. 6: EDX spectra of TiO₂.

5.3.4 Field Emission Scanning Electron Microscopy (FESEM)

To confirm the creation of TiO₂ nanostructured films, field emission scanning electron microscopy (FESEM) measurements are often performed [86]. When TiO₂ films were heated to less than 450 °C, they were found to produce an imperceptible current even in the A range, making them ideal for solar cells [87]. Even the TiO₂ film that has been created is sintering at 500°C. Cracks in the TiO₂ layer are clearly visible in the FESEM picture seen in Figures 5.7 and 5.8. In order to address this issue, a second TiO₂ layer was placed on top of the first, and the TiO₂ film was annealed at 500 °C before being exposed to light. Figures (5.7 and 5.8) show a FESEM image of a TiO₂ film with two layers. It would seem that the TiO₂ film is denser than the other films when compared to one layer. On the other hand, in spite of the fact that

there are still a few minor fractures in the FTO glass, its surface quality has finally improved.

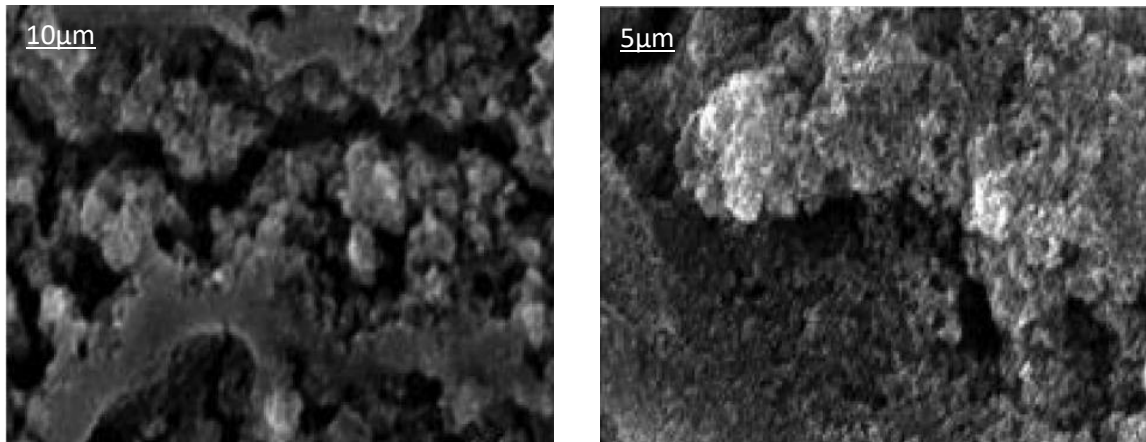


Figure 5. 7: At 500 °C, FESEM pictures of a single TiO₂ layer at 5 μm and 10 μm.

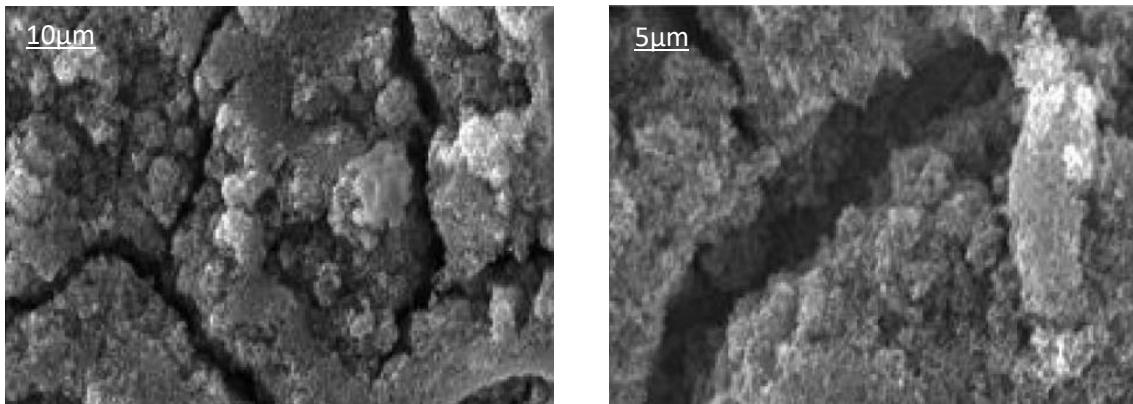


Figure 5. 8: At 500 °C, FESEM pictures of a two TiO₂ layer at 5 μm and 10 μm.

The exact structural property of TiO₂ film was also examined using FESEM, as shown in Figure 5.9, which shows that TiO₂ is oriented in the form of random and spherical grains with a size of (27 ± 3) nm covering the FTO substrate. These particles are formed due to assembly during the annealing process and good agglomeration. This makes it suitable for enhanced FTO glass surface coverage, which improves electrical conductivity within the particle network and converts light energy (photons) into electrical energy.

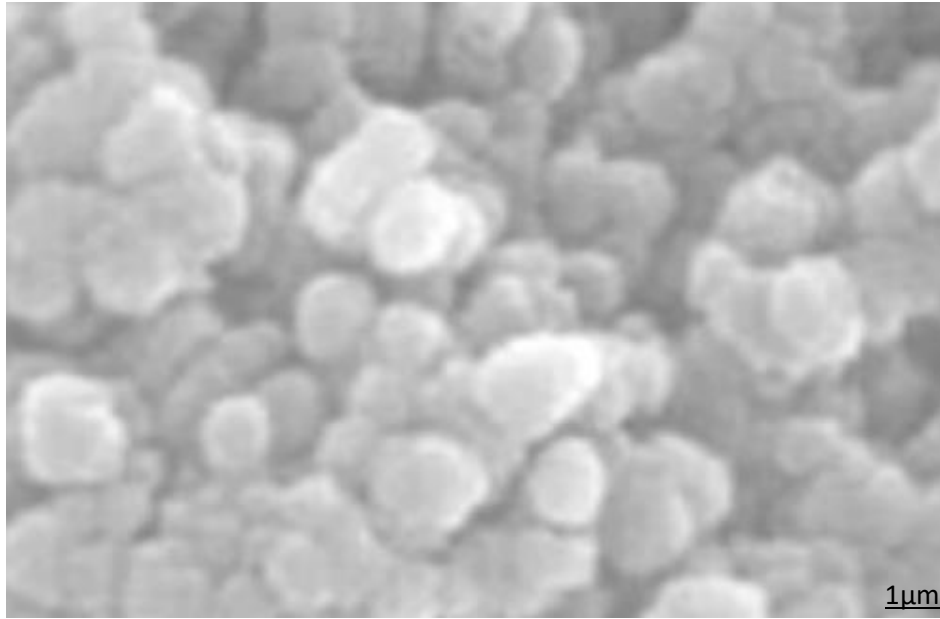


Figure 5. 9: FESEM image of TiO₂

5.4. The results of optical measurements for TiO₂

Figure 5.10 shows the adsorption behavior of the as-prepared TiO₂. It shows that the TiO₂ film annealed at 500 °C had an absorption peak of 318 nm for the single layer of TiO₂ while the absorption peaks for the two layers were 320 nm with a capacity bandgap of 3.899 eV and 3.875 eV, respectively. The energy bandgap of dyes adsorbed by a TiO₂ surface was calculated using Eq. 3.9.

The results of this study on the optical energy bandgap are consistent with previous studies[88][89].

The results show that the absorbance in the visible light region decreases significantly for TiO₂ with one or two layers. Also, the absorbance of the films depends on the thickness of those films in terms of the absorption peak and the amount of absorption.

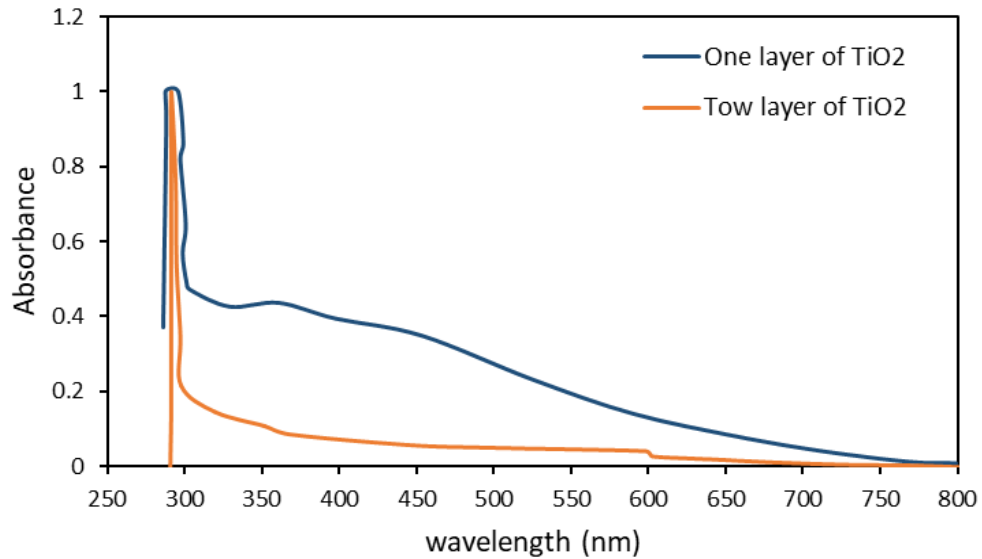


Figure 5. 10: Absorption spectrum of TiO₂.

Figure 5.11 shows that the TiO₂ film that was poured on FTO glass allows the transmission of visible light and absorbs ultraviolet rays. The average visible light transmission of TiO₂ after casting on the FTO substrate reduces to about 74.34%. However, FTO coating allows maximum transmission of visible light to the dye (sensitive material) for optimal absorption and conversion to electricity in DSSC, while blocking harmful UV rays.

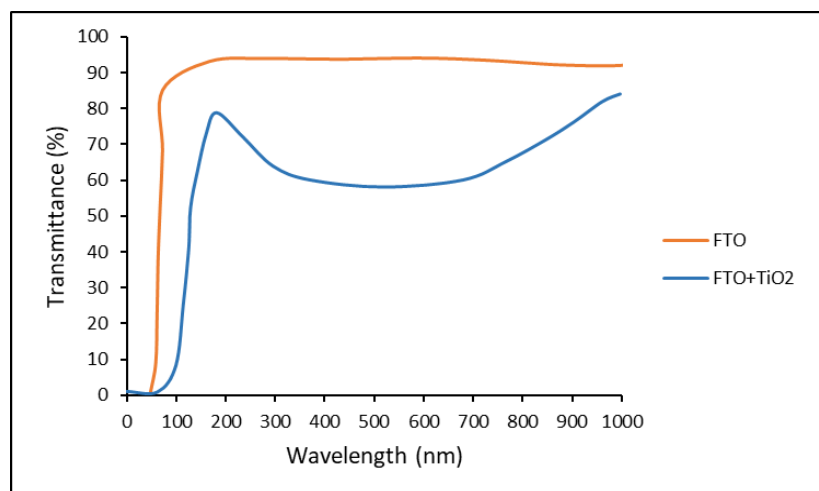


Figure 5. 11: Transmitter spectra of FTO and TiO₂ film cast on FTO.

5.4.1 Absorption Coefficient

The radiation intensity through different media decreases exponentially from type ($e^{-\alpha t}$) where (α) the absorption coefficient in the flux of radiation energy. To calculate the absorption coefficient, the absorbance data (A) and the thickness of one film (t) are used.

Calculating the value of the optical absorption coefficient is done in several ways, the most important of which is based on equation No. (3.14) after making the necessary corrections to the absorption spectrum. The thickness of the two layers of TiO₂ is 30 μm , while the thickness of one layer is 12 μm .

From Figure (5.12), the change of the absorption coefficient with the photon energy of the TiO₂ film, as we note that its value is greater than ($7 \cdot 10^4 \text{ cm}^{-1}$) for the wavelength range from (250-800) nm, this value changes with the increase of the photon energy, which intern helps to predict the occurrence of direct electronic transitions within the above-mentioned wavelength range.

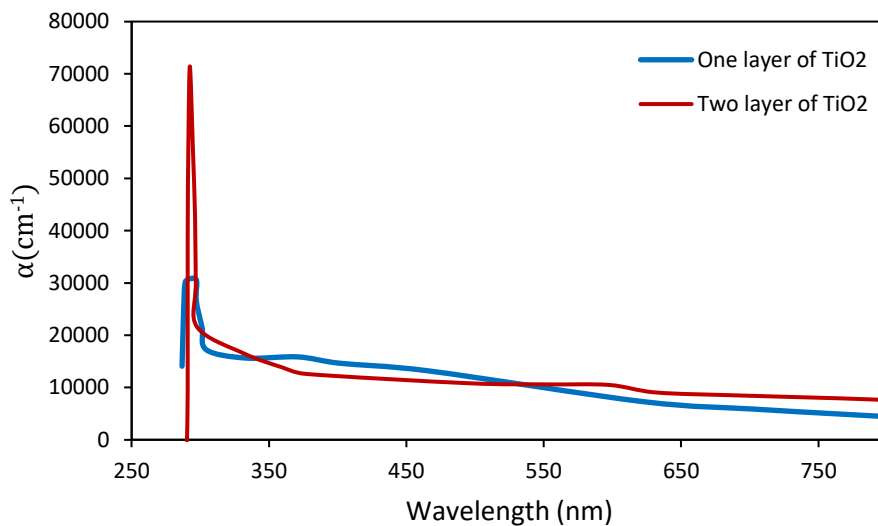


Figure 5. 12: Relationship of the absorption coefficient and wavelength of TiO₂.

5.4.2 Reflectance

The reflectivity was calculated using a UV-vis device. Figure 5.13 shows the reflectivity spectrum of TiO₂ films, where we notice that the reflectivity of TiO₂ begins to increase and decrease gradually due to the increase in the photon energy within the wavelength range (250-800nm), as the reflectivity behavior of TiO₂ varies from case to case. because the reflection coefficient R varies according to the method of preparation.

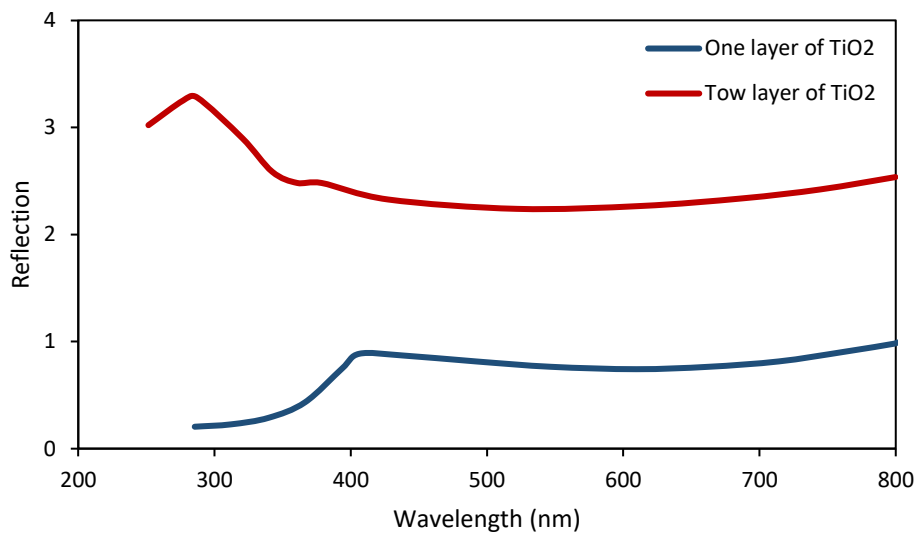


Figure 5. 13: The relationship between the reflection coefficient and the wavelength of the TiO₂ film.

5.4.3 Refractive Index

The refractive index of TiO₂ films was calculated from Equation No. (3.12). Figure 5 .14. Changing the refractive index as a function of photon energy for TiO₂ films We note that the nature of the refractive index curve is almost similar to the nature of the reflectivity curve due to the correlation of the reflectivity with the refractive index as in Equation No. (3.12). The refractive index of TiO₂ films increases with increasing energy, and the lowest value of the refractive index is (1).

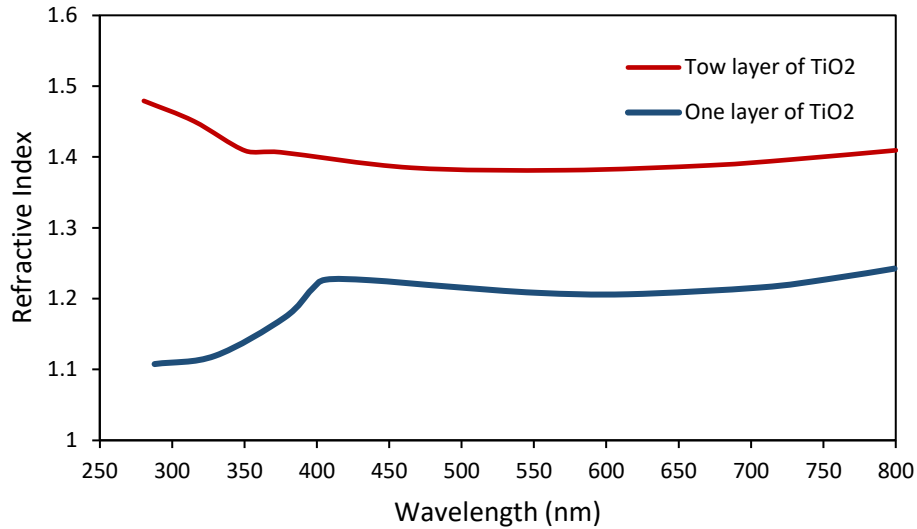


Figure 5. 14: The relationship between the refractive index and the wavelength of the TiO₂ film.

5.4.4 Extinction Coefficient

The imaginary part of the complex refractive index is called the damping index (K_0) as mentioned in equation (3.11).

The extinction coefficient of TiO₂ was calculated using equation (3.13) and it is noted that the inertia coefficient is directly related to the absorption coefficient (α). Figure 5.15 shows the change of the damping coefficient as a function of the photon energy for TiO₂ films. We see that the peaks of the damping coefficient are almost the same and get smaller as the energy of the photon goes up in the 300-800 nm range. The reason for the low attenuation coefficient within this range of the spectrum is the high light transmittance of TiO₂ films within the visible light region.

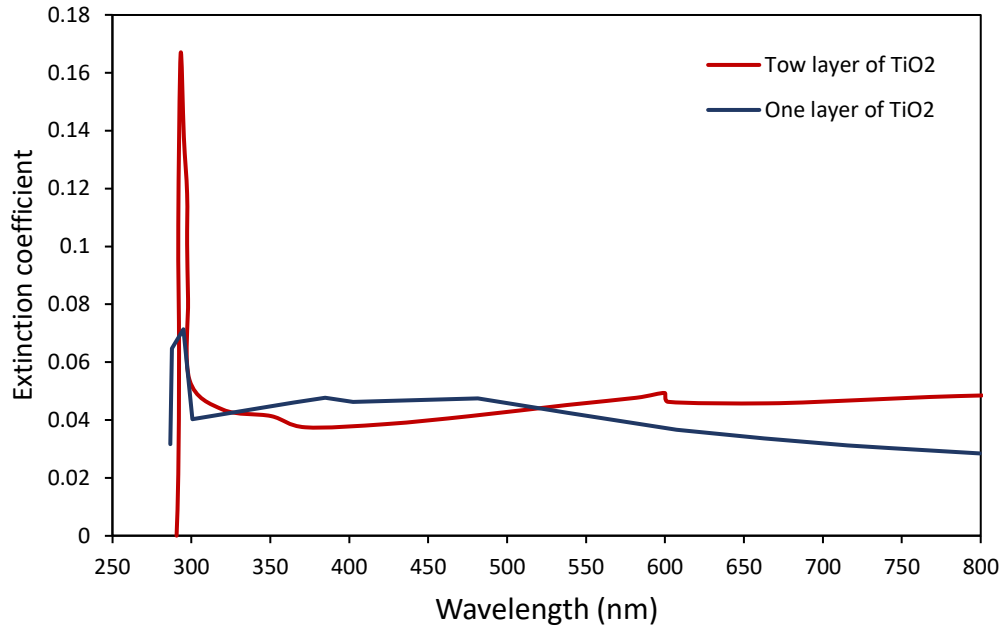


Figure 5. 15: Relationship of the damping coefficient with the wavelength of the TiO₂ film.

5.4.5 Dielectric Constant

The complex dielectric constant of the medium (ϵ) can be calculated using equations (3.16) and (3.17), and from equations (3.18) and (3.19) the real and imaginary parts of the dielectric constant were calculated for TiO₂ films, from Figure (5.16) it is clear that the real part of the dielectric constant changes with similar photon energy. Because of the nature of the change in refractive index with photon energy, and this is consistent with relationship No. 3.18, where the effect of the damping coefficient is very small in comparison to the effect of the refractive index. It was noticed that the peak values of the real dielectric constant increase gradually with increasing energy.

Figure (5.17) shows the imaginary part of the dielectric constant, and it is noted that the nature of its change with photon energy is similar to the nature of changing the damping coefficient with photon energy, as we find that it

increases gradually at low energies, and then we get a rapid increase at high photon energies and the reason for this is the correlation of the damping coefficient with this constant with the relation (3.19).

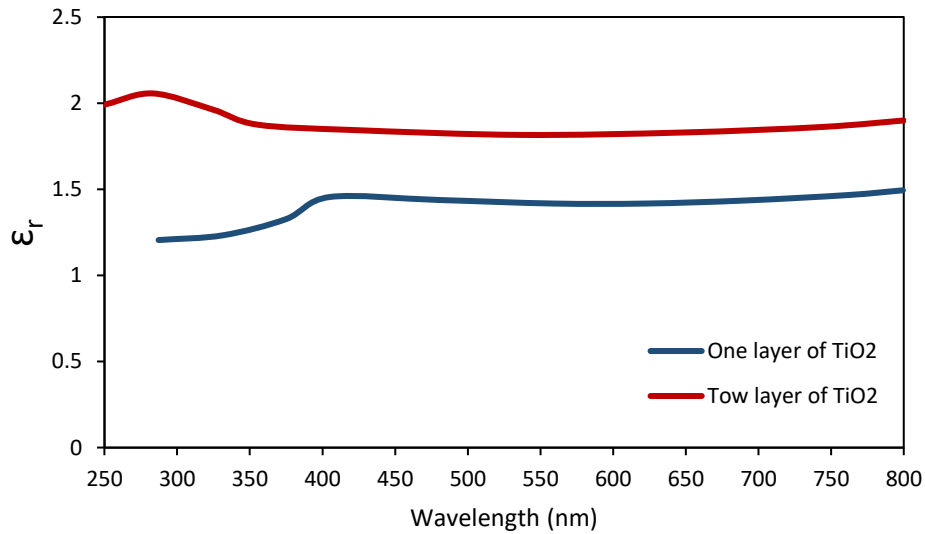


Figure 5. 16: Relationship of the true dielectric constant with the wavelength of the TiO_2 film.

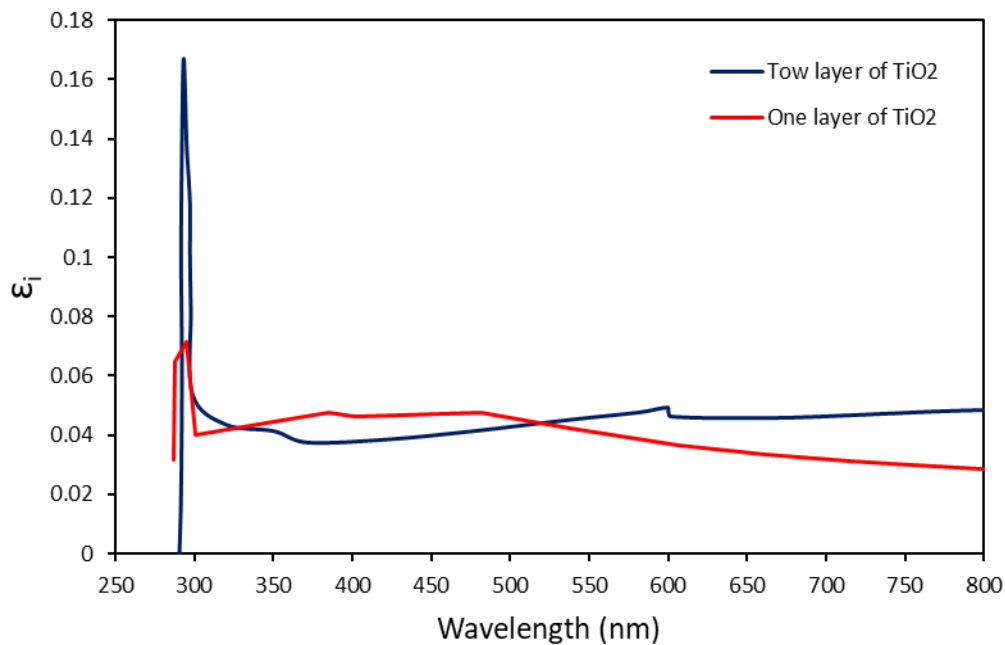


Figure 5. 17: Relationship of the imaginary dielectric constant with the wavelength of the TiO_2 film.

5.5. Optical characterization of dyes

UV-visible spectroscopy was used to measure the optical properties of the prepared dyes (*Helianthus annuus* leaves, *Mentha* leaves, and *Fragaria*) when they were dissolved in acetone, ethanol, and methanol to find out the best solvent. It is also used to find out the absorption of dyes in the visible region (300–800 nm), which is plotted and presented in Figure (5.18), Figure (5.19), and Figure (5.20), where it was observed that the three dyes can absorb light in the visible region when dissolved in any of the solvents used, making them suitable for use as inducers in DSSCs. When acetone was used as a solvent to extract the dyes, it showed a higher absorption density than the dyes extracted using ethanol and methanol as solvents, and the reason for this may be due to their respective organic groups.

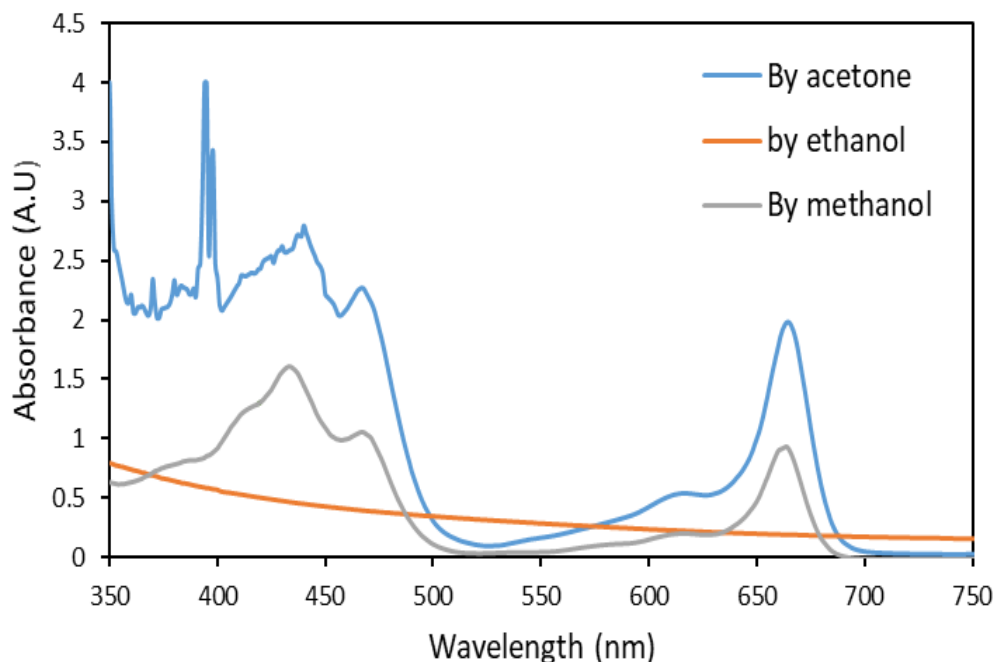


Figure 5. 18: UV-V is absorption spectra of *Helianthus annuus* in different solvents.

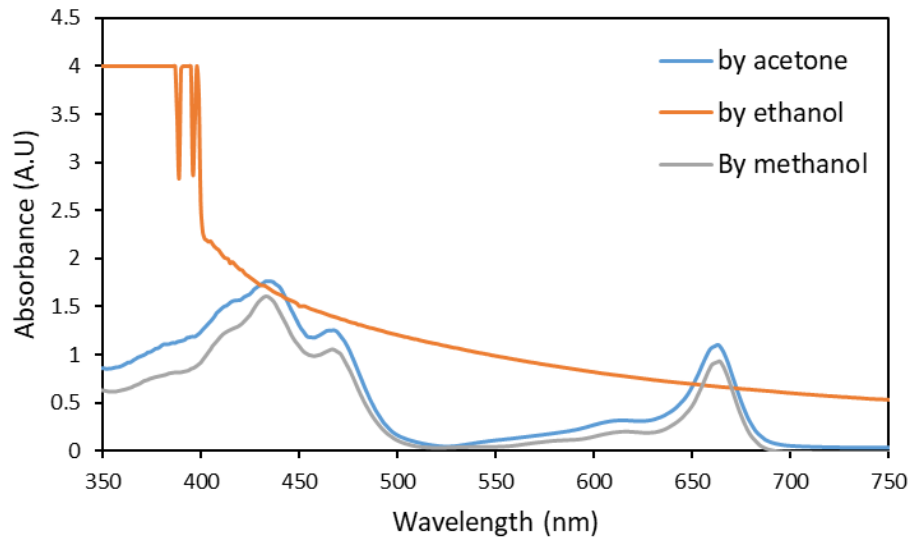


Figure 5. 19: UV-V is absorption spectra of Mentha leaves in different solvents.

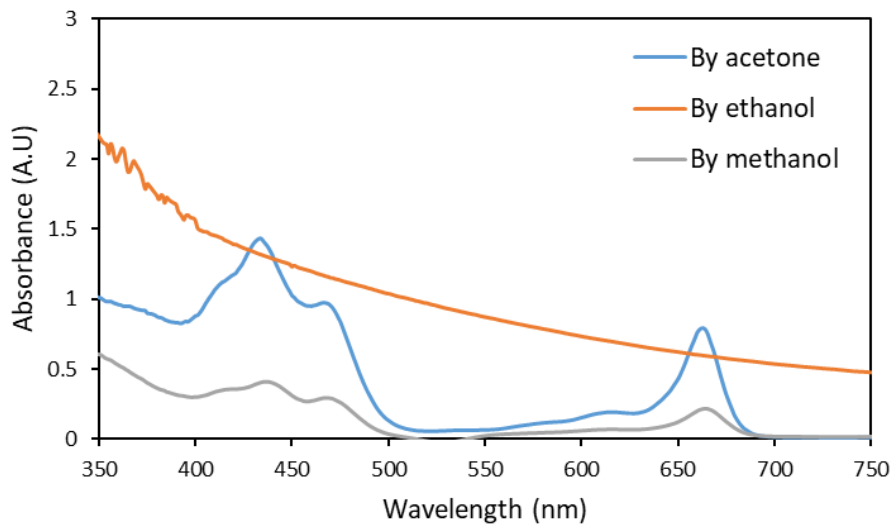


Figure 5. 20: UV-V is absorption spectra of Fragaria in different solvents.

Referring to Table 5.2, it was noted that the dyes extracted using acetone had the highest energy gap compared to other solvents, as *Helianthus annuus* leaf dye had the highest energy gap equal to 3.02 eV, while it showed the highest energy gap for Mentha leaves and Fragaria at 2.82 eV and 2.83 eV, respectively. In the year 2020, researcher S. Sowmya and others confirmed that a smaller energy gap leads to a lower voltage [90].

Table 5. 2: Absorption peaks and band gap energies of the isolated dyes.

Name of the dye	solvent	Absorption wavelength peak (nm)	Band-gap energy (eV)	
Helianthus annuus leaves	Ethanol	-	-	
	Methanol	443	2.79	
		451	2.75	
		663	1.87	
	Acetone	410	3.02	
		451	2.99	
		445	2.78	
		456	2.72	
		609	2.04	
	Mentha leaves	Ethanol	401	3.09
Methanol			442	2.80
			465	2.67
		664	1.87	
Acetone		440	2.82	
		465	2.67	
		665	1.86	
Fragaria	Ethanol	338	3.67	
	Methanol	447	2.77	
		453	2.74	
		651	1.90	
	Acetone	439	2.83	
		464	2.67	
664		1.87		

This result was similar to what researchers S. Sowmya et.al [39] and M.Z. Najihah et.al [41].

Equal amounts of each extract were mixed to form a new dye. Which was checked for absorbance and compared with the rest of the dyes as shown in Figure (5.21). The absorption spectra showed that each type of dye had its own absorption peak in the visible range.

Mentha leaves: The optical absorption spectrum of Mentha leaves shows the peak absorption rate in the visible region at wavelengths of (425 - 451) nm, (474 - 460) nm, and (649 - 687) nm, thus three peaks appear at 440 nm, 465 nm, and 665 nm. Such areas appeared to have Fragaria, but Fragaria absorption was lower at each top.

Helianthus annuus: The optical absorption spectrum of Helianthus annuus shows the highest absorption peaks in the visible region from the lowest (409-450) nm, to the highest (640-689) region, where the absorption peaks appear at 410 nm, 415 nm, 445, 465, 609 nm, and 665 nm.

Mixture of dyes: The optical absorption spectrum of the mixture shows the peak absorption rate in the visible region at wavelength (405 - 450) nm, (450 - 458) nm, (458-500) nm, (556-593) nm, (600-645) nm, and (647 - 697) nm. It also shows a large number of peaks.

Thus, it can be concluded that the nature of the solvent used to extract the dyes can affect the concentration of the dye due to the presence of different chemical compounds in plants, and accordingly, they have different solubilities in different solvents. Also, it can be concluded that the optimal combination of dyes showed better cumulative absorption properties and that the absorption spectrum was broader and higher. Absorption in the visible range increases the possibility of converting higher solar energy into an electrochemical form.

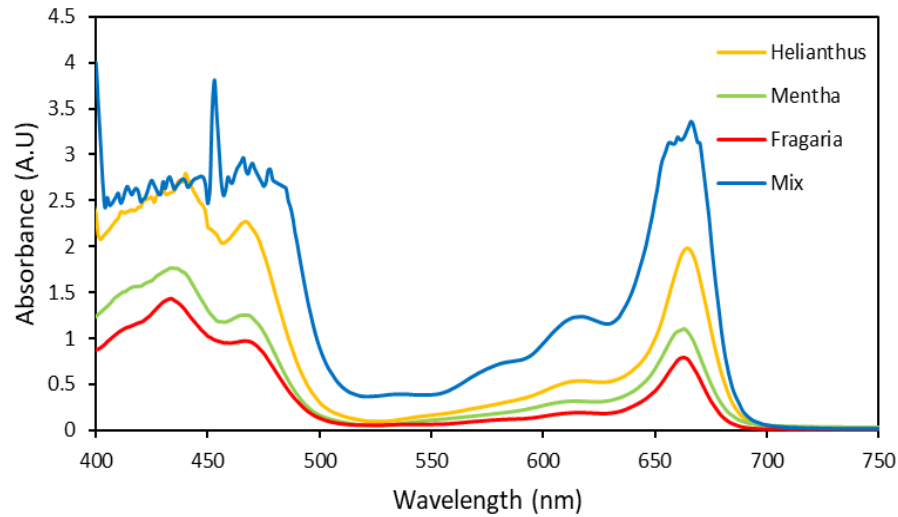


Figure 5. 21: UV-V is absorption spectra of Mentha leaves, Helianthus annuus, Fragaria, and a mixture of the three with various peak locations.

5.6. Optical properties of electrolytes

The absorption and transmittance spectra of the electrolyte were studied using a UV-vis device, and it was found that the light transmittance is the highest possible in the visible light region and that its absorption peak is in the ultraviolet region of the solar spectrum. Figures (5.22 and 5.23) show the absorption and transmittance spectra of the electrolyte.

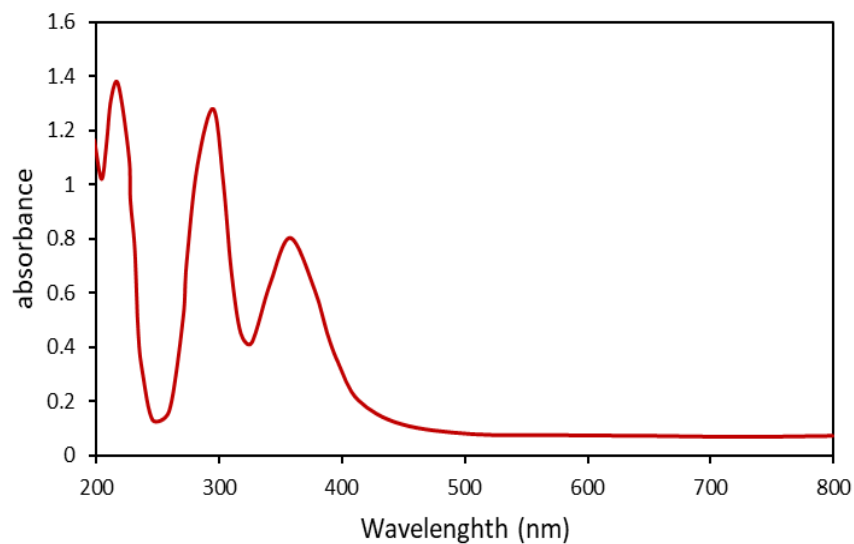


Figure 5. 22: Electrolyte absorption spectrum.

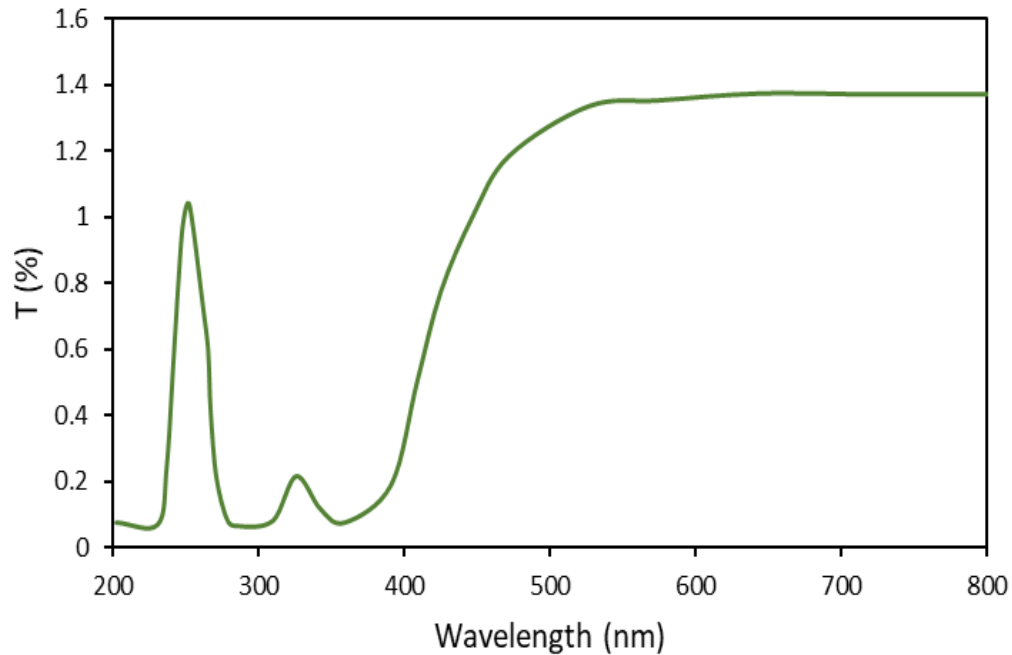


Figure 5. 23: Electrolyte permeability spectrum.

5.7. Solar cell surface temperature with time

The performance of DSSCs devices as a function of temperature is crucial for technical development and for accurate commercial information. Along with solar irradiance, temperature is the most important operating factor in the DSSCs device's performance.

Figure 5.24 shows that the temperature of the cell increases with time when a light of intensity $1000\text{W}/\text{m}^2$ is shone vertically on it. The total test time of the cell under the light was 30 minutes. The highest temperature the cell reached after a half hour was 57.3 degrees Celsius. Because of the rise in the surface temperature of the cell, the effect of this on cell efficiency was studied in the next few paragraphs.

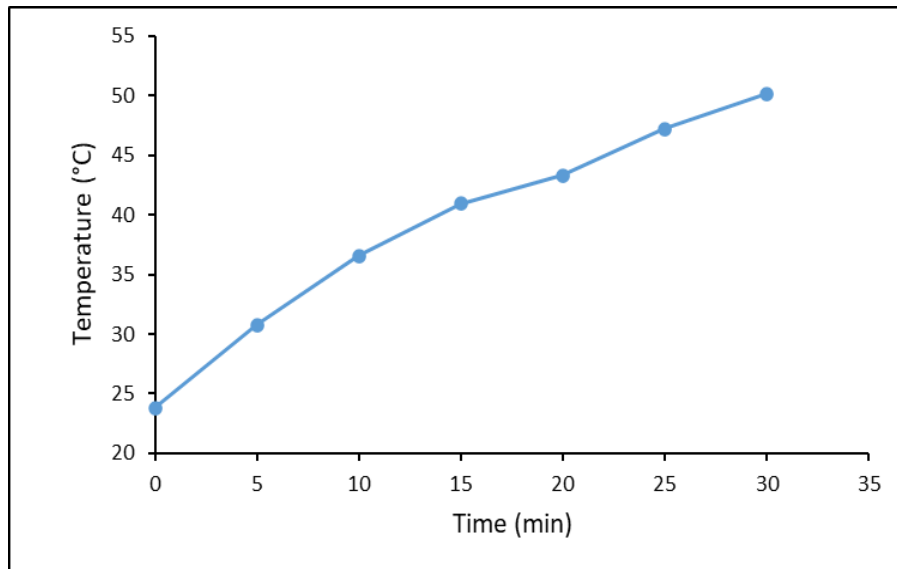


Figure 5. 24: DSSC surface temperature with time.

5.8. DSSCs measurement results

5.8.1. Study the effect of types of dyes on performance of DSSCs

Photovoltaic tests of DSSCs using natural dyes as catalysts were performed by measuring the I-V curve of each cell under white light (1000 W/m^2) from a high-pressure mercury arc lamp. An evaluation of the performance of the natural dye as a catalyst in DSSCs was performed using the following parameters: short circuit current, fill factor, open circuit voltage, and power conversion efficiency. When using dyes derived from Mint, Helianthus annuus, and Fragaria, as well as, a fourth dye consisting of equal amounts of each of the three dyes above, and the I-V curve shown in Figure (5.25). Therefore, sensitizer dyes have a significant effect on the performance of DSSCs.

The short-circuit current has the highest value in DSSC based on the mixture of dyes. While it showed the highest open circuit voltage with DSSC based on Mentha leaves. Power output of the DSSC was computed using IV data as $P = I V$. Figure (5.26) shows the power estimated as a function of V

for DSSC sensitized by a dye combination as an example. The photoelectrochemical properties of the DSSCs sensitized with natural dyes are listed in Table 5.2. The fill factor of the fabricated DSSC ranges between 46.44% and 73.55%. The V_{oc} changes from (0.38 to 0.59) V and the J_{sc} varies from (0.51 to 1.59) mA/cm^2 . The DSSC sensitized by a dye combination produced the greatest results, with a cell efficiency of 0.69%.

The higher efficiency of the cell based on the mixture of dyes can be attributed to the energy gap range, which is narrower than the rest of the dyes and the wider absorption spectrum. The narrow bandgap causes electrons to be easily promoted from the highest vacant moving orbital (HUMO) to the lowest orbital (LUMO). Also, the broad absorption spectrum of the dye mixture is commensurate with the performance of DSSCs, which makes them an improved mechanism for transferring electrons to TiO_2 .

The strong J_{sc} indicates a high excitation energy as the J_{sc} depends on: the area of the DSSCs, the number of photons falling on the cell, the absorption spectrum, optical properties, and the method of cell assembly [91]. All the factors mentioned above are the same for all cells based on different pigments, except for the optical properties of the dyes, which are explained in paragraph (5.12). The dyes prepared with acetone (specifically the dye mixture) have better absorbance than other dyes, which makes a difference in the optical properties of DSSCs. Therefore, DSSCs based on the mixture dye showed the height current as they have a high-power band (3.08 eV, 2.69 eV, 2.23 eV and 2.17 eV), and accordingly, with the increase of the power bandgap, the current increases and the voltage increases.

In other experiments, when adding Ag to the dye and conducting the required examination of the cell, there was no efficiency for DSSCs, the reason for this is that the dye was completely dissolved when Ag was added to it, as explained by Md. Rashid et al.[92]. This causes the light-absorbing part to be absent in DSSCs, causing cell failure.

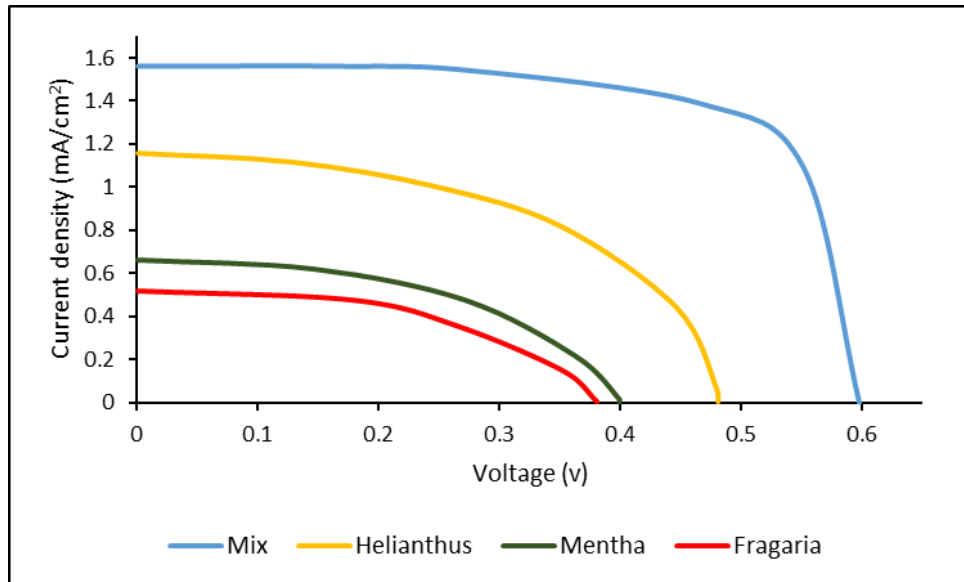


Figure 5. 25: I-V curve for DSSCs depends on dyes

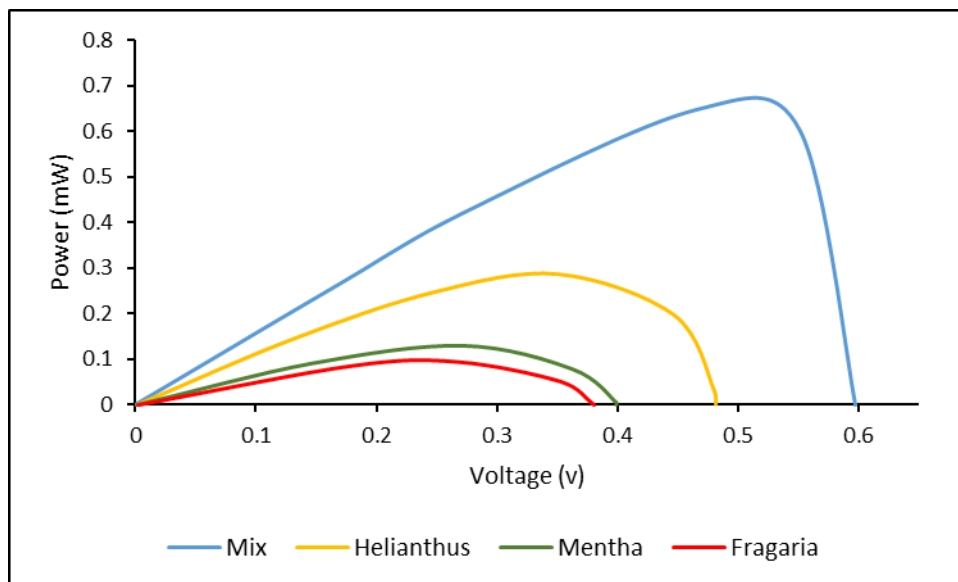


Figure 5. 26: P-V curve for DSSCs depends on dyes.

Table 5. 3: Performance of DSSCs based on dyes.

Dye	$V_{oc}(v)$	$J_{sc}(mA)$	η (%)	FF (%)
Fragaria	0.38	0.51	0.09	46.44
Mentha leaves	0.41	0.64	0.15	57.16
Helianthus annuus leaves	0.48	1.19	0.29	50.77
Mix	0.59	1.59	0.69	73.55

5.8.2. Study the effect of types of counter electrodes

In another experiment, carbon soot was used as counter electrodes instead of Pt for DSSCs based on a dye mixture. Despite the very low cost of carbon, the efficiency of DSSC based on carbon soot is $1.52 \times 10^{-5}\%$, which is much lower than DSSC based on Pt. Also, as shown in Figures (5.27) and (5.28), the current density is very small, which caused a decrease in efficiency. This decrease is due to the fact that carbon soot has very weak electrical stimulation and is also very weak for adhesion with FTO, which causes problems in the stability of the cell, and the electron transfer is slow to achieve the performance of DSSCs. Whereas Pt has excellent catalytic properties accompanied by light reflectance properties. It also showed excellent electrocatalytic activity which promoted smooth and rapid transfer of electrons to electrolyte through reduction reaction.

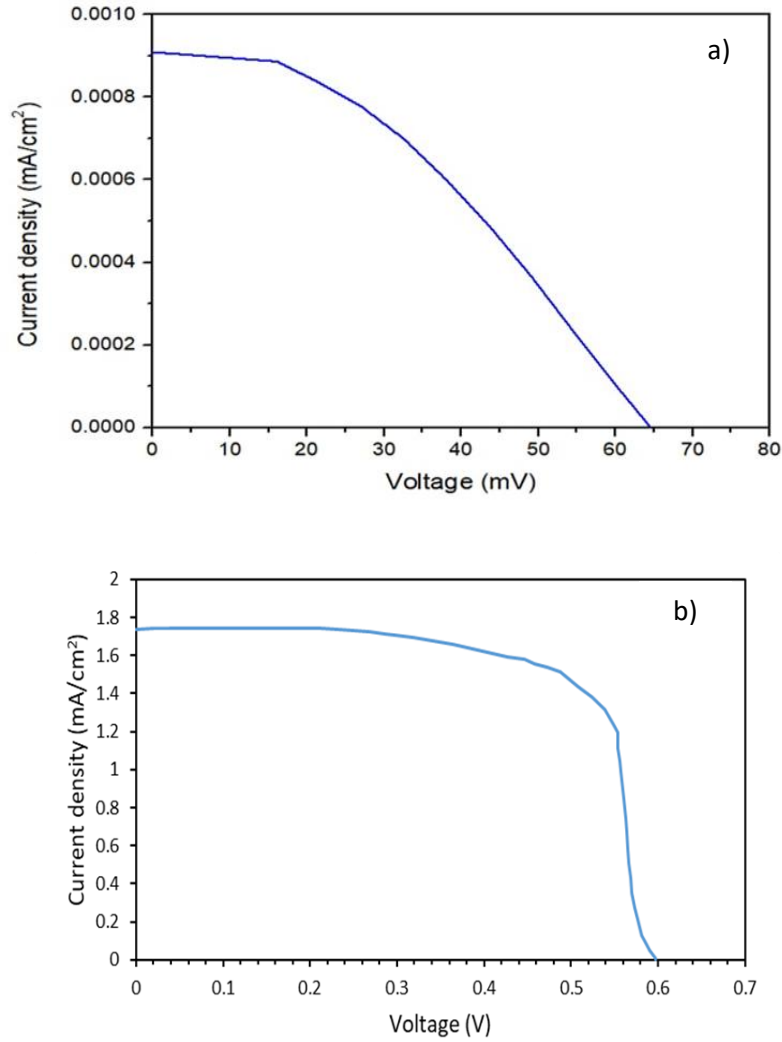
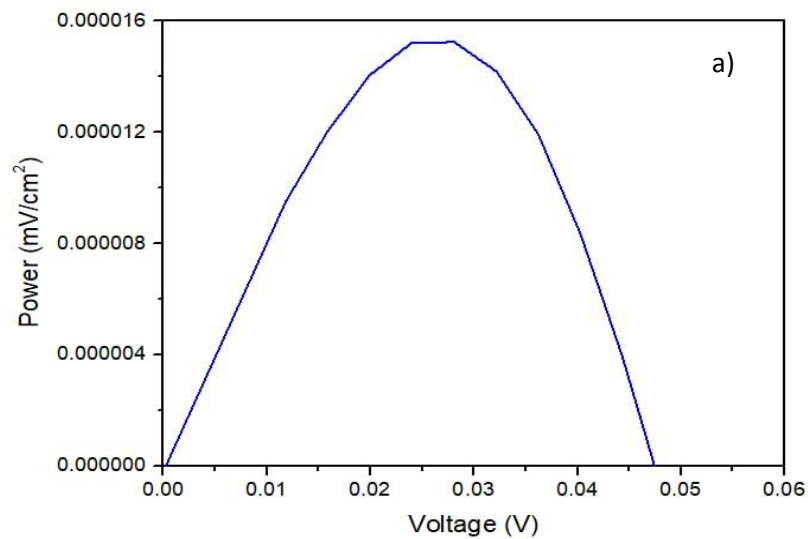


Figure 5.27: I-V of DSSCs with a) carbon soot b) pt.



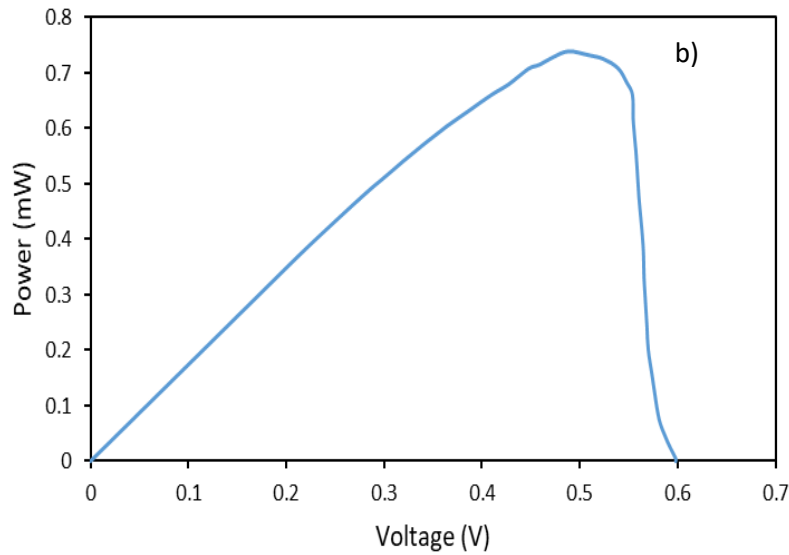


Figure 5. 28: P-V of DSSCs with a) carbon soot b) pt.

5.8.3. Study the effect of thickness of TiO_2 Layers on Performances of DSSCs

Figure (5.29) compares two-layer TiO_2 DSSCs with other single-layered DSSCs. It shows an increase in performance for two-layered DSSCs. Table 5.4 shows that an increase in short circuit current (J_{SC}) of 4.8 mA/cm^2 is responsible for this improved performance. However, in comparison with other DSSCs, the open circuit voltage (V_{OC}) was found to be somewhat reduced. The second layer strengthens the protected contact between the electrolyte and the FTO glass by filling most of the cracks in the first layer by adding a second layer of TiO_2 . This improvement in the J_{SC} may be due to this fact. The fractions of TiO_2 in the first layer of the DSSC is decreased its performance. This comparison was made based on the mixture of dyes.

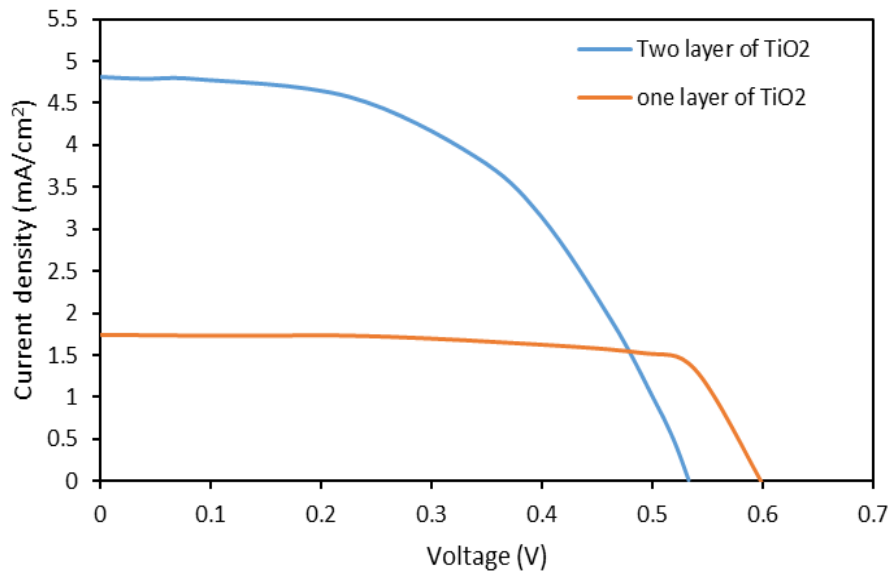


Figure 5. 29: I-V diagram of DSSCs for TiO_2 layers.

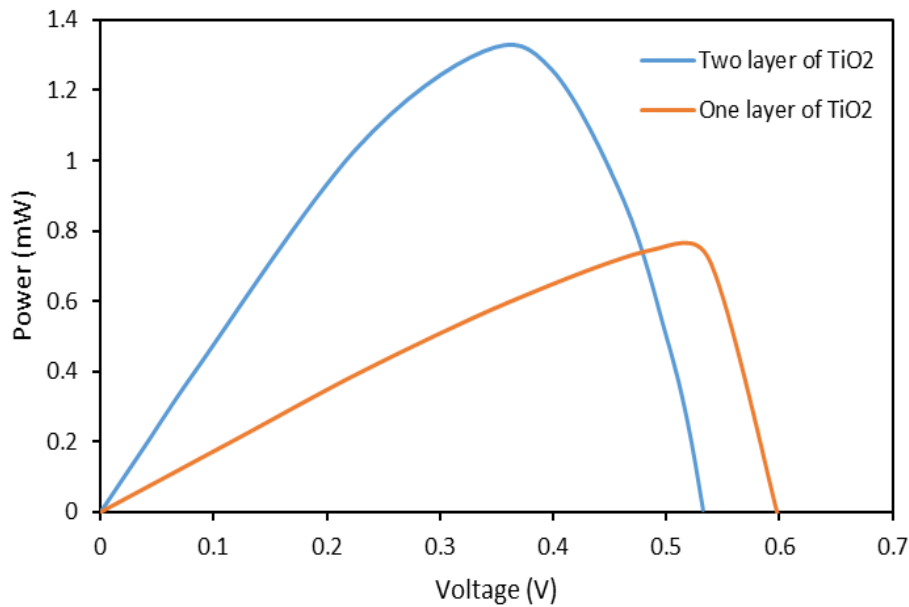


Figure 5. 30: P-V diagram of DSSCs for TiO_2 layers.

Table 5. 4: Comparison of experimental results of single-and two-layered DSSCs for TiO_2

TiO_2 layers number	V_{oc} (v)	J_{sc} (mA)	η (%)	FF
one	0.59	1.59	0.69	73.44
two	0.534	4.80	1.13	0.441

5.8.4. Study the effect of temperature on performance of DSSCs

Curves of current density and voltage for DSSCs in minutes as shown in Figure (5.31), soaking a continuous increasing light the curves show a slight decrease in J_{sc} , V_{oc} , and η of the cells for the entire duration of the light soaking test. While Figure (5.32) shows a decrease in the maximum power.

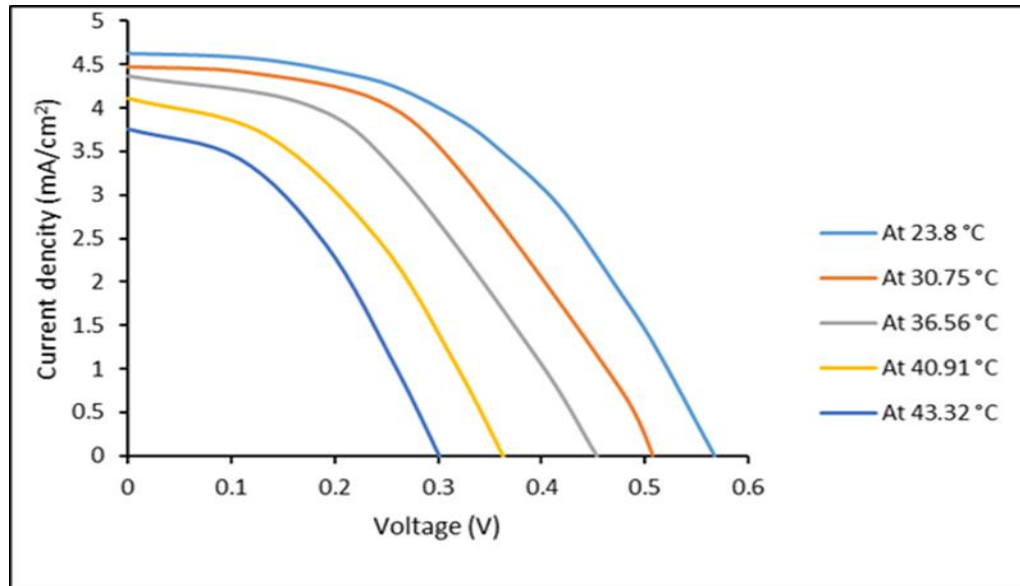


Figure 5. 31: Current density-voltage curves of DSSC at 30 min of continuous light soaking.

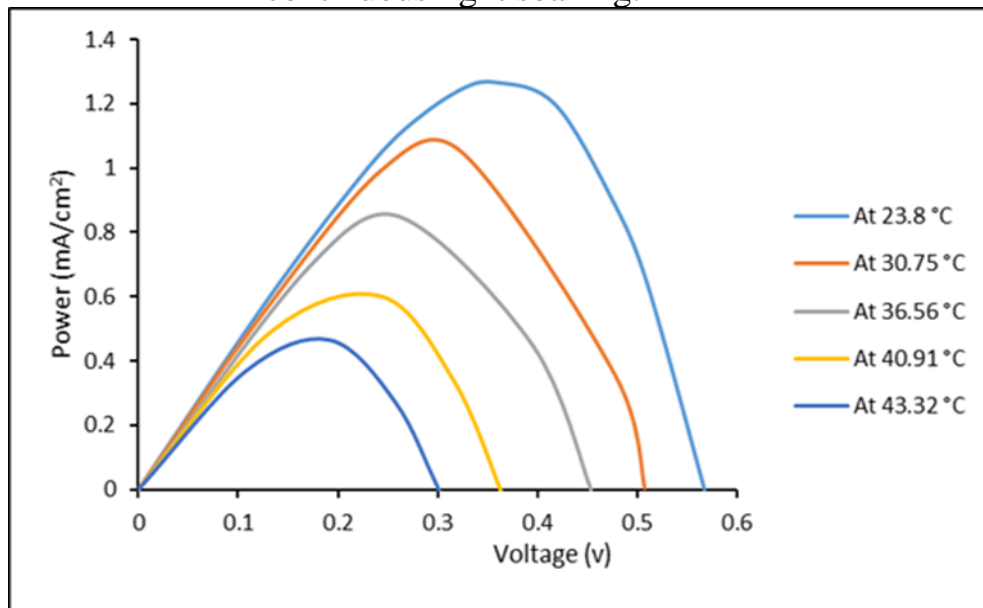


Figure 5. 32: Current density-voltage curves of DSSC at 30 min of continuous light soaking.

In Figure (5.33), it is noted that FF is not stable with time (at different temperatures) as it increases at 30.75 °C. It starts decreasing when the temperature increases, as the increase in the shunt resistance can lead to an increase in FF at 10 min. That is, there may be a slight temperature buildup in the DSSC at min. 10 (at 30.75°C) after 10 min of the continuous light soaking test. changes in the corresponding opening circuit voltage and short current cause the photo-transformation efficiency of DSSC to be reduced.

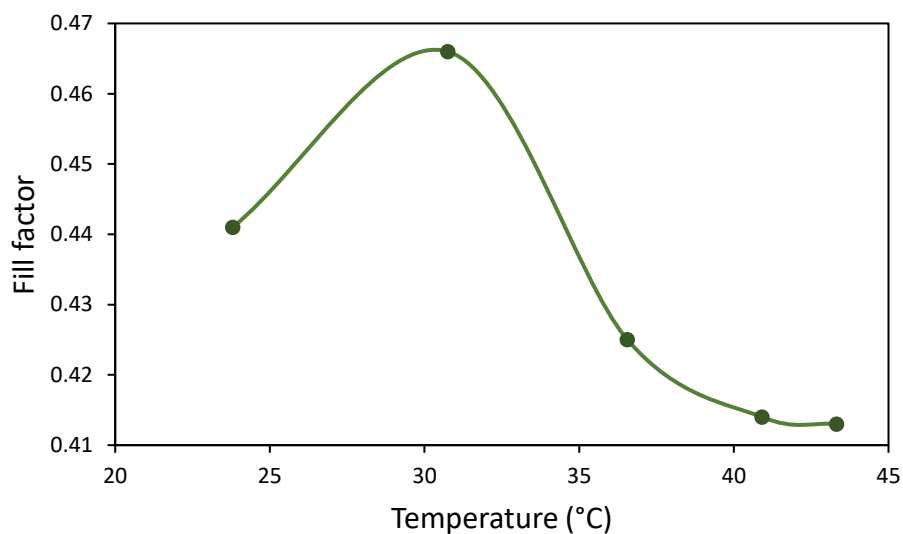


Figure 5. 33: FF change with temperature.

Figures (5.34), (5.35), and (5.36) show that the decrease in I_{sc} , V_{oc} , and η can be attributed to recombination in the surface state of TiO_2 . It was reported that electron injection from photo-excited dye into the TiO_2 conduction band can be improved during a light soaking test, due to additional energy levels from trap-states below the TiO_2 conduction band edge. The trap-states originated from the intercalation of a light-induced proton into the TiO_2 lattice. The interaction of the photo-induced proton with the lattice of TiO_2 generates new electronic (trapping) states in the forbidden energy band gap of TiO_2 . No formation of electron trapping states hinders charge transport since

protons originate from the dye or water traces within the electrolyte thereby promoting recombination between the electrons and triiodide ions in the electrolyte.

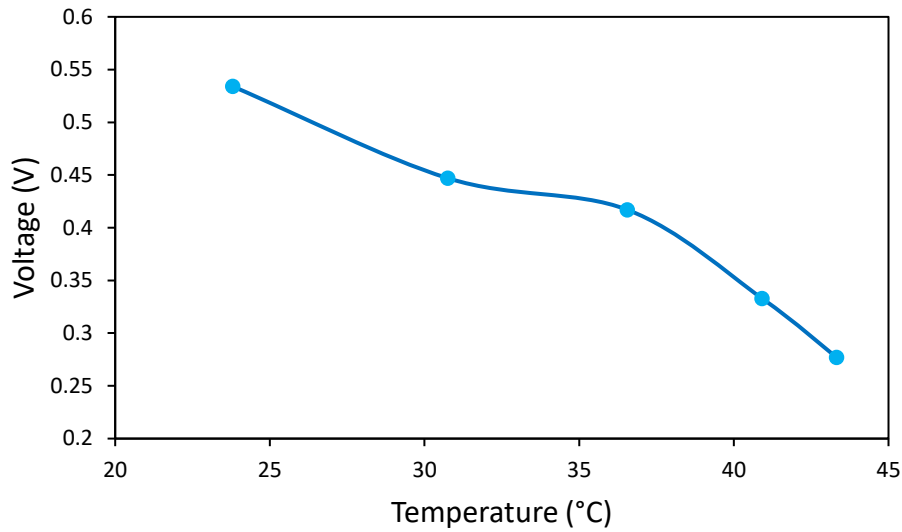


Figure 5. 34: voltage change with temperature.

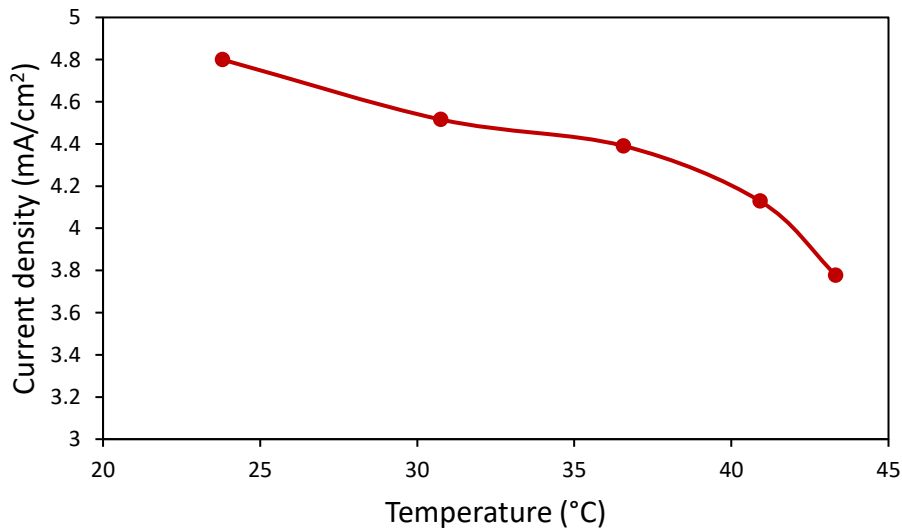


Figure 5. 35: current density changes with temperature.

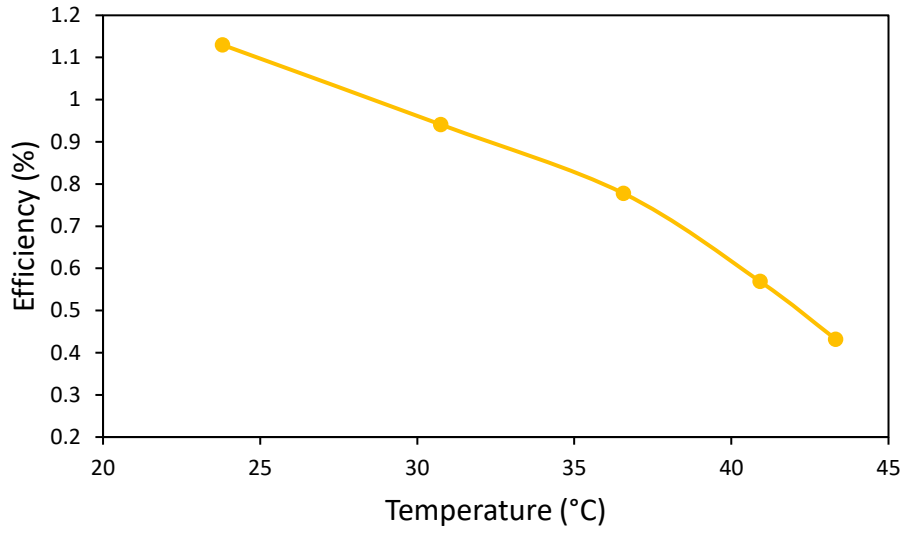


Figure 5. 36: Efficiency change with temperature.

CHAPTER SIX**CONCLUSIONS AND RECOMMENDATIONS****6.1. Conclusion**

The current study examines the effect of different types of dyes on the performance of DSSCs, as well as, focusing on the semiconductor layer of the TiO₂ type and studying a number of changes such as its thickness and nano-size and their effect on cell performance. The effect of temperature on the performance of DSSCs was also studied.

1. Natural dyes such as mint leaves, helianthus leaves, and *Fragaria* fruit were studied experimentally on many DSSCs if their efficiency was 0.15 %, 0.29 %, and 0.09 %, respectively, but and was noted that the best cells were those based on a mixture of the three mentioned dyes with efficiency 0.69% at 23.8°C. Because it showed the best cumulative absorption properties.
2. The best type of solvent used to extract natural dyes is acetone. Because the pigment that was extracted with acetone had a higher energy gap compared to other solvents.
3. FESEM shows that when two layers of TiO₂ are poured, they have fewer cracks.
4. When studying a change in the thickness of the TiO₂ layer, it was noticed that the efficiency of DSSC was increased when using two layers of TiO₂, where the performance efficiency increased from 0.69 to 1.13 percent.

5. The efficiency of DSSCs decreases with time due to the increase in temperature at which they are exposed to light and evaporate the electrolyte.
6. When adding nanomaterials with dyes, they cause decomposition of the sensitizers, and therefore the cell cannot absorb light.

6.2. Recommendations

This study focused on the sensitizers (dyes) and the semiconductor layer used in the improvement of the performance of dye solar cells. To improve this work, some ideas should be included in future studies:

1. Using different methods to prepare titanium dioxide
2. Use different dyes and work on improving the performance of natural dyes to get the highest efficiency of DSSCs.
3. Replacing the liquid electrolyte with the polymer electrolyte.
4. Researching the cell temperature stabilization method, which is one of the main problems that causes instability in DSSCs

References

- [1] A. Agrawal, S. A. Siddiqui, A. Soni, and G. D. Sharma, “Advancements, frontiers and analysis of metal oxide semiconductor, dye, electrolyte and counter electrode of dye sensitized solar cell,” *Sol. Energy*, vol. 233, no. January, pp. 378–407, 2022, doi: 10.1016/j.solener.2022.01.027.
- [2] S. Manju and N. Sagar, “Progressing towards the development of sustainable energy: A critical review on the current status, applications, developmental barriers and prospects of solar photovoltaic systems in India,” *Renew. Sustain. Energy Rev.*, vol. 70, no. November 2016, pp. 298–313, 2017, doi: 10.1016/j.rser.2016.11.226.
- [3] D. Devadiga, M. Selvakumar, P. Shetty, M. Sridhar Santosh, R. S. Chandrabose, and S. Karazhanov, “Recent developments in metal-free organic sensitizers derived from carbazole, triphenylamine, and phenothiazine for dye-sensitized solar cells,” *Int. J. Energy Res.*, vol. 45, no. 5, pp. 6584–6643, 2021, doi: 10.1002/er.6348.
- [4] Y. Zhao, Y. Zhu, H. W. Cheng, R. Zheng, D. Meng, and Y. Yang, “A review on semitransparent solar cells for agricultural application,” *Mater. Today Energy*, vol. 22, no. 2, pp. 354–361, 2021, doi: 10.1016/j.mtener.2021.100852.
- [5] Z. Wang *et al.*, “Efficiency Accreditation and Testing Protocols for Particulate Photocatalysts toward Solar Fuel Production,” *Joule*, vol. 5, no. 2, pp. 344–359, 2021, doi: 10.1016/j.joule.2021.01.001.
- [6] A. Sahu, A. Garg, and A. Dixit, “A review on quantum dot sensitized solar cells: Past, present and future towards carrier multiplication with a possibility for higher efficiency,” *Sol. Energy*, vol. 203, no. March, pp.

210–239, 2020, doi: 10.1016/j.solener.2020.04.044.

- [7] D. Kishore Kumar *et al.*, “Functionalized metal oxide nanoparticles for efficient dye-sensitized solar cells (DSSCs): A review,” *Mater. Sci. Energy Technol.*, vol. 3, pp. 472–481, 2020, doi: 10.1016/j.mset.2020.03.003.
- [8] G. V. Belessiotis, M. Antoniadou, I. Ibrahim, C. S. Karagianni, and P. Falaras, “Universal electrolyte for DSSC operation under both simulated solar and indoor fluorescent lighting,” *Mater. Chem. Phys.*, vol. 277, no. October 2021, p. 125543, 2022, doi: 10.1016/j.matchemphys.2021.125543.
- [9] B. Maldon and N. Thamwattana, “A fractional diffusion model for dye-sensitized solar cells,” *Molecules*, vol. 25, no. 13, 2020, doi: 10.3390/molecules25132966.
- [10] A. Bist and S. Chatterjee, “Review on Efficiency Enhancement Using Natural Extract Mediated Dye-Sensitized Solar Cell for Sustainable Photovoltaics,” *Energy Technol.*, vol. 9, no. 8, pp. 1–19, 2021, doi: 10.1002/ente.202001058.
- [11] J. MaçAira, L. Andrade, and A. Mendes, “Modeling, simulation and design of dye sensitized solar cells,” *RSC Adv.*, vol. 4, no. 6, pp. 2830–2844, 2014, doi: 10.1039/c3ra46295a.
- [12] L. K. Singh and B. P. Koiry, “Natural Dyes and their Effect on Efficiency of TiO₂ based DSSCs: A Comparative Study,” *Mater. Today Proc.*, vol. 5, no. 1, pp. 2112–2122, 2018, doi: 10.1016/j.matpr.2017.09.208.

- [13] M. Z. Bin Mukhlis, Y. Horie, K. Higashi, A. Ichigi, S. Guo, and T. Nomiyama, “Self-standing conductive ITO-silica nanofiber mats for use in flexible electronics and their application in dye-sensitized solar cells,” *Ceram. Int.*, vol. 43, no. 11, pp. 8146–8152, 2017, doi: 10.1016/j.ceramint.2017.03.140.
- [14] A. Orona-Navar, I. Aguilar-Hernández, K. D. P. Nigam, A. Cerdán-Pasarán, and N. Ornelas-Soto, “Alternative sources of natural pigments for dye-sensitized solar cells: Algae, cyanobacteria, bacteria, archaea and fungi,” *J. Biotechnol.*, vol. 332, no. October 2020, pp. 29–53, 2021, doi: 10.1016/j.jbiotec.2021.03.013.
- [15] N. Tomar, A. Agrawal, V. S. Dhaka, and P. K. Surolia, “Ruthenium complexes based dye sensitized solar cells: Fundamentals and research trends,” *Sol. Energy*, vol. 207, no. April, pp. 59–76, 2020, doi: 10.1016/j.solener.2020.06.060.
- [16] J. Theerthagiri *et al.*, “A review on ZnO nanostructured materials: Energy, environmental and biological applications,” *Nanotechnology*, vol. 30, no. 39, 2019, doi: 10.1088/1361-6528/ab268a.
- [17] S. Bera, D. Sengupta, S. Roy, and K. Mukherjee, “Research into dye-sensitized solar cells: A review highlighting progress in India,” *JPhys Energy*, vol. 3, no. 3. IOP Publishing Ltd, Jul. 01, 2021, doi: 10.1088/2515-7655/abff6c.
- [18] S. Joseph, A. J. P. Paul Winston, S. Muthupandi, P. Shobha, S. M. Margaret, and P. Sagayaraj, “Performance of Natural Dye Extracted from Annatto, Black Plum, Turmeric, Red Spinach, and Cactus as Photosensitizers in TiO₂NP/TiNT Composites for Solar Cell

- Applications,” *J. Nanomater.*, vol. 2021, 2021, doi: 10.1155/2021/5540219.
- [19] J. E. Ikpesu, S. E. Iyuke, M. Daramola, and A. O. Okewale, “Synthesis of improved dye-sensitized solar cell for renewable energy power generation,” *Sol. Energy*, vol. 206, no. March, pp. 918–934, 2020, doi: 10.1016/j.solener.2020.05.002.
- [20] G. Nandan Arka, S. Bhushan Prasad, and S. Singh, “Comprehensive study on dye sensitized solar cell in subsystem level to excel performance potential: A review,” *Sol. Energy*, vol. 226, no. March, pp. 192–213, 2021, doi: 10.1016/j.solener.2021.08.037.
- [21] F. Grifoni *et al.*, “Toward Sustainable, Colorless, and Transparent Photovoltaics: State of the Art and Perspectives for the Development of Selective Near-Infrared Dye-Sensitized Solar Cells,” *Adv. Energy Mater.*, vol. 11, no. 43, 2021, doi: 10.1002/aenm.202101598.
- [22] M. F. Don, P. Ekanayake, H. Nakajima, A. H. Mahadi, C. M. Lim, and A. Atod, “Acetylene carbon black-graphite composite as low-cost and efficient counter electrode for dye-sensitized solar cells (DSSCs),” *Ionics (Kiel)*, vol. 25, no. 11, pp. 5585–5593, 2019, doi: 10.1007/s11581-019-03071-9.
- [23] C. Sima, C. Grigoriu, and S. Antohe, “Comparison of the dye-sensitized solar cells performances based on transparent conductive ITO and FTO,” *Thin Solid Films*, vol. 519, no. 2, pp. 595–597, 2010, doi: 10.1016/j.tsf.2010.07.002.
- [24] N. Ruba *et al.*, “Recent Advancement in Photo-Anode, Dye and Counter Cathode in Dye-Sensitized Solar Cell: A Review,” *J. Inorg. Organomet.*

- Polym. Mater.*, vol. 31, no. 5, pp. 1894–1901, 2021, doi: 10.1007/s10904-020-01854-6.
- [25] M. Yahya, A. Bouziani, C. Ocak, Z. Seferoğlu, and M. Sillanpää, “Organic/metal-organic photosensitizers for dye-sensitized solar cells (DSSC): Recent developments, new trends, and future perceptions,” *Dye. Pigment.*, vol. 192, no. January, 2021, doi: 10.1016/j.dyepig.2021.109227.
- [26] K. Gossen and A. Ehrmann, “Influence of FTO glass cleaning on DSSC performance,” *Optik (Stuttg.)*, vol. 183, no. January, pp. 253–256, 2019, doi: 10.1016/j.ijleo.2019.02.041.
- [27] A. Pervez *et al.*, “Fabrication and comparison of dye-sensitized solar cells by using TiO₂ and ZnO as photo electrode,” *Optik (Stuttg.)*, vol. 182, pp. 175–180, 2019, doi: 10.1016/j.ijleo.2018.12.044.
- [28] D. Sinha, D. De, D. Goswami, A. Mondal, and A. Ayaz, “ZnO and TiO₂ Nanostructured Dye sensitized Solar Photovoltaic Cell,” *Mater. Today Proc.*, vol. 11, pp. 782–788, 2019, doi: 10.1016/j.matpr.2019.03.043.
- [29] M. Hosseinneshad, J. Movahedi, and S. Nasiri, “High stability photosensitizers for dye-sensitized solar cells: Synthesis, characterization and optical performance,” *Opt. Mater. (Amst.)*, vol. 109, no. June, p. 110198, 2020, doi: 10.1016/j.optmat.2020.110198.
- [30] P. Dhamodharan, J. Chen, and C. Manoharan, “Fabrication of In doped ZnO thin films by spray pyrolysis as photoanode in DSSCs,” *Surfaces and Interfaces*, vol. 23, no. July 2020, p. 100965, 2021, doi: 10.1016/j.surfin.2021.100965.

- [31] U. I. Ndeze, J. Aidan, S. C. Ezike, and J. F. Wansah, “Comparative performances of nature-based dyes extracted from Baobab and Shea leaves photo-sensitizers for dye-sensitized solar cells (DSSCs),” *Curr. Res. Green Sustain. Chem.*, vol. 4, no. May, p. 100105, 2021, doi: 10.1016/j.crgsc.2021.100105.
- [32] F. Kabir, M. M. H. Bhuiyan, M. S. Manir, M. S. Rahaman, M. A. Khan, and T. Ikegami, “Development of dye-sensitized solar cell based on combination of natural dyes extracted from Malabar spinach and red spinach,” *Results Phys.*, vol. 14, no. June, p. 102474, 2019, doi: 10.1016/j.rinp.2019.102474.
- [33] F. Kabir *et al.*, “Improvement of efficiency of Dye Sensitized Solar Cells by optimizing the combination ratio of Natural Red and Yellow dyes,” *Optik (Stuttg.)*, vol. 179, no. October 2018, pp. 252–258, 2019, doi: 10.1016/j.ijleo.2018.10.150.
- [34] T. Jalali, P. Arkian, M. Golshan, M. Jalali, and S. Osfouri, “Performance evaluation of natural native dyes as photosensitizer in dye-sensitized solar cells,” *Opt. Mater. (Amst.)*, vol. 110, no. October, p. 110441, 2020, doi: 10.1016/j.optmat.2020.110441.
- [35] M. Golshan, S. Osfouri, R. Azin, T. Jalali, and N. R. Moheimani, “Co-sensitization of natural and low-cost dyes for efficient panchromatic light-harvesting using dye-sensitized solar cells,” *J. Photochem. Photobiol. A Chem.*, vol. 417, no. May, p. 113345, 2021, doi: 10.1016/j.jphotochem.2021.113345.
- [36] B. Arjun Kumar, G. Ramalingam, D. Karthigaimuthu, T. Elangovan, and V. Vetrivelan, “Fabrication of natural dye sensitized solar cell using

- tridax procumbens leaf and beetroot extract mixer as a sensitizer,” *Mater. Today Proc.*, no. xxxx, 2021, doi: 10.1016/j.matpr.2021.04.221.
- [37] S. A. Taya, “Dye-Sensitized Solar Cells Using Fresh and Dried Natural Dyes,” *Int. J. Mater. Sci. Appl.*, vol. 2, no. 2, p. 37, 2013, doi: 10.11648/j.ijmsa.20130202.11.
- [38] Sakshi, P. K. Singh, and V. K. Shukla, “Widening spectral range of absorption using natural dyes: Applications in dye sensitized solar cell,” *Mater. Today Proc.*, vol. 49, no. xxxx, pp. 3235–3238, 2020, doi: 10.1016/j.matpr.2020.12.287.
- [39] S. Sowmya, N. Ruba, K. Inbarajan, P. Prakash, and B. Janarthanan, “Dye-sensitized solar cells concocted with dyes extracted from fresh and dried leaves of Henna using different solvents,” *Opt. Quantum Electron.*, vol. 53, no. 5, 2021, doi: 10.1007/s11082-021-02953-5.
- [40] N. A. Norhisamudin *et al.*, “The Effect of Different Solvents in Natural Dyes from Roselle (*Hibiscus Sabdariffa*) and Green Tea Leaves (*Camellia Sinensis*) for Dye-Sensitized Solar Cell,” *J. Phys. Conf. Ser.*, vol. 1755, no. 1, 2021, doi: 10.1088/1742-6596/1755/1/012024.
- [41] N. M.Z. and W. Tan, “Dye extracted from *Costus woodsonii* leave as a natural sensitizer for dye-sensitized solar cell,” *Sci. Lett.*, vol. 15, no. 1, p. 58, 2021, doi: 10.24191/sl.v15i1.11794.
- [42] S. Sowmya, K. Inbarajan, N. Ruba, P. Prakash, and B. Janarthanan, “A novel idea of using dyes extracted from the leaves of *Prosopis juliflora* in dye – Sensitized solar cells,” *Opt. Mater. (Amst)*, vol. 120, no. July, p. 111429, 2021, doi: 10.1016/j.optmat.2021.111429.

- [43] S. Venkatesan, I. P. Liu, W. N. Hung, H. Teng, and Y. L. Lee, “Highly efficient quasi-solid-state dye-sensitized solar cells prepared by printable electrolytes for room light applications,” *Chem. Eng. J.*, vol. 367, no. 1, pp. 17–24, 2019, doi: 10.1016/j.cej.2019.02.118.
- [44] Rahul *et al.*, “Eco-friendly dye sensitized solar cell using natural dye with solid polymer electrolyte as hole transport material,” *Mater. Today Proc.*, vol. 34, no. xxxx, pp. 760–766, 2019, doi: 10.1016/j.matpr.2020.04.775.
- [45] P. Khammee, Y. Unpaprom, T. Thurakitseree, N. Dussadee, S. Kojinok, and R. Ramaraj, “Natural dyes extracted from Inthanin bok leaves as light-harvesting units for dye-sensitized solar cells,” *Appl. Nanosci.*, no. 0123456789, 2021, doi: 10.1007/s13204-021-01769-9.
- [46] S. Çakar, C. Soykan, and M. Özacar, “Polyacrylonitrile/polyindole and poly(glycidyl methacrylate)/polyindole composites based quasi solid electrolyte materials for dye sensitized solar cells,” *Sol. Energy*, vol. 215, no. October 2020, pp. 157–168, 2021, doi: 10.1016/j.solener.2020.12.039.
- [47] M. T. Z. Butt, K. Preuss, M. M. Titirici, H. ur Rehman, and J. Briscoe, “Biomass-derived nitrogen-doped carbon aerogel counter electrodes for dye sensitized solar cells,” *Materials (Basel)*, vol. 11, no. 7, pp. 1–11, 2018, doi: 10.3390/ma11071171.
- [48] D. Kishore Kumar *et al.*, “Screen printed tin selenide films used as the counter electrodes in dye sensitized solar cells,” *Sol. Energy*, vol. 190, no. July, pp. 28–33, 2019, doi: 10.1016/j.solener.2019.07.066.
- [49] G. F. C. Mejica, Y. Unpaprom, and R. Ramaraj, “Fabrication and

- performance evaluation of dye-sensitized solar cell integrated with natural dye from *Strobilanthes cusia* under different counter-electrode materials,” *Appl. Nanosci.*, no. 0123456789, 2021, doi: 10.1007/s13204-021-01853-0.
- [50] M. S. Abusaif *et al.*, “New carbazole-based organic dyes with different acceptors for dye-sensitized solar cells: Synthesis, characterization, dssc fabrications and density functional theory studies,” *J. Mol. Struct.*, vol. 1225, p. 129297, 2021, doi: 10.1016/j.molstruc.2020.129297.
- [51] G. Richhariya and A. Kumar, “Performance evaluation of mixed synthetic organic dye as sensitizer based dye sensitized solar cell,” *Opt. Mater. (Amst.)*, vol. 111, no. September, p. 110658, 2021, doi: 10.1016/j.optmat.2020.110658.
- [52] A. Agrawal, S. A. Siddiqui, A. Soni, K. Khandelwal, and G. D. Sharma, “Performance analysis of TiO₂ based dye sensitized solar cell prepared by screen printing and doctor blade deposition techniques,” *Sol. Energy*, vol. 226, no. August, pp. 9–19, 2021, doi: 10.1016/j.solener.2021.08.001.
- [53] A. Siddika, M. Sultana, M. S. Bashir, S. Tabassum, S. Aziz, and M. A. Ali Shaikh, “Improved performance of dye sensitized solar cell by exploration of photoanode and ruthenium based dye,” *Opt. Mater. (Amst.)*, vol. 125, no. February, p. 112042, 2022, doi: 10.1016/j.optmat.2022.112042.
- [54] I. Chandra Maurya, S. Singh, P. Srivastava, B. Maiti, and L. Bahadur, “Natural dye extract from *Cassia fistula* and its application in dye-sensitized solar cell: Experimental and density functional theory

- studies,” *Opt. Mater. (Amst.)*, vol. 90, no. February, pp. 273–280, 2019, doi: 10.1016/j.optmat.2019.02.037.
- [55] M. Z. Iqbal, S. R. Ali, and S. Khan, “Progress in dye sensitized solar cell by incorporating natural photosensitizers,” *Sol. Energy*, vol. 181, no. December 2018, pp. 490–509, 2019, doi: 10.1016/j.solener.2019.02.023.
- [56] K. B. Erande *et al.*, “Extraction of natural dye (specifically anthocyanin) from pomegranate fruit source and their subsequent use in dssc,” *Mater. Today Proc.*, vol. 43, no. xxxx, pp. 2716–2720, 2020, doi: 10.1016/j.matpr.2020.06.357.
- [57] K. Obi, L. Frolova, and P. Fuierer, “Preparation and performance of prickly pear (*Opuntia phaeacantha*) and mulberry (*Morus rubra*) dye-sensitized solar cells,” *Sol. Energy*, vol. 208, no. August, pp. 312–320, 2020, doi: 10.1016/j.solener.2020.08.006.
- [58] M. A. Almutairi, W. A. Farooq, and M. S. AlSalhi, “Photovoltaic and impedance properties of dye-sensitized solar cell based on nature dye from beetroot,” *Curr. Appl. Phys.*, no. November 2019, 2021, doi: 10.1016/j.cap.2021.07.010.
- [59] A. N. Ossai, S. C. Ezike, P. Timtere, and A. D. Ahmed, “Enhanced photovoltaic performance of dye-sensitized solar cells-based *Carica papaya* leaf and black cherry fruit co-sensitizers,” *Chem. Phys. Impact*, vol. 2, no. March, p. 100024, 2021, doi: 10.1016/j.chphi.2021.100024.
- [60] D. J. Yun *et al.*, “Well-aligned ZnO nanorod array covered with ruthenium layers for alternative counter electrodes in dye-sensitized solar cells,” *Appl. Surf. Sci.*, vol. 550, no. November 2020, p. 149273,

2021, doi: 10.1016/j.apsusc.2021.149273.

- [61] D. K. Hwang, B. Lee, and D. H. Kim, “Efficiency enhancement in solid dye-sensitized solar cell by three-dimensional photonic crystal,” *RSC Adv.*, vol. 3, no. 9, pp. 3017–3023, 2013, doi: 10.1039/c2ra22746k.
- [62] F. L. Chawarambwa *et al.*, “Effects of concentrated light on the performance and stability of a quasi-solid electrolyte in dye-sensitized solar cells,” *Chem. Phys. Lett.*, vol. 781, no. May, p. 138986, 2021, doi: 10.1016/j.cplett.2021.138986.
- [63] R. P. Chahal, S. Mahendia, A. K. Tomar, and S. Kumar, “UV irradiated PVA-Ag nanocomposites for optical applications,” *Appl. Surf. Sci.*, vol. 343, pp. 160–165, 2015, doi: 10.1016/j.apsusc.2015.03.074.
- [64] A. Kühn, “Lecture 1,” *Lect. Dev. Physiol.*, pp. 1–11, 1971, doi: 10.1007/978-3-642-87286-0_1.
- [65] M. Freitag and G. Boschloo, “The revival of dye-sensitized solar cells,” *Curr. Opin. Electrochem.*, vol. 2, no. 1, pp. 111–119, 2017, doi: 10.1016/j.coelec.2017.03.011.
- [66] U. S. A. E. Commission, “RADIATIONLESS MOLECULAR ELECTRONIC TRANSITIONS,” 1967.
- [67] G. Gruner and M. Dressel, “Electrodynamics of Solids,” 2003.
- [68] T. Zdanowicz, T. Rodziewicz, and M. Zabkowska-Waclawek, “Theoretical analysis of the optimum energy band gap of semiconductors for fabrication of solar cells for applications in higher latitudes locations,” *Sol. Energy Mater. Sol. Cells*, vol. 87, no. 1–4, pp. 757–769, 2005, doi: 10.1016/j.solmat.2004.07.049.

- [69] J. G. Solé, L. E. Bausá, and D. Jaque, *An Introduction to the Optical Spectroscopy of Inorganic Solids*, vol. 6. 2005.
- [70] H. Bakr, Q. M. A. Hassan, and H. A. Sultan, “Diffraction Ring Patterns And Z-Scan Measurements Of The Nonlinear Refraction Index Of 5W20 Oil,” *J. Coll. Educ. Pure Sci.*, vol. 9, no. 2, pp. 226–232, 2019, doi: 10.32792/utq.jceps.09.02.24.
- [71] M. A. Mahdi and S. K. J. Al-Ani, “Optical characterization of chemical bath deposition Cd 1-xZn xS thin films,” *Int. J. Nanoelectron. Mater.*, vol. 5, no. 1, pp. 11–24, 2012.
- [72] M. Abdel Rafea and A. A. M. Farag, “Preparation and optical properties of SeS Thin films semiconducting chalcogenide glasses,” *Chalcogenide Lett.*, vol. 5, no. 3, pp. 27–33, 2008.
- [73] R. K. H. Manshad and Q. M. A. Hassan, “Nonlinear characterization of orcein solution and dye doped polymer film for application in optical limiting,” 2012.
- [74] “Unconfirmed 658731.crdownload.” .
- [75] M. S. Hussain, Q. M. A. Hassan, H. A. Sultan, A. S. Al-Asadi, H. T. Chayed, and C. A. Emshary, “Preparation, characterization, and study of the nonlinear optical properties of a new prepared nanoparticles copolymer,” *Mod. Phys. Lett. B*, vol. 33, no. 36, pp. 1–17, 2019, doi: 10.1142/S0217984919504566.
- [76] F. O. Lenzmann and J. M. Kroon, “Recent advances in dye-sensitized solar cells,” *Adv. Optoelectron.*, vol. 2007, no. 2, 2007, doi: 10.1155/2007/65073.

- [77] H. Zhong, Y. Hu, Y. Wang, and H. Yang, "TiO₂/silane coupling agent composed of two layers structure: A super-hydrophilic self-cleaning coating applied in PV panels," *Appl. Energy*, vol. 204, pp. 932–938, 2017, doi: 10.1016/j.apenergy.2017.04.057.
- [78] M. Law, L. E. Greene, A. Radenovic, T. Kuykendall, J. Liphardt, and P. Yang, "ZnO-Al₂O₃ and ZnO-TiO₂ core-shell nanowire dye-sensitized solar cells," *J. Phys. Chem. B*, vol. 110, no. 45, pp. 22652–22663, 2006, doi: 10.1021/jp0648644.
- [79] E. M. Abdou, H. S. Hafez, E. Bakir, and M. S. A. Abdel-Mottaleb, "Photostability of low cost dye-sensitized solar cells based on natural and synthetic dyes," *Spectrochim. Acta - Part A Mol. Biomol. Spectrosc.*, vol. 115, pp. 202–207, 2013, doi: 10.1016/j.saa.2013.05.090.
- [80] N. A. Karim, U. Mehmood, H. F. Zahid, and T. Asif, "Nanostructured photoanode and counter electrode materials for efficient Dye-Sensitized Solar Cells (DSSCs)," *Sol. Energy*, vol. 185, no. January, pp. 165–188, 2019, doi: 10.1016/j.solener.2019.04.057.
- [81] X. Chen and S. S. Mao, "Titanium dioxide nanomaterials: Synthesis, properties, modifications and applications," *Chem. Rev.*, vol. 107, no. 7, pp. 2891–2959, 2007, doi: 10.1021/cr0500535.
- [82] J. Ahmad, K. Deshmukh, M. Habib, and M. B. Hägg, "Influence of TiO₂ Nanoparticles on the Morphological, Thermal and Solution Properties of PVA/TiO₂ Nanocomposite Membranes," *Arab. J. Sci. Eng.*, vol. 39, no. 10, pp. 6805–6814, 2014, doi: 10.1007/s13369-014-1287-0.
- [83] Y. Zhang, J. Han, G. Pan, Y. Xu, and F. Wang, "A multi-stage predicting

- methodology based on data decomposition and error correction for ultra-short-term wind energy prediction,” *J. Clean. Prod.*, vol. 292, p. 125981, 2021, doi: 10.1016/j.jclepro.2021.125981.
- [84] N. G. Park, J. Van De Lagemaat, and A. J. Frank, “Comparison of dye-sensitized rutile- and anatase-based TiO₂ solar cells,” *J. Phys. Chem. B*, vol. 104, no. 38, pp. 8989–8994, 2000, doi: 10.1021/jp9943651.
- [85] A. Zatirostami, “Increasing the efficiency of TiO₂-based DSSC by means of a double layer RF-sputtered thin film blocking layer,” *Optik (Stuttg.)*, vol. 207, no. November 2019, 2020, doi: 10.1016/j.ijleo.2020.164419.
- [86] V. Dhas *et al.*, “Enhanced DSSC performance with high surface area thin anatase TiO₂ nanoleaves,” *Sol. Energy*, vol. 85, no. 6, pp. 1213–1219, 2011, doi: 10.1016/j.solener.2011.02.029.
- [87] S. Saadaoui *et al.*, “Performance of natural-dye-sensitized solar cells by ZnO nanorod and nanowall enhanced photoelectrodes,” *Beilstein J. Nanotechnol.*, vol. 8, no. 1, pp. 287–295, 2017, doi: 10.3762/bjnano.8.31.
- [88] A. Sclafani and J. M. Herrmann, “Comparison of the photoelectronic and photocatalytic activities of various anatase and rutile forms of titania in pure liquid organic phases and in aqueous solutions,” *J. Phys. Chem.*, vol. 100, no. 32, pp. 13655–13661, 1996, doi: 10.1021/jp9533584.
- [89] S. C. Ezike, “Effect of Concentration Variation on Optical and Structural Properties of TiO₂ Thin Films,” vol. 7, no. 1, pp. 1–6, 2020.
- [90] S. Sowmya, Pooja Prakash, N. Ruba, B. Janarthanan, A. Nagamani

Prabu, and J. Chandrasekaran, “A study on the fabrication and characterization of dye-sensitized solar cells with *Amaranthus red* and *Lawsonia inermis* as sensitizers with maximum absorption of visible light,” *J. Mater. Sci. Mater. Electron.*, vol. 31, no. 8, pp. 6027–6035, 2020, doi: 10.1007/s10854-020-03154-8.

- [91] A. Hariyadi, M. A. Swasono, and A. C. Augusty, “Combination of dragon fruit, hibiscus and bitterleaf as dye sensitizer to increase efficiency of DSSC,” *Int. J. Adv. Sci. Eng. Inf. Technol.*, vol. 7, no. 3, pp. 936–942, 2017, doi: 10.18517/ijaseit.7.3.2445.
- [92] M. R. Al-Mamun, M. N. Karim, N. A. Nitun, S. Kader, M. S. Islam, and M. Z. H. Khan, “Photocatalytic performance assessment of GO and Ag co-synthesized TiO₂ nanocomposite for the removal of methyl orange dye under solar irradiation,” *Environ. Technol. Innov.*, vol. 22, p. 101537, 2021, doi: 10.1016/j.eti.2021.101537.

Appendices:

Appendix -A: Titanium Dioxide certificate

This appendix represents the certificate of Titanium Dioxide (TiO₂) Nano-particles properties processing from HWNANO-COMPANY. figure. A represents the Nanoparticles characteristics, and Figure.A2 represents the Nano size verification as a scanning electron microscope test (SEM) to verify the grain Nano-size under the microscope.

Product Name	Titanium oxide (氧化铜)	
Electrical resistivity	251.4 $\mu\Omega$ ·m	合格 Conform
Electric conductivity	397.840066 S/m	合格 Conform
Specific surface area	98 m ² /g	合格 Conform
Bulk density	1.7 g/cm ³	合格 Conform
True density	3.78 g/cm ³	合格 Conform
Thermal conductivity	4.7 W/m·K	合格 Conform

For and on behalf of
HONGWU INTERNATIONAL GROUP LTD
宏武國際集團有限公司

Authorized Signature(s)

Tel: (86) 20-87226359, (86) 20-87748617
Website: www.xuzhounano.com E-mail: hwnano@xuzhounano.com

Figure A1. Titanium Dioxide certificate.

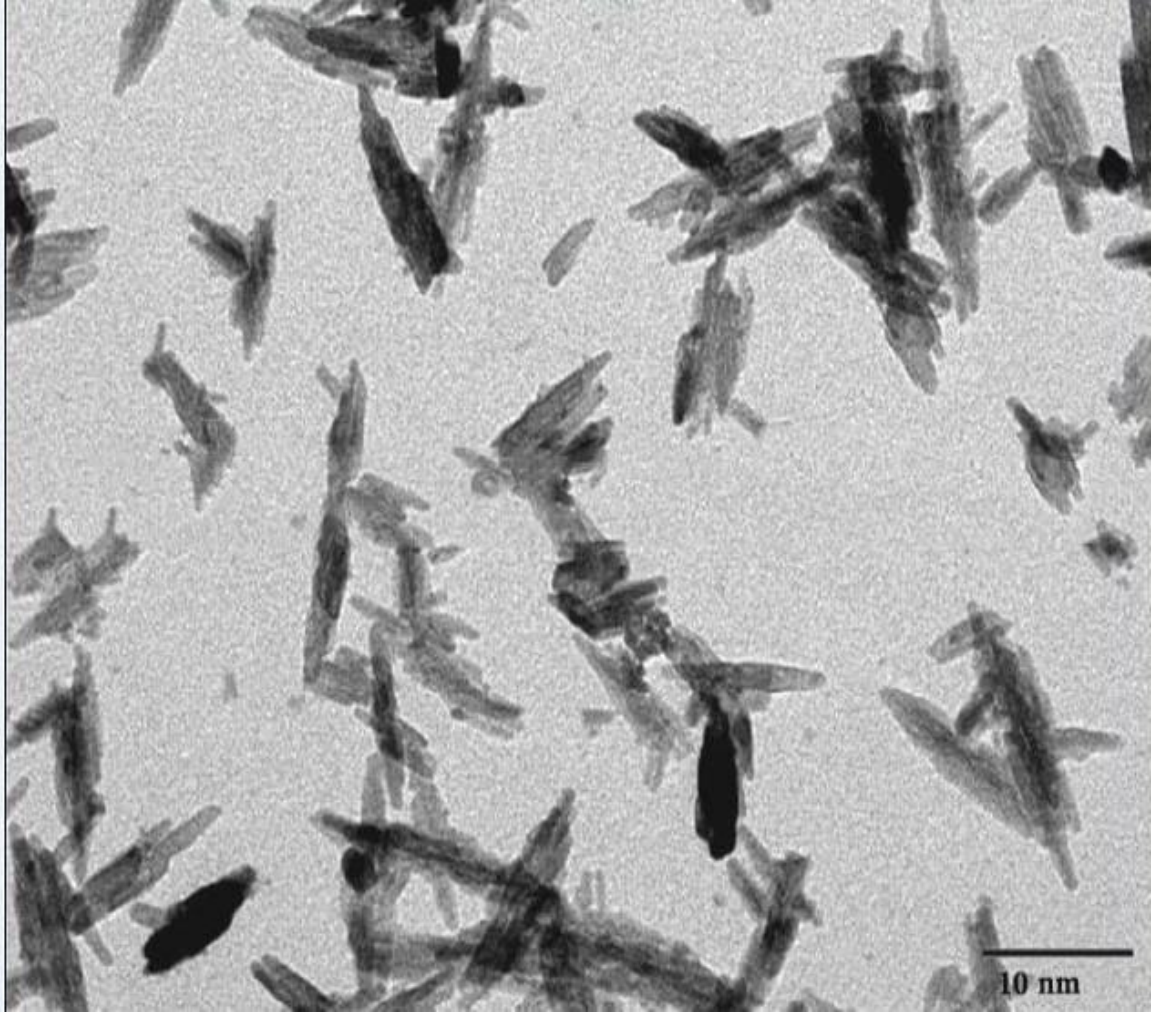


Figure A.2 Titanium Dioxide Scanning electron microscopy (SEM).

Appendix –B: Water Bath Ultrasonic Device (Elmasonic P180H)

This appendix shows the main characteristics of the Water Bath Ultrasonic Device Specifications (Elmasonic P180H) as shown in the table. B1.

Table B.1 Ultrasonic water-bath properties.

Property	Value
Electrical Characteristics	110/220 VAC
Frequency	37 / 80 kHz
Power consumption	1330W
Weight	8.5 kg
Volume tank	12 liters
Drain size	3/8”
Materials	Stainless steel V2A
sound level (LPZ), (dB)	96 / 87

Appendix -C: Coating Thickness Gauge.

Property	Value
Temperature range	0~60°C
Humidity	20% ~90%RH
Power source	1.2V, 600mA
Dimensions	270mm×86 mm×47 mm
Weight	530g
Probe-type	N400
Coating thickness-range	0~400μm

Appendix-D: Thermocouples calibration system.

This appendix represents the calibration process for K-Type thermocouples which was used in this work, figure B.1, 2, and 3 show the calibration data.

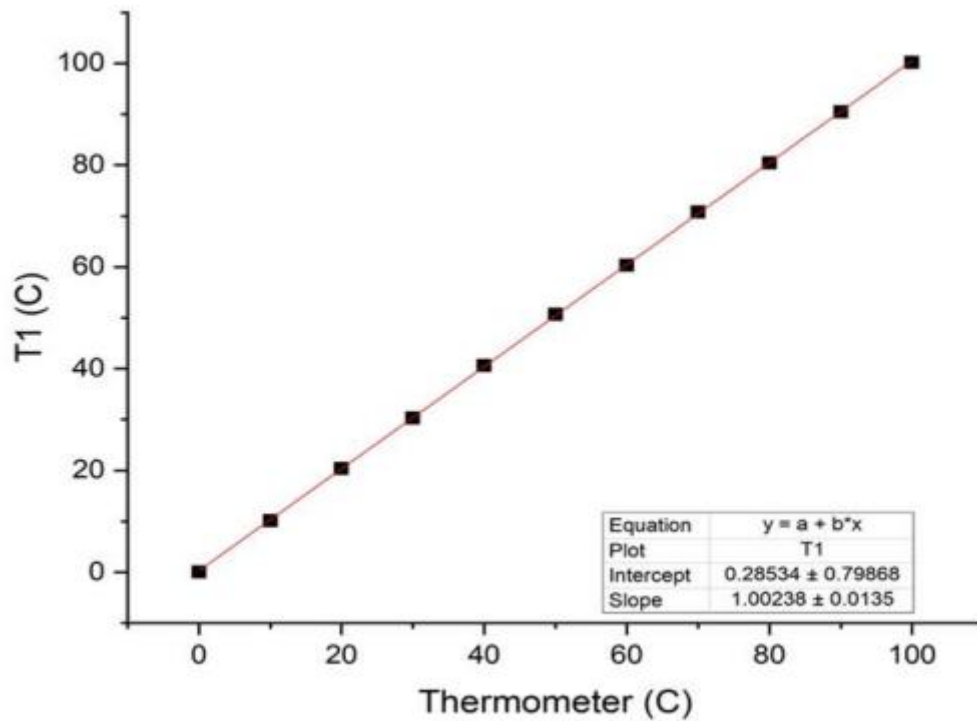


Figure B.1 Temperature calibration T1.

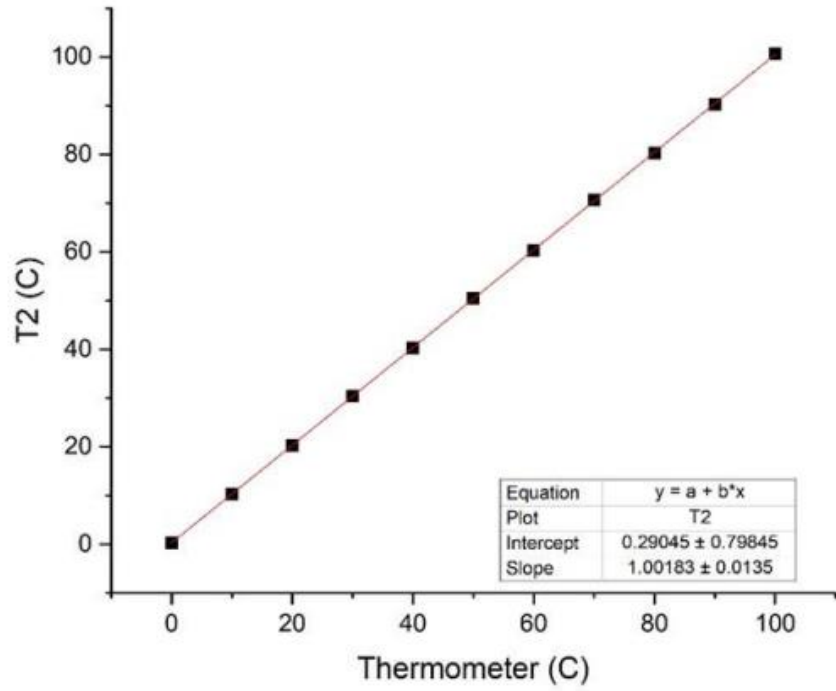


Figure B.2 Temperature calibration T2.

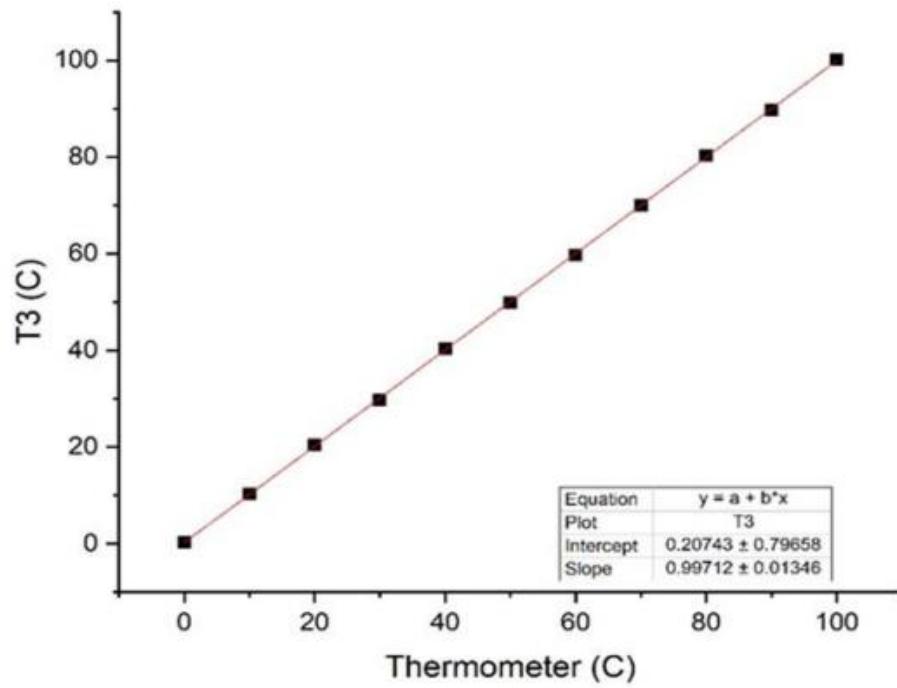


Figure B.3 Temperature calibration T3

Appendix-E. Solar Meter Calibration:

Figure and table C.1. Represent the calibration process for the solar meter (Pyranometer) device which was used in this work.

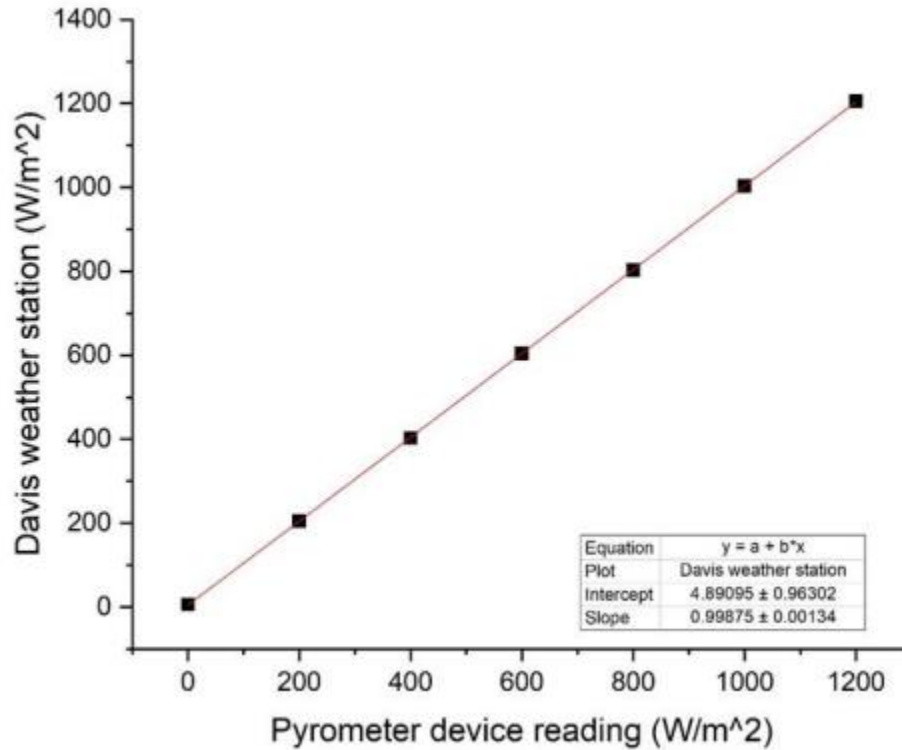


Figure C.1 solar meter calibration (Pyranometer)

Table C.1 solar meter characteristics (Pyranometer).

Property	Value
Model	TENMARS TM 207
Temperature error	±0.38°C
Accuracy	±10W/m ²
Sample time	0.25 second
Operating under temperature effect	0°C – 50 °C
Humidity	<80% RH
Dimension L/W/H	22 cm, 15cm, and 4.5cm

Appendix -F: List of publications

1. Comparative performances of natural dyes extracted from Mentha leaves, Helianthus leaves, and fragaria fruit for dye-sensitized solar cells.



Article

Comparative Performances of Natural Dyes Extracted from Mentha Leaves, Helianthus Annuus Leaves, and Fragaria Fruit for Dye-Sensitized Solar Cells

Zainab Haider Abdulrahman ¹, Dhafer Manea Hachim ², Ahmed Salim Naser Al-murshedi ², Furkan Kamil ², Ahmed Al-Manea ³ and Talal Yusaf ^{4,5,*}

¹ Department of Power Mechanics, Najaf Technical College, Al-Furat Al-Awsat Technical University, Najaf 31001, Iraq

² Najaf Technical College, Al-Furat Al-Awsat Technical University, Najaf 31001, Iraq

³ Al-Samawah Technical Institute, Al-Furat Al-Awsat Technical University, Al-Samawah 66001, Iraq

⁴ School of Engineering and Technology, Central Queensland University, Brisbane 4000, Australia

⁵ Institute of Sustainable Energy, University Tenaga Nasional, Putrajaya Campus, Kajang 43000, Malaysia

* Correspondence: t.yusaf@cqu.edu.au

Abstract: During the last four centuries, there have been extensive research activities looking for green and clean sources of energy instead of traditional (fossil) energy in order to reduce the accumulation of gases and environmental pollution. Natural dye-sensitized solar cells (DSSCs) are one of the most promising types of photovoltaic cells for generating clean energy at a low cost. In this study, DSSCs were collected and experimentally tested using four different dyes extracted from Mentha leaves, Helianthus annuus leaves, Fragaria, and a mixture of the above extracts in equal proportions as natural stimuli for TiO₂ films. The result show that solar energy was successfully turned into electricity. Additionally, DSSCs based on mixtures of dyes showed better results than those based on single dyes. Efficiency (η) was 0.714%, and the fill factor (FF) was 83.3% for the cell area.

Keywords: natural dyes; dye-sensitized solar cells; DSSCs

Citation: Abdulrahman, Z.H.; Hachim, D.M.; Al-murshedi, A.S.N.; Kamil, F.; Al-Manea, A.; Yusaf, T. Comparative Performances of Natural Dyes Extracted from Mentha Leaves, Helianthus Annuus Leaves, and Fragaria Fruit for Dye-Sensitized Solar Cells. *Designs* **2022**, *6*, 100. <https://doi.org/10.3390/designs6060100>

Academic Editors: Xia Lu and Xueyi Lu

Received: 14 September 2022

Accepted: 19 October 2022

Published: 25 October 2022

1. Introduction

Nowadays, the used energy in the industry sector is transitioning towards a more environmentally-friendly future. Fossil fuels are an environmental menace that will be depleted sooner. To triumph over this situation, alternatives to these fossil fuel reserves

2. A Review Study to Manufacture each Part of Dye-Sensitized Solar Cells.



1st International Conference on Achieving the Sustainable Development Goals

(6th – 7th) June 2022 in Istanbul- Turkey

Final Acceptance Letter

Manuscript Number: 6

Dear: Zainab Haider Abdulrahman

Co-Authors: Dhafer Manea Hachim and Ahmed Salim Naser Al-Murshedi

Congratulations!

It's a great pleasure to inform you that, after the peer review process, your manuscript entitled

(A Review Study to Manufacture each Part of Dye-Sensitized Solar Cells)

had been **ACCEPTED** for participating in the **1st International Conference on Achieving the Sustainable Development Goals**, and considered for publication in **(AIP Conference proceeding)**.

Thank you for your valuable participation in the ICASDG2022 conference.

A handwritten signature in green ink, appearing to read 'Ahmed G. Wadday'.



Prof. Dr. Ahmed G. Wadday
ICASDG2022 Scientific Committee Chair | AIP Conference Proceeding Editor
6th – 7th June 2022 | Istanbul | Turkey

3. Investigation of the Thermal Effect on the Performance of Dye-Sensitive Solar Cells

From: <ices2023@atu.edu.iq>
Date: Sat, Feb 4, 2023 at 11:47 AM
Subject: [3rd ICES 2023] Editor Decision
To: Prof.Dr.Dhafer M. Hachim <cj.dfr@atu.edu.iq>

Dear Prof.Dr.Dhafer M. Hachim,

We have reached a decision regarding your submission to 3rd International Conference on Engineering & Science (ICES), "Investigation of the Thermal Effect on the Performance of Dye-Sensitive Solar Cells".

Our decision is to: Accept the Submission

Best Regards,

Dr. Ahmed Razzaq H. Al-Manea
Scientific Committee of ICES 2023 | Guest editor AIP Proceedings
3-4 MAY 2023 | Al-Samawa Technical Institute | IRAQ

WWW.ices2023.atu.edu.iq

ICES2023 Scientific Committee | Al-Samawa | IRAQ

[3rd International Conference on Engineering & Science \(ICES\)](#)

الخلاصة

تعتبر الخلايا الشمسية (الخلايا الكهروضوئية; غالباً ما يعبر عنها بالرمز PV) الحل الأمثل للتخلص من مشاكل التلوث البيئي الناتجة من عمليات إنتاج الطاقة الكهربائية. فهي تحول الطاقة الشمسية مباشرة الى طاقة كهربائية بفعل خاصية (Photovoltaic Effect) بدون ضوء وتلوث بيئي أو أجزاء متحركة يجعل الخلايا الشمسية الخيار الأمثل للطاقة النظيفة في العالم. الا ان هناك العديد من العوامل البيئية التي تحد من كفاءة الخلايا الشمسية وتجعلها قليلة نسبياً.

تمثل الخلايا الشمسية نوع (Dye-Sensitized solar cell (DSSC)) أحد أنواع خلايا الجيل الثالث للخلايا الكهروضوئية والتي تعرف كباقي الخلايا الشمسية الأخرى بأنها جهاز يحول الفوتونات الشمسية (ضوء الشمس) الى طاقة كهربائية. جذبت DSSC الكثير من الاهتمام لقلّة تكلفتها مقارنة بالخلايا الكهروضوئية الأخرى. في هذا العمل تم تصنيع خلايا نوع DSSCs باستخدام اصباغ طبيعية حساسة للضوء حيث تمتاز بسهولة استخلاصها وكلفتها المنخفضة جداً كما انها صديقة للبيئة كما تستخدم هذه الخلايا غشاءً رقيقاً من مادة ثنائي أكسيد التيتانيوم مغطى بطبقة من الاصبغ الطبيعية لامتناس الطاقة الشمسية وتحويلها الى الكترونات حرة بحيث تحقن الى طبقة TiO_2 الذي يعمل كجامع للإلكترونات. وتتكون أيضاً من محلول الكتروليتي سائل للتعويض عن الإلكترونات المفقودة من جزيئات الصبغة الطبيعية.

في هذه الدراسة تم تصنيع DSSCs باستخدام ثلاث اصباغ طبيعية جديدة مختلفة والمتمثلة بالاصباغ المستخلصة من أوراق النعناع (لاحتوائها على نسبة عالية من الكلوروفيل الذي يمثل اهم العناصر في امتصاص الطاقة الشمسية) وزهرة عباد الشمس (لاحتوائها على هرمون الاوكسين الذي يسبب دوران هذه الزهرة مع الشمس) وفاكهة الفراولة (لاحتوائها على الانثوسيانين). أفضل النتائج التي تم الحصول عليها كانت ل DSSC القائمة على الصبغة المستخلصة من زهرة عباد الشمس اذ كان لها اكبر عدد من قمم الامتناس حيث كانت نتائج الخلية $V_{oc}=0.48V$, $FF=50.77\%$, $I_{sc}=1.19mA$ و $\eta=0.29\%$ ولتحسين كفاءة أداء الخلية تم مزج الاصبغ الثلاثة لتصنيع خلية جديدة قائمة على مزيج الاصبغ بنسب متساوية كصبغة فكانت نتائج تلك الخلية $V_{oc}=0.59V$, $I_{sc}=1.59mA$ و $FF=73.55\%$ و $\eta=0.69\%$.

وفي تجارب أخرى تم خلط مواد نانوية مع الاصبغ الا ان نتائجها كانت سلبية حيث تسببت إضافة المادة النانوية الى تحلل الصبغة وبذلك اختفى جزء الخلية الحساس للضوء فلم تظهر أي نتائج للخلايا

كما تم في هذه الدراسة مقارنة النتائج بين خلية ذات طبقة واحدة من TiO_2 وأخرى ذات طبقتين ; كلا الخليتين قائمة على مزيج الاصباغ كمحسس للضوء وبعد اجراء فحص FESEM أظهرت الصور ان الطبقة الواحدة من TiO_2 تظهر شقوق أكثر واكبر مما هو عليه بالنسبة لطبقتين TiO_2 وبذلك تم معالجة عيب أساسي من عيوب DSSCs اذا كان هناك ارتفاع واضح في نتائج الخلية المكونة من طبقتين من TiO_2 حيث ارتفعت كفاءة DSSCs من 0.69 % الى 1.13 %.

تم دراسة التدهور الحاصل في كفاءة DSSCs نتيجة ارتفاع درجة حرارة المحيط. من خلال الفحوصات المختبرية التي اجريه وباستخدام جهاز (Keithlye 2400) وتسليط ضوء شدة اشعاعه 1000 واط/م² لاحظت النتائج ان كفاءة DSSCs تقل بنسبة عالية بارتفاع درجة الحرارة اذ قلت الكفاءة من 1.13 % عند درجة الحرارة الأولى التي كانت تعادل $23.8^{\circ}C$ الى 0.49 % عند حرارة $43.32^{\circ}C$.



التحقق من اداء الخلايا الشمسية الصبغية بطلائها بصبغات طبيعية مع مواد نانوية

رسالة مقدمة الى

قسم هندسة تقنيات ميكانيك القوى في الكلية التقنية الهندسية-نجف /جامعة الفرات الاوسط التقنية
كجزء من متطلبات نيل درجة الماجستير في هندسة تقنيات ميكانيك الحرارية

تقدمت بها

زينب حيدر عبد الرحمن محمد

اشراف

الدكتور احمد سالم ناصر

الاستاذ الدكتور ظافر مانع حاجم

1444 هـ



جمهورية العراق

وزارة التعليم العالي والبحث العلمي

جامعة الفرات الاوسط التقنية

الكلية التقنية الهندسية/النجف

دراسة تجريبية للتحقق من اداء الخلايا الشمسية الصبغية بطلانها بصبغات
طبيعية مع مواد نانوية

زينب حيدر عبد الرحمن محمد

بكالوريوس في هندسة تقنيات الطيران

1444 هـ